Study of Hard Magnetic Properties of Hexagonal Ferrites using Magnetite from Cox's Bazar Beach Sand with the Addition of Rare-earth Oxides

M. Phil Thesis

By

Mohammad Mahbubur Rahman

Department of Physics
Khulna University of Engineering & Technology
Khulna-920300
Bangladesh

Study of Hard Magnetic Properties of Hexagonal Ferrites using Magnetite from Cox's Bazar Beach Sand with the Addition of Rare-earth Oxides

M. Phil Thesis

By

Mohammad Mahbubur Rahman

Roll No. 0455551

Session: July 2004

A DISSERTATION SUBMITTED O THE DEPARTMENT OF PHYSICS OF KHULNA UNIVERSITY OF ENGINEERING & TECHNOLOGY IN THE PARTIAL FULFILLMENT OF THE REQIREMENT FOR DEGREE OF MASTER OF PHILOSOPHY

Department of Physics
Khulna University of Engineering & Technology
Khulna-920300
Bangladesh

AUGUST 2007

Declaration

This is to certify that the thesis work entitled **"Study of Hard Magnetic Properties of Hexagonal Ferrites using Magnetite from Cox's Bazar Beach Sand with the Addition of Rare-earth Oxides"** has been carried out in the partial fulfillment for the requirement of M. Phil degree in the department of Physics, Khulna University of Engineering & Technology, Khulna-920300 does not contain any material extracted from elsewhere or from a work published by any body else. The above research work or any part of this work has not been submitted anywhere for the award of any degree or diploma. No other person's work has been used without due acknowledgement.

Candidate

Mohammad Mahbubur Rahman

Supervisor

Prof. Dr. S. S. Sikder

KHULNA UNIVERSITY OF ENGINEERING & TECHNOLOGY
DEPARTMENT OF PHYSICS
CERTIFICATION OF THESIS WORK

A THESIS ON

STUDY OF HARD MAGNETIC PROPERTIES OF HEXAGONAL FERRITES USING MAGNETITE FROM COX'S BAZAR BEACH SAND WITH THE ADDITION OF RARE-EARTH OXIDES

By
MOHAMMAD MAHBUBUR RAHMAN

has been accepted as satisfactory in partial fulfillment for the degree of Master of Philosophy in Physics and certified that the student has demonstrated a satisfactory knowledge on the field covered by this thesis in an oral examination held on August 18, 2007.

Panel of Examiners

1. **Prof. Dr. Shibendra Shekher Sikder**
   Department of Physics
   Khulna University of Engineering & Technology
   ..... 18/08/07
   Chairman & Supervisor

2. **Head**
   Department of Physics
   Khulna University of Engineering & Technology
   ..... 18/08/07
   Member

3. **Dr. A. K. M Abdul Hakim**
   Chief Engineer & Head
   Materials Science Division
   Atomic Energy Centre, Dhaka-1000
   ..... 18.08.07
   Member & Joint Supervisor

4. **Prof. Dr. Md. Mahbub Alam**
   Department of Physics
   Khulna University of Engineering & Technology
   ..... 18.08.07
   Member

5. **Prof. Dr. Jiban Podder**
   Department of Physics
   Bangladesh University of Engineering & Technology
   Dhaka-1000
   ..... 18/08/07
   Member (External)

Acknowledgements

First and foremost, I would like to express my deep sense of sincere gratitude to my supervisor Professor Dr. Shibendra Shekher Sikder, Head, Department of Physics, Khulna University of Engineering & Technology and my Co-Supervisor Dr. A. K. M. Abdul Hakim, Chief Engineer and Head, Materials Science Division, AECD for their continuous guidance, excellent cooperation, fruitful comments and suggestions and encouragement for the completion of the research work in proper and smooth way. I am very grateful to them for giving me the opportunity to carry out research under their sincere guidance, supervision and knowledge. I would like to extend my sincere gratitude to Dr. D. K. Saha, P. S. O of MSD, AECD for his kind cooperation during the XRD study of the samples.

It is a matter of great pleasure for me to record the deepest sense of gratitude to Professor Dr. Md. Mahbub Alam, Department of Physics, Khulna University of Engineering & Technology who has given me a strong support in various ways during the entire period of my study in this department.

I gratefully acknowledge Mr. Md. Abdullah Elias Akhter, Mrs. Jolly Sultana and Mr. Md. Kamrul Hasan Reza, Assistant Professors, Department of Physics, Khulna University Engineering & Technology for their co-operation and inspiration during my study in this department. I wish to express my thanks to Mr. Enamul Hoque Buiyan, and Mr. Asaduzzaman, Lecturers, Department of Physics for their cooperation in various ways during the period of my study in this department.

I am indebted to Ms. Sheikh Manjura Hoque, S. S. O., Mr. Mohammed Nazrul Islam Khan, S. O. of MSD, AECD and Mr. Md. Manjurul Haque, Assistant Professor, Department of Electronics & Applied Physics, Islamic University, Kushtia and for their valuable suggestions, experiences and many interesting discussions to develop the thesis.

I would like to acknowledge gratefully to Dr. Sundaresan and Ph. D. student Mr. Pranav of Jawharlal Nehru Centre for Advanced Scientific Research (JNCASR), India for their cooperation and assistance in Physical property measurement system (PPMS) measurements.

I must express my gratitude and very very special thanks to Mr. Asit Kumar Gain, a metallurgist from BUET and Mr. Shiba Pada Mondal, M. Phil student of Department of Physics, KUET, Khulna for their cooperation and assistance at different times during the research work.

I am very much indebted to the Chairman BCSIR, Dhaka for allowing me the laboratory facility with a considerable low price for the microstructure study of the samples by using Scanning Electron Microscope (SEM). I wish to express my thanks to Dr. Tofazzol Hosain, P. S. O. and Mr. Syed Farid Uddin Farhad, S. O., Industrial Physics Division (IPD), BCSIR, Dhaka for their assistance during the microstructure study of the samples by SEM.

I have the pleasure to thank Mr. Sultan Mahmud, Assistant Professor, Department of Physics, University of Asia and Pacific, Dhaka to inspire me by his nice and popular behavior during my research work.

My sincere thanks to Anjuman Ara Apa, for her consistent and heartfelt help during the entire period of my research work at the laboratory of MSD, AEC, Dhaka. My thanks to all the staffs of Materials Science Division, AECD Mrs. Parveen, Mrs. Sadia Halima, Ms. Nazmunnahar, Mr. Mohsin, Mr. Mostafiz and Mr. Jewell for their cooperation during the preparation of the sample and experimental measurements.

I am immensely grateful to my father, elder brothers, sisters and bhabies for their sacrifice, constant love, patience, inspiration and providing me lot of supports in various ways during the whole period of my student life. In this connection, I would like give a very special thank to Misha, my niece for her cooperation and sharing about different matter of practical life during my stay in Dhaka for the research work.

A very special thanks to Mrs. Nandita Sikder wife of Prof. Dr. S. S. Sikder for her heartfelt encouragement, care and helps throughout the entire period of my M. Phil study. She bears an excellent hand of cooking. I will never forget the tests of different nice foods taken different times during the period of valuable discussion about the research work at his residence.

I would like to mourn and pay my deepest sense of all respect to the departed soul of my heavenly mother Mrs. Rabya Khatun, whose blessings enabled me to complete such a noble work in a smooth and comfortable way.

My thanks are due to Director Atomic Energy Centre, Dhaka for his kind permission to use the Laboratory of Materials Science Division, Atomic Energy Center, Dhaka.

I am grateful to the authority of KUET for providing me the relevant facilities and financial assistance for the research work.

The financial support of this research work of Dutch-Bangla Bank Foundation (DBBF) by their fellowship programme is gratefully acknowledged. The DBBF is

playing a very important role by their fellowship programme for the development of higher education and research in the country.

Finally, all the thanks to almighty Allah, the most merciful, the sustainer and controller of the universe, whose command makes all the above mentioned facilities available to me.

Mohammad Mahbubur Rahman

THIS NOBLE WORK HAS BEEN

DEDICATED

TO

MY HEAVENLY MOTHER, THE MOST LOVING PERSON OF ME

CONTENTS

CHAPTER ONE: INTRODUCTION

CHAPTER TWO: THEORETICAL ASPECTS

CHAPTER THREE: SPECIMEN PREPARATION

CHAPTER FOUR: EXPERIMENTAL DETAILS

CHAPTER FIVE: RESULTS AND DISCUSSION

LIST OF THE SYMBOLS USED

a	=	Lattice parameter
c	=	Lattice parameter
tan δ	=	loss factor or loss tangent
T_c	=	Curie temperature
L	=	Self inductance of the sample core
L_o	=	Inductance of the winding coil without sample
λ	=	Wave length of the X-ray
(hkl)	=	Indices of the planes
V	=	Unit cell volume
I	=	X-ray beam of intensity
XRD	=	X-ray diffraction
CPS	=	Counts per second
FWHM	=	Full Width at half maximum
μ	=	Initial permeability
μ′	=	Real part of the complex permeability
μ″	=	Imaginary part of the complex permeability
B_0	=	Magnetic induction in free space
H_0	=	Magnetic field in free space
Z	=	Complex impedance
X	=	Reactance
R	=	Resistance
ω	=	Frequency
RF	=	Radio frequency
d	=	Diameter
Q	=	Quality factor
SEM	=	Scanning electron microscope
D_g	=	Grain size
PPMS	=	Physical property measurement system
VSM	=	Vibrating sample magnetometer
M_s	=	Saturation magnetization
H	=	Magnetic field
M	=	Magnetization
M_r	=	Remanent magnetization
H_c	=	Coercivity

LIST OF PUBLICATIONS

1. **M. MAHBUBUR RAHMAN**[1], S. S. SIKDER[1], S. MONJURA HOQUE[2], M. A. HAKIM[2], "*Effect of Additives on Structural and Magnetic Properties of M-type Ba-Hexaferrites*", in Press; Jahangirnagar University Journal of Science, July 2007.

2. **M. MAHBUBUR RAHMAN**[1], S. S. SIKDER[1], M. A. HAKIM[2], "*Synthesis and Characterization of Rare-earth Oxide and (CaO + SiO_2) Substituted Barium Hexaferrites*", Presented on the Annual Conference of Bangladesh Physical Society (BPS), Held on 4-5 May, 2007, pp. 19

3. **M. MAHBUBUR RAHMAN**[1], S. S. SIKDER[1], D. K. SAHA[2] & M. A. HAKIM[2], "*Study Of Structural and Magnetic Properties of Sr-Hexaferrites Using Additives*", Accepted by the Bangladesh Journal of Physics for the Issue to be Published on December 2007.

ABSTRACT

The structural and magnetic properties of Sr- and Ba-hexaferrites with magnetoplumbite structure of composition $(MeO)_{1-x}$ $(La_2O_3)_x$ 5.7 Fe_2O_3, where x = 0.00, 0.04, 0.08 and MeO. 5.7 Fe_2O_3 + [0.7wt% CaO +0.3wt% SiO_2] and where Me = Sr and Ba prepared by standard ceramic technology at different sintering temperature using magnetite from Cox's Bazar beach sand, Bangladesh have been investigated in the present research work. The detailed work carried out by the measurement of density, porosity, identification of crystalline structure through X-ray diffraction (XRD) technique, unit cell volume, lattice parameters, Curie temperature, microstructure analyses of the samples following Scanning Electron Microscope (SEM), permeability, resistivity and study of hysteresis parameters viz. saturation magnetization, remanent magnetization and coercivity using quantum design physical property measurement system (PPMS) vibrating sample magnetometer (VSM). The density of the sintered hexaferrite samples has been found to be dependent with the additives and the sintering temperature. During the study it has been observed that the porosity and the lattice parameter a and c of the hexaferrites are also to be varied with addition of La_2O_3 and with the simultaneous addition of (CaO + SiO_2). The Curie temperature of Sr-hexaferrites has been found to be almost unchanged with the addition of La_2O_3 but with the addition of CaO and SiO_2 the Curie temperature has been found to be increased a little. At the same time Curie temperature of Ba-hexaferrite samples decreases with the addition of La_2O_3 and increases with the simultaneous addition of (CaO + SiO_2).

The phase identification and hexagonal shape particle morphology has been confirmed by XRD analyses of hexaferrites. SEM study of the SrM and BaM hexaferrites show that the particles are of elongated and irregular shaped and the average grain size decreases with the addition of La_2O_3. Throughout the investigation it has also been found that grain size increases with increasing sintering temperature.

The hysteresis measurements show that the additives have a significant effect of the hysteresis parameters of the hard ferrites. In the case of Sr-hexaferrites the value of saturation magnetization, M_s increases first with the La_2O_3 addition and then decreases. But in the case of BaM the value of M_s and coercivity has been found to be increased with the La_2O_3 addition. In our observation it has been found that the magnetic properties of the sintered barium and strontium hexaferrite samples having off-stoichiometric composition increases remarkably with the addition of La_2O_3 and ($CaO + SiO_2$).

CHAPTER ONE

Introduction

1.1 Introduction

In addition to the conventional three types of magnetic materials: diamagnetic, paramagnetic and ferromagnetic, there are two other types of magnetic materials with extraordinary magnetic properties. These are antiferromagnetic and ferrimagnetic materials. Ferrites fall into the category of ferrimagnetic materials. The history of ferrites began centuries before the birth of Christ with the discovery of stones that attract iron. The most abundant deposits of these stones were found in the district of Magnesia in Asia Minor, and hence the name of the minerals becomes magnetite (Fe_3O_4).

Ferrites constitute a special branch of ferrimagnetics. The term ferrites mean certain double oxide of iron and another metal, which have two unequal sublattices and are ordered anti-parallel to each other. Each sublattice exhibits spontaneous magnetization at room temperature, like the ferrimagnetics. Because of unequal magnitudes the magnetization is similar to ferromagnetics. Again like ferromagnetics, thus ferrites have spontaneously magnetized domains and show the phenomena of magnetic saturation and hysteresis and have a critical temperature T_c, called the Curie temperature, above which they become paramagnetic. But what makes these materials more interesting is their high resistivity. The resistivity of ferrites varies from 10^2 to 10^{10} ohm-cm which is about 15 orders of magnitude higher than that of iron. This outstanding property of ferrites makes them highly demandable for high frequency applications.

Ferrites are essentially ceramic materials, compound of iron, boron, barium, strontium, lead, zinc, magnesium or manganese. The ingredients are mixed, pre-fired, milled/crushed, dried, shaped and finally pressed and fired into their final hard and brittle state. Now a days newer family of ferrite materials have been

discovered, which are rare-earth types. Additives of rare-earth metals like lanthanum oxide (La_2O_3) are used to study the effect of enhancing the magnetic properties. They are primarily used as permanent magnets. These ferrites are very stable with the excellent characteristic of high resistivity.

Hard ferrites referred to as permanent magnets retain their magnetism after being magnetized. The development of permanent magnets came in the 1950's with the introduction of hard hexagonal ferrites. Ferrites with hexagonal structure such as barium, strontium and lead ferrites with the composition $MeFe_{12}O_{19}$ where Me = Ba, Sr or Pb have attracted considerable interest for permanent magnet applications, as the media for magnetic and magneto-optical recording as well as for high frequency core materials [1.1]. The unique feature of high coercivity and high energy product of the hexagonal ferrites is their high uniaxial magnetocrystalline anisotropy about 100 times higher than the soft ferrite with cubic structured. Therefore, hard ferrites constitute the major fraction since they are used where energy per unit weight and cost are important considerations [1.2]. General formula of hexagonal ferrite can be represented as m(MeO). n(Fe_2O_3), where m and n are natural numbers and Me is bivalent metal. For m =1 and n = 6, one obtains the formula for the so-called M-type ferrites. MeO. 6 (Fe_2O_3). The most common M-type ferrites are those where Me = Ba, Sr or Pb. When the hexaferrites are off-stoichiometric composition n can have the value between 6 and 5. Hence, enormous opportunities are associated with these materials to carry out research to upgrade the magnetic properties by changing the above-mentioned parameters. Wide spectrums of research have been performed by several authors on hexagonal ferrites [1.3-1.5]. The effects of additives like La_2O_3 [1.6], CaO and SiO_2 [1.7] and Al_2O_3 [1.8] on hexagonal ferrite in particular on Sr-ferrite have been investigated.

1.2 Review of Some Earlier Works

Now a days different synthesis methods are employed with various doopants to produce materials with modified magnetic parameters suitable for magnetic, high-density magneto-optical recording media and microwave applications [1.9-1.10]. There are several processes of preparing M-type hexaferrites such as chemical co-precipitation method [1.11], hydrothermal precipitation-calcination technique [1.12], sol-gel method [1.13], microemulsion synthesis [1.14], glass crystallization method [1.15], sputtering technique [1.16], liquid mix technique/ the organic resin method [1.17], salt-melt technique [1.18], aerosol pyrolysis [1.19] and organometallic precursor technique [1.20]. Recently a simple route to produce ferrite powders of very small particles and morphology have been widely used known as ball milling by using conventional ceramic method [1.21-1.22]. Babu and Padaikathan [1.5] studied the structural and hard magnetic properties of barium hexaferrites with and without La_2O_3 prepared by standard ceramic method. They investigated the data using XRD, SEM and VSM technologies. They showed that the magnetic properties were improved significantly with the addition of La_2O_3, which acts as grain refiner. In the meantime, the researches on improving the structural, physical and magnetic properties have never been stopped [1.24-1.26].

Various efforts have been made by different investigators to improve the structural and magnetic properties of M-type hexaferrite permanent magnets because of their good energy product and the best performance to cost ratio [1.27] incorporating cationic substitution. Besides these, ferrites are chemically much more stable than rare earth based materials. Rare-earth ions like La in substitution for Ba taking into account the ionic radius of the elements. Therefore, any improvement of the properties of M-type hexaferrites is of relevance for the large market.

Since their discovery of M-type hexagonal ferrites tremendous efforts have been made in enhancing their magnetic qualities. In order to improve their fundamental magnetic qualities of hexaferrites, many attempts have been made incorporating cationic substitution. Liu et al. [1.28] in their work, have prepared La-substituted M-type strontium hexaferrite by conventional ceramic process and systematically studied the influences of La^{3+} substituted amount on the magnetic properties. Moreover, the detailed effect of the sintering temperature on the magnetic properties has also been studied throughout their investigation. Throughout their study it was found that the suitable amount of La^{3+} substitution might remarkably increase saturation magnetization M_s and intrinsic coercivity H_c. With the La^{3+} addition for the same sintering temperature saturation magnetization and intrinsic coercivity increase at first then decrease gradually.

During the past few years, it has become possible to synthesize new hexaferrite particles in which intrinsic coercivity can be decreased by cation substituting techniques. At present, studies on these substitutions are mainly concentrated on transition-metal cations, for example, Zn^{2+}, Co^{2+}, Mn^{2+}, Ni^{2+}, Ti^{4+} and Ir^{4+} to substitute Fe^{3+} ions of hexaferrite [1.29-1.31]. Experiments demonstrated that the coercivity was reduced effectively. However, it can be found that the magnetization of doped particles also reduces, which is limit of the use of hexaferrite for magnetic recording. Hence how to decrease coercive force and simultaneously increase the saturation magnetization has attracted much attention. Recently, Fang [1.32] in their work shown the effect of substitution on the structure and magnetic characteristics of intrinsic and Cr^{3+} substituted Sr-hexaferrite particles. Throughout the work they showed that the Cr doping Sr-hexaferrite exhibits higher values of saturation magnetization and lower coercive

field when the substitution content $x \leq 0.14$, which is more suitable for high density magnetic recording.

Almost all the authors have been concentrated their investigations to enhance the magnetic anisotropy by partly substituting Me or Fe in the hexagonal ferrite by various elements including rare-earth elements. The substitution of small amounts of SrO by La_2O_3 in the hexagonal Sr-ferrites has been found to lead to an improvement of the magnetic properties [1.33-1.37]. In this regard Niem et al. [1.38] presented the influence of La doping on the structure and properties of a BaSr hexaferrite. They showed that the doping of La not only improves the coercivity and magnetization but the maximum energy product is also enhanced due to increase of the squareness. It was also concluded that doping of La leads to an increase of the hysteresis loop parameters of isotropic samples. The appropriate La_2O_3 and the small SiO_2 doping contribute to the creation of needle shape particle with the size of a single magnetic domain, leading to an increase of the magnetization as well as the magnetic anisotropies.

Ba-hexaferrite with magneto-plumbite structure have been studied and used broadly in permanent magnets because of their low cost along with reasonable magnetic properties [1.39]. They have high saturation magnetization, high resistivity, high chemical stability, high Curie temperatures and their coercive field can be adjusted for a wide range of applications. An important aspect of improving magnetic properties of barium hexaferrite was done by La or Pr substitution by Ounnunkad [1.40]. The author studied the sintered samples powder X-ray diffraction and vibrating sample magnetometry (VSM). All XRD patterns show the single phase of magnetoplumbite barium ferrite without other intermediate phase. Report also shows magnetization (M_s) and coercive field (H_c) could be

mproved by substitutions of La or Pr ions on Ba ion basis sites. The M_s reveal magnetic behaviour with respect to La or Pr ions content, showing an increase first then a decrease. The H_c increases remarkably with increasing La or Pr content. Barium hexaferrite and its derivative can be used for permanent magnets, magnetic recording media and microwave applications because of their improved magnetic properties.

The magnetic and microstructural properties of both polycrystalline and single crystal samples of barium hexaferrites have been investigated by Dho et al. [1.41] to elucidate the relationship between the grain boundary and the grain boundary pinning effect. They report that with the increasing in sintering temperature of the polycrystalline sample from 1100 to 1300°C, the grain size gradually increases while the coercivity largely drops from about 4 kOe to a few Oe.

After several decades of applications, hexaferrites cover more than 50% of the permanent magnet market since the lower price compensates for the superior magnetic performance of the rare-earth based permanent magnets developed in the last couple of years. Besides these, ferrites are chemically much more stable than rare-earth based materials. Therefore, any improvement of the properties of M-type ferrites is of relevance for the large market. Different attempts have been made to improve their magnetic properties by doping and substitutions within the complex structure but without significant success [1.42]. Grossinger et al. [1.43] studied the combined La-Co substitution on Ba-hexaferrite and reported that the anisotropy as well as the coercivity increases with the increase in La-Co content on the barium hexaferrite. Although La-Co substituted M-type ferrites and their related compounds were discovered a long time ago, only recently these ferrites

found a new industrial interest in the field of permanent magnets [1.44] because of their essentially improved coercivities.

Ba- or Sr-hexaferrites are manufactured on large scale worldwide [1.45]. The improvement of ferrite materials is a vital field of research. One crucial issue is the development of ferrite grades with large remanence and energy product. The formation of the desired dense microstructure with small oriented grains is controlled by the addition of sintering additives. The mechanism of the introduction of SiO_2 in ferrites was studied by Haberey and Kools [1.46-1.47]. Simultaneous addition of 0.45% CaO and 0-0.6% SiO_2 as another option to suppress grain growth has been investigated; a large remanence and coercivity of 250 kA/m were obtained [1.48]. Moreover, there are some indications that the size of the additives might also play a crucial role in determining their effectiveness for microstructure control. Topfer et al. [1.49] reported microstructural control of the magnetic properties by simultaneously adding CaO and SiO_2 in a concentration range from 0 to 1 wt%.

1.3 Recent Improvement and Applications of Hard Ferrites

Ferrites are commercially important magnetic materials pervade almost every sphere of modern technology. Magnetic materials are fundamental functional materials of electronic industry. As an important magnetic materials, hard ferrite materials play heavy role in electronic industry, electronic information industry, car industry, motor cycle industry etc, mean while, they are also widely used in medical treatment, mining and metallurgy, industrial automation, oil industry and civil industry. Ferrites are broadly used in the cores of inductors and transformers. Cassettes and videotapes use ferrites coated into the plastic base to record the signal. Ferrites are also used as memory core devices in computers.

Since their discovery ceramic materials based on M-type hexagonal have always enjoyed a significant market share thanks to their main applications in the DC motors for the automotive industry and consumer goods. Because of their improved magnetic properties and cost effectiveness hard ferrites still remain the permanent magnetic material both in tonnage and in value. To fulfill the market requirements, hard ferrites with higher magnetic properties have always been developed. The latest breakthrough is based on partial substitutions with rare-earth elements preferably lanthanum and with transition metals, preferable cobalt [1.50-1.52]. The improvement of magnetic properties stems from the modified intrinsic magnetic properties, in particular from a drastic change of the magneto-crystalline anisotropy field, which increases with the in substituted metals [1.53].

Ferrite applications may be classified into two broad categories for high frequency range as microwave and non-microwave. Perhaps the most important use of ferrites in recent times as a medium for transmitting microwaves. A microwave ferrite is defined as highly resistive magnetic materials used at frequencies between 100 MHz to 500 GHz, the highest microwave frequency now in use. Microwave ferrites are of two types: non-reciprocal and reciprocal. Ferrites showing non-reciprocal effect are almost irreplaceable have the greatest number of applications. This means that electromagnetic waves passing through them behave differently traveling in different directions. This phenomenon allows the construction of one-way transmission lines, junctions that can control the 'traffic' of microwaves, and other microwave control devices. The modern telecommunication system of today would have been impossible without ferrites. Another important use of ferrite is in resonance circuit. Cores of inductors use ferrites. To control and minimize various loss factors, ferrites become the very best inductor cores having high initial permeability and attractive small physical

size. Power transformer, where high saturation magnetization and low hysteresis losses are requires, also uses ferrites as core materials.

1.4 Importance of Ferrite Research in Our Country

Hexagonal ferrites are ceramic hard magnets with hexagonal crystal structure prepared from various metallic oxides like Fe_2O_3, BaO, SrO and PbO having various proportion. Hexagonal ferrites are technically important hard magnetic materials, which have extensive uses in electrical and electronic devices.

Presently Bangladesh is fully dependent upon the imported ferrite cores as well as other soft magnetic materials. Therefore, there is a huge scope to upgrade the quality of ferrite by developing ferrite industry, which may alleviate the existing problem.

Though the present use of magnetite from Cox's Bazar beach sand as a major ingredient (85% by weight) for the manufacture of permanent magnets with a small addition of rare-earth oxide such as La_2O_3 and controlled amount of SiO_2 and CaO would be tested. It has already been confirmed previously by various research activities carried out by different researchers [1.54] that commercial grade permanent magnets could be manufactured by using magnetite and hematite. In the present study addition of La_2O_3 and (CaO + SiO_2) about 1 wt% possibly enhance the hard magnetic properties because La_2O_3 act as grain refiner and SiO_2 is expected to activate the reaction kinetics for the formation of hexagonal ferrite during synthesis process while CaO promotes plate like grain growth oriented perpendicular to the basal plane enhancing the directional property of the hard magnets. It is well known the small grain size close to one micron in size effectively increases the hard magnetic properties, which we are expecting from

the addition of La_2O_3. Since SiO_2 activates the reaction kinetics, it was expected that the sintering could be done at relatively lower temperature compared with the sample without addition SiO_2. In the present case, it has been expected that the grain size will not be increased when synthesized at lower temperature because the grain size generally increases with the increase of sintering temperature. When the optimum grain size and their distribution are optimized, good hard magnetic properties can be attained.

As Bangladesh is fully dependent upon the imported hard ferrite cores as well as other soft ferrite materials. Successful completion of this research work will add some fruitful technological information for the development of hard magnetic materials in our country and these information would help to develop small-scale industries for the production of low cost permanent magnet using locally available raw materials, that may alleviate the present problem.

1.5 Our Aim

Ceramic materials permanent magnets are now well established in many areas of everyday use. The improvements in performance, service life, savings in operational costs and savings in maintenance are clear evidence of the benefits of the hard ferrites. The production of hard ferrites is complex and sophisticated equipments, highly specialized and well-trained people are required.

In the present study, our aim is the development of hard magnetic materials with special emphasis on more recent developments in this field. Our specific attention will be concentrated on the following points:

- To look into the possibility of develop of hard magnets using magnetite from Cox's Bazar beach sand.
- Effect of additives like La_2O_3 to enhance the hard magnetic properties of the synthesized samples which is generally found in case of using hematite Fe_2O_3.
- Effect of ($CaO + SiO_2$) addition to improve the properties of hard magnets would be studied at various synthesis temperatures.
- Characterize the synthesized materials as regard their crystal structure and microstructure.
- Optimize the best magnetic properties related to the practical application of these materials through appropriate heat treatment at different temperatures and duration of time.
- The results of experimentally determined parameters would be compared with the standard published results.
- Through this research to develop and standardize the indigenous technology for the manufacture of low cost hard magnets from the locally available raw materials.
- To establish specifications for raw materials required for the manufacturing of the barium and strontium hexaferrites.
- To increase the rate of sintering thus decreasing the sintering temperature and time using the additives like La_2O_3, CaO and SiO_2.
- To achieve better magnetic properties by controlling the grain size and inhabiting grain growth of the product.

1.6 Layout of the Dissertation

The contents of the dissertation have been arranged in the following way:

History of the ferrites, importance of ferrites, advantages of the ferrites, objectives of the present work and a review of some earlier works have been presented in **Chapter-I**.

The **Chapter-II** includes the general structure of crystals and ferrites, how atoms are arranged in some common crystals, theoretical background of the research work, mathematical formulation.

Chapter-III contains the methodology of the sample preparation.

The phenomenon of X-ray diffraction related to interplanar spacings in the crystalline powder following a mathematical relation called "*Bragg's Law*", using known wavelength λ, the spacing d of various planes and indexing the planes in a crystal for its structural and magnetic property analysis, different experimental techniques and measurements for the expected outcome are described in details in **Chapter-IV**.

The results and discussions of our investigations are presented in **Chapter-V.**

The conclusions of the research work as extracted from the experimental results and discussions are displayed in **Chapter-VI**.

Bibliography is given in the **Chapter-VII.**

CHAPTER TWO

Theoretical Aspects

2.1 Introduction

A crystal is a solid in which the constituent atoms, molecules, or ions are packed in a regularly ordered, repeating pattern extending in all three spatial dimensions. All the atoms in the solid fit into the same crystal structure forms a single crystal structure. However, generally, many crystals form simultaneously during solidification, leading to a polycrystalline solid. Most of the metals encountered in everyday life are polycrystals. Crystals are often symmetrically intergrown to form crystal twins. In Which, fluid forms a crystal structure, depends on the chemistry of the fluid, the conditions under which it is being solidified, and also on the ambient pressure. The process of forming a crystalline structure is often referred to as crystallization [2.1].

Almost all metal exists in a polycrystalline state; amorphous or single-crystal metals must be produced synthetically, often with great difficulty. Ionically bonded crystals can form upon solidification of salts, either from a molten fluid or when it condenses from a solution. Covalently bonded crystals are also very common, notable examples being diamond, silica, and graphite. Weak Van der Waals forces can also play a role in a crystal structure; for example, this type of bonding loosely holds together the hexagonal-patterned sheets in graphite. Most crystalline materials have a variety of crystallographic defects. The types and structures of these defects can have a profound effect on the properties of the materials. While the term "crystal" has a precise meaning within materials science and solid-state physics, colloquially "crystal" refers to solid objects that exhibit well-defined and often pleasing geometric shapes. The shape of these crystals is dependent on the types of molecular bonds between the atoms to determine the structure, as well as on the conditions under which they formed. Snowflakes, diamonds, and common salt are common examples of crystals. Crystallography is the scientific study of crystals and crystal formation.

2.2 Single Crystal

A single crystal, also called monocrystal, is a crystalline solid in which the crystal lattice of the entire sample is continuous and unbroken to the edges of the sample, with no grain boundaries. The opposite of a single crystal sample is a polycrystalline sample, which is made up of a number of smaller crystals known as crystallites. Because of a variety of

entropic effects on the microstructure of solids, including the distorting effects of impurities and the mobility of crystallographic defects and dislocations, single crystals of meaningful size are exceedingly rare in nature, and can also be difficult to produce in the laboratory under controlled conditions. Because grain boundaries can have significant effects on the physical and electrical properties of a material, single crystals are of interest to industry, and have important industrial applications. The most notable of these is the use of single crystal silicon in the fabrication of semiconductors. On the quantum scale that microprocessors operate on, the presence of grain boundaries would have a significant impact on the functionality of field effect transistors by altering local electrical properties. Therefore, microprocessor fabricators have invested heavily in facilities to produce large single crystals of silicon. Fabrication of single crystals usually involves the building of a crystal layer by layer of atoms. Some thin film deposition techniques can be used for epitaxy, forming a new layer of material with the same structure on the surface of an existing single crystal.

2.3 Lattices

A crystal may be defined as a solid composed of atoms arranged in a pattern periodic in three dimensions. Not all solids are crystalline, however, some are amorphous, like glass and do not have any regular interior arrangement of atoms. In thinking about crystals, it is often convenient to ignore the actual atoms composing the crystals and their periodic arrangement in space, and to think instead of a set of imaginary points which has a fixed relation in space to the atoms of the crystals and which may be regarded as a sort of framework of skeleton on which the actual crystal is built [2.2]. The space dividing planes will intersect each other in a set of lines shown figure 2.1, and these lines in turn in interest in the set of points so referred to above. A set of points so formed has an important property: it constitutes a point lattice, which is defined as an array of points in space so, arranged that each points has identical surrounding. By "identical surrounding" we mean that the lattice of points, when viewed in a particular direction from one lattice point would have exactly the same appearance when viewed in the same direction from any other lattice point.

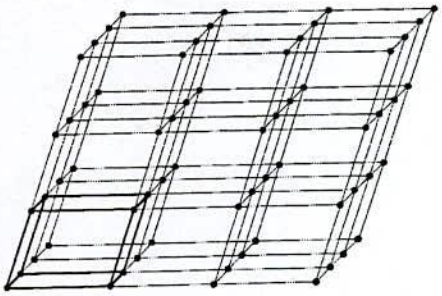

Fig-2.1: A point lattice

According to the figure 2.1 all the cells of the lattices are identical, we may choose any one, for example the heaving out lined one, as a unit cell. The size and shape of the unit cell can in turn be described by the three vectors ***a***, ***b*** and ***c*** drawn from one corner of the cell taken as origin as shown in figure 2.2. The cell is defined by these vectors called the crystallographic axes of the cell. They may also be described in terms of their lengths (*a, b, c*) and the angles between them (α, β, γ). These lengths and angles are the lattice constants or lattice parameters of the unit cell.

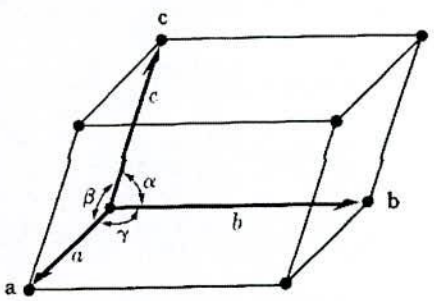

Fig-2.2: A unit cell

2.4 Classification of Ferrites and its Relevance

Ferrites are essentially ceramic materials, compound of iron, boron, barium, strontium, lead, zinc, magnesium or manganese. The ingredients are mixed, pre-fired, milled/crushed, dried, shaped and finally pressed and fired into their final hard and brittle state. Now a days newer family of ferrite materials have been discovered, which are rare-earth types. Additives of rare-earth metals like lanthanum oxide (La_2O_3) are used to study the effect of enhancing the magnetic

properties. They are primarily used as permanent magnets. These ferrites are very stable with the excellent characteristic of high resistivity.

Ferrites are classified into two categories based on their coercive field strength. They are

i) Soft ferrite with coercive field strength < 10 Oe

ii) Hard ferrite with coercive field strength > 125 Oe

Most common ferrite contains 50% iron oxide. One of the most common types of soft ferrite is made up of oxides of manganese (Mn) and zinc (Zn). Hard ferrites like Ba-ferrite, Sr-ferrite, Pb-ferrite are used in communication devices operating with high frequency currents because of their high resistivity, negligible eddy currents and lower loss of energy due to joule heating and hysteresis.

Hard ferrites referred to as permanent magnets retain their magnetism after being magnetized. The development of permanent magnets came in the 1950's with the introduction of hard hexagonal ferrites. Ferrites with hexagonal structure such as barium, strontium and lead ferrites with the composition $MeFe_{12}O_{19}$ where Me = Ba, Sr or Pb have attracted considerable interest for permanent magnet applications, as the media for magnetic and magneto-optical recording as well as for high frequency core materials [2.3]. The unique feature of high coercivity and high-energy product of the hexagonal ferrites is their high uniaxial magnetocrystalline anisotropy about 100 times higher than the soft ferrite with cubic structured. Therefore, hard ferrites constitute the major fraction since they are used where energy per unit weight and cost are important considerations [2.4].

According to the crystallographic structures ferrites fall into three categories

i) Cubic ferrites of spinel type

ii) Cubic ferrites of the garnet type and

iii) Hexagonal ferrites

Ferrites fallen into two groups with different crystal structures are shown in the following block diagram shown in fig-2.3

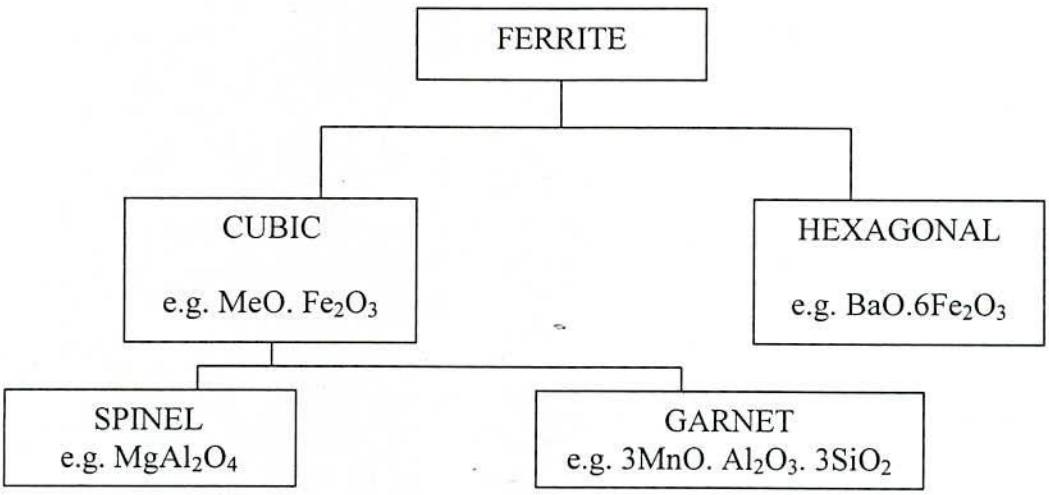

Fig-2.3: Classification of Ferrites

2.4.1 Cubic Ferrites of the Spinel Type

These ferrites are also called ferrospinels because they crystallize in the same crystal structure as the mineral spinel and they derive their general formula $MeFe_2O_4$ from that ($MgAl_2O_4$) of spinel. In this formula, Me represents a divalent ion of metal. Besides the divalency, another condition to qualify a metal in ferrospinels is its ionic radius which should fall between 0.6 and 1.0 Å. Mg, Fe, Co, Ni, Cu, Zn and Cd all satisfy these two conditions and thus form various single cubic ferrites. Magnetic, which contains one ferrous ion and two ferric ions in each formula unit is a typical ferrite.

The crystal structure of ferrites is based on a face-centered cubic lattice of the oxygen ions. Each unit cell contains eight formula units. Therefore, there are $32O^{2-}$ anions, 16 Fe^{3+} cations and 8 Me^{2+} cations in the cell, and the lattice constant is rather large, of the order of 8.5 O. In each unit cell, there are 64 tetrahedral, or A-sites and 32 octahedral, or B-sites. These sites are so named

because they are surrounded by four and six oxygen ions at equal distances, respectively.

2.4.2 Cubic Ferrites of Garnet Type

The mineral garnet refers to a group of mixed oxides, of which the widely known one has the chemical formula $Mn_3Al_2Si_3O_{12}$, or equivalently, $3MnO.\ Al_2O_3.3SiO_2$. Single magnetic garnets have the general formula $3M_2O_3.\ 5Fe_2O_3 = 2\,M_3^{III}Fe_5^{III}\,O_{12}$. In magnetic garnets, the 24 positive charge units per formula units are divided unequally between the ferric ions (15 units) and another species of trivalent ions (9 units). Technically useful garnets are those with M = Sm, Eu, Gd, Tb, Dy, Ho, Er, Tm, Yb, or Y.

A code system has been adopted to name them: REG stands for the rare-earth garnets, GdIG for the gadolinium –iron garnet ($Gd_3Fe_5O_{12}$), YIG for the yttrium-iron garnet ($Y_3Fe_5O_{12}$), etc. Garnets crystallize in the cubic system with two-fifths of the ferric ions forming a body-centered cubic lattice. Like the ferrospinels, the garnets, too, pack a large number (160) of ions in eight formula units into a unit cell. The lattice constant is ≈ 12.5Ο, about 50% larger than those of ferrospinel. Also, the crystal structure of garnets is more complicated than the spinel structure because of the size (0.85 – 1.10Ο) of the M^{III} ions. They are too large to be accommodated at the interstitial sites between the oxygen ions. Hence the oxygen ions are prohibited from forming a close-packed structure as in the spinel. In each until cell, which contains eight formula units, there are three kinds of cation sites, of which

i) 16 octahedral [a] sites are occupied by Fe^{III} ions
ii) 24 tetrahedral (d) sites are also occupied by Fe^{III} ions and
iii) 24 dodecahedral {c} sites are occupied by M^{III} ions [2.5]

2.4.3 Hexagonal Ferrites

Ferrite having a complex, close-packed, hexagonal structure similar to that of the mineral magnetoplumbite have found their application as permanent magnet materials because of their very high coercivities combined with a moderate saturation magnetization. Hexagonal ferrites are Ceramic hard magnets with hexagonal crystal structure prepared from various metallic oxides such as Fe_2O_3, BaO, SrO and PbO having various proportion. These materials are broadly known as ferrimagnetic materials. Hexagonal ferrites are technically important hard magnetic materials, which have extensive uses in electrical and electronic devices. There are many hexagonal ferrites but the only ones of commercial importance are barium ferrite $BaO.6Fe_2O_3$ (= $BaFe_{12}O_{19}$) and strontium ferrite $SrO.6Fe_2O_3$ (= $SrFe_{12}O_{19}$) [2.3]. General formula of hexaferrite can be represented as $m(MeO).n(Fe_2O_3)$ where m and n are natural numbers and Me is a divalent metal. For m = 1 and n = 6 one obtains the formula for the so-called M-type ferrites, $MeO.\ 6(Fe_2O_3)$. The most common M-type ferrites are those where Me = Ba, Sr, or Pb. When the hexaferrites are of off-stoichiometric composition n can have the value between 6 and 5.

The atomic arrangement of the hexagonal close-packed structure is shown in the following fig-2.4. The atoms in the second layer are above the hollows in the first layer, so that the layer stacking sequence can be summarized as ABABAB….[2.6].

A group of ferromagnetic oxides exists possessing closely related hexagonal crystal structures. The following figure 2.5 shows the chemical compositions of different types of hexaferrites. The corners of the diagram represent the oxides BaO, MeO and Fe_2O_3. The symbol Me represents a divalent ion from the first transition series, or it may represent Zn, Mg or a combination of for instance Li^{I} and Fe^{III}, just as occur in spinel structure [2.8].

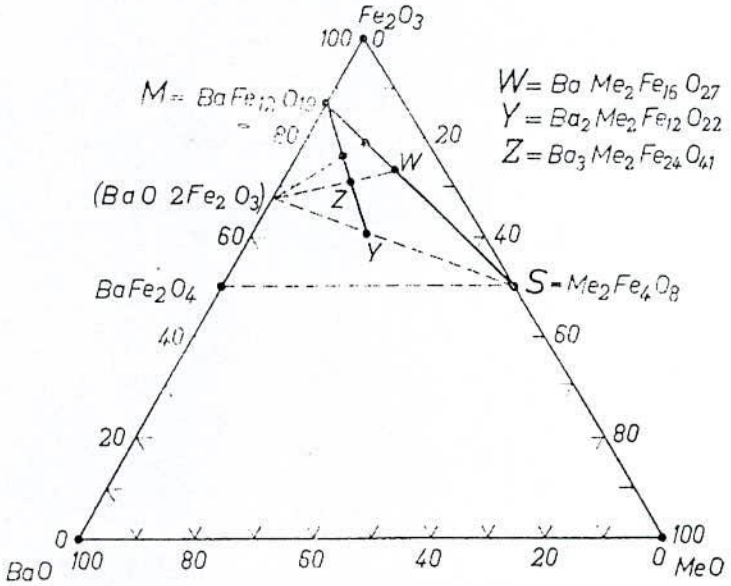

Fig-2.5: Composition diagram for the ferromagnetic ferrites. The symbol Me represents a divalent ion

The hexagonal closed-packed structure is schematically in the following figure 2.6. The centers of the ions B lie in a horizontal plane and form equilateral triangles. On this layer can now be placed a new layer of identical ions, shown in the diagram as A. These ions are also closely packed in a horizontal plane. With a hexagonal close-packed structure there exists under the layer with B ions another layer ions whose centers lie vertically below those of the ions in the A layer. Continuing in the vertical direction we thus obtain in a hexagonal structure the sequence of layers ABABA and so on. It is evident that this produces uniaxial hexagonal crystal structure in which the c axis is perpendicular to the oxygen layers [2.8].

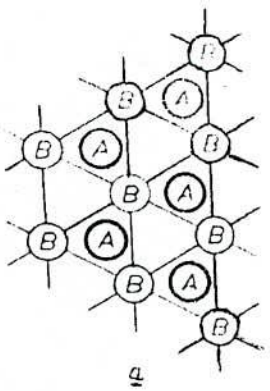

Fig-2.6: Schematic representation of the close-packed hexagonal structure

2.4.4 The Magnetoplumbite (M) Structure

The structure of M-type barium ferrite is symbolically described as RSR*S*, where R is a one-layer block with composition $Ba^{2+}\,Fe_3^{3+}\,O_3^{2-}$ and S is a four O_4-layer block with composition $Fe_9^{3+}\,O_{16}^{2-}$, where the asterisk means that the corresponding block has been turned 180° around the hexagonal c-axis. All the metal ions are arranged in the interstices of oxygen atom. The magnetoplumbite structure can be built up from spinel blocks S and S*, which are connected by a block R containing the barium ion shown in figure 2.8. Blocks R* and S* are obtained from blocks R and S, respectively, by rotation over 180° around the c axis. The layer containing barium is hexagonally packed with respect to two oxygen layers at each side. The four oxygen layers between those containing barium are cubically packed. There is an overlap of cubically and hexagonally packed sections in the structure. The basal plane containing the barium ion is a mirror plane of the R block, and consequently the blocks preceding and succeeding the R blocks (S and S*) must be rotated over 180° with respect to each other. This is also the reason why the elementary cell of the M structure contains 10 and not 5 oxygen layers. There are five Fe sites: two ions have tetrahedral surroundings ($4f_1$), and one Fe ion is located in a trigonal bipyramid (2b) with five-fold coordination [2.9]; three octahedral positions (2a, $4f_2$ and 12k) are occupied by one, two and six Fe ions, respectively, as shown in figure 2.7. In an elementary cell each layer contains four large ions. There are in four successive

layers always four oxygen ions, but each fifth layer contains three oxygen ions and one barium ion. In general it can be said that when one block is passed in a structure the following blocks must be rotated over 180° around the c axis. Only after a second R block is passed is the original situation found again. The crystallographic structure can thus be as RSR*S*, and the elementary cell contains a number of ions corresponding to $2(BaFe_{12}O_{19})$. The unit S, then, contains two molecules $MeFe_2O_4$. It would be possible to say that in the M structure the spinel block consists of two more oxygen layers [2.10], but the block then obtained would not contain the metal and oxygen ions in the ration 3 : 4.

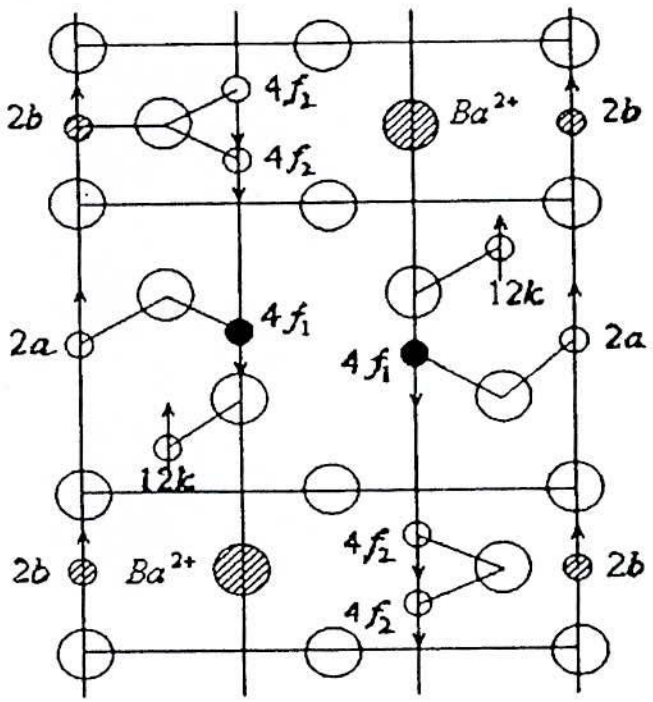

Fig- 2.7: Structure of M-type Ba-hexaferrite

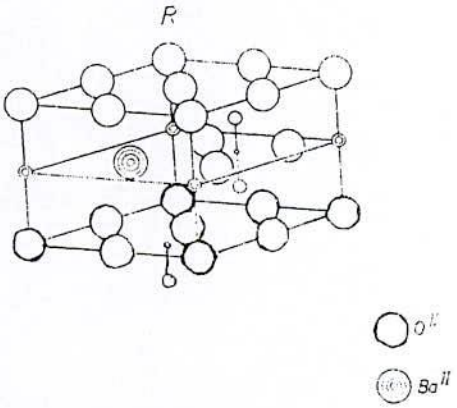

Fig- 2.8: Perspective drawing of the R block occurring in the M

For the ferric ions there are three different kinds of interstitial sites present. Along with octahedral and tetrahedral sites there exists a new type of interstitial site which is not found with spinels and which is surrounded by five oxygen ions constituting a triagonal bipyramid. Theses site occur in the same layer as the barium ion, and they can be compared with tetrahedral sites. In the hexagonal structure two tetrahedral sites are adjacent to each other, and for these two only one metal ion is available. This metal ion now occupies a position halfway between them, amidst the three oxygen ions. According to the ideal parameters the available space is extremely small. This means that the three oxygen ions are certainly displaced outwards, as it is also the case with the more spacious tetrahedral sites in the spinel lattice. In the R block two adjacent octahedral sites are occupied by ferric ions. There are now, however, two ions available, so that in this case there is no abnormal environment.

2.5 Magnetic Ordering

Magnetic ordering in solids has two basic requirements:

i) Individual atoms should have magnetic moments (spins) and

ii) Exchange interactions should exist that couple them together [2.11]

In solids magnetic moments originate as a consequence of overlapping of the electronic wave functions with those of neighboring atoms. Some transition and rare-earths metals satisfy this condition. The exchange interaction is strongly dependent upon the inter-atomic distance and the nature of the chemical bonds, particularly of nearest neighbor atoms. When the positive exchange dominates, which corresponds to parallel coupling of neighboring spins, the magnetic system becomes ferromagnetic below a certain temperature T_c, called the Curie temperature. The common spin directions of the crystal are determined by the minimum magneto-crystalline anisotropy energy. That is why; ferromagnetic substances are characterized by spontaneous magnetization. In the demagnetized state, a ferromagnetic material shows no net magnetization in zero field because in the demagnetized state a ferromagnet of macroscopic size is divided into a number of small regions called domains, spontaneously magnetized to saturation value and the directions of these spontaneous magnetization of the various domains are such that the net magnetization of the specimen is zero. The existence of domains is a consequence of energy minimization. The size and formation of these domains is in a complicated manner dependent on the shape of the specimen as well as its magnetic and thermal history. Whenever, the negative exchange dominates, adjacent atomic moments (spins) align anti-parallel to each other, and the substance is said to be anti-ferromagnetic below a characteristic temperature, T_N, termed as Neel temperature. In the simplest case, the lattice of an antiferromagnet is divided into two sub-lattices with the magnetic moments in anti-parallel alignment. The net magnetization becomes zero. This results a special case of anti-ferromagnetism known as ferrimagnetism.

In ferrimagnetic substances there are two sub-lattices with magnetic moments opposite to each other, but the magnetization of the sub-lattices are of unequal strength resulting in a net magnetization, called spontaneous magnetization. In the macroscopic level the domain structures of ferromagnetic and ferrimagnetic materials are of similar type. The Curie and Neel temperatures characterize a

phase transition between the magnetically ordered and disordered states viz. ferromagnetic to paramagnetic or ferrimagnetic to paramagnetic states. From above simple cases of magnetic ordering, different types of magnetic ordering may exist in metallic substances. Due to long-range ordering and oscillatory nature of the exchange interaction, mediated by the conduction electrons, structures like helical, conical and modulated patterns might occur. Different possible of magnetic ordering are shown in figure 2.9[2.12]

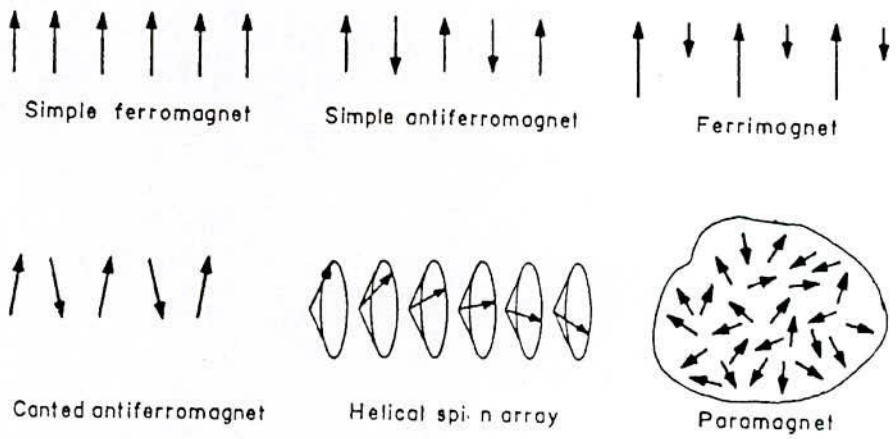

Fig-2.9: Magnetic order using a linear array of localized moments, including paramagnet

2.6 Theory of Ferrimagnetism

Like ferromagnetic materials, ferrimagnetic substances exhibit spontaneous magnetization at room temperature, which led them commercially important and they consist of self-saturated domains, exhibit the phenomena of magnetic saturation and hysteresis. Above a certain critical temperature, T_c called Curie temperature spontaneous magnetization of these substances disappears, and become paramagnetic. Ferrimagnetic materials were not recognized as forming a distinct magnetic class until 1948. In 1948, Neel described the theoretical key to an understanding of ferrimagnetism. Neel describes the properties of those substances, which below a certain temperature exhibit spontaneous magnetization

arising from a non-parallel alignment of atomic magnetic moments. In his work, Neel envisaged a partitioning of the moments into two sub-lattices, which because of their mutual interaction are aligned antiparallel to each other, thus producing a total magnetic moment equal to the difference between their individual magnitudes. Almost all known ferrimagnetic compounds have rather complex structures, to provide a basis for the sub-lattices, with at least two crystallographically inequivalent sites for the magnetic ions. At long-range order, the characteristic temperature generally known as the Neel point, T_N determined largely by the strength of the interaction between nearest neighbors, though under special conditions of symmetry [13].

Figs.2.10 illustrate the different ways of arising ferrimagnetism due to various arrangements of the sub-lattices [14]. Fig 2.10 (a) represents the case in which there are different numbers of similar magnetic moments in the sub-lattices. In some respects this arrangement superficially resembles that of a normal antiferromagnetic substance with unequal partitioning of the sub-lattices, but many of the properties of such a substance are similar to those of a ferromagnet with a reduced number of magnetic moments. Fig-2.10 (b) shows the case of equal numbers of moments having unequal opposite magnitude. This type of dissimilarity may arise if the magnetic ions are chemically different, or a different local environment leads to different effective magnetic moments in ions having the same spin. So far only the first of these two possibilities has been observed. In fig-2.10 (c) a third type of arrangement is shown, which was originally considered by Neel and describes the large number of substances, including most of the ferrites. In this arrangement one sub-lattice contains two different types of magnetic moment, one of which also occurs in equal numbers on the second sub-lattice, so that the net effect is that of just the one type of moment. An extension of the case fig-2.10 (c) may also arise when the second sub-lattice also contains two types of moments, as shown in fig-2.10 (d). An extensive description of Neel's theory has been given by Yafet and Kittel (1952) [15], who pointed out that if

there are strong interactions between the ions within a given sub-lattice, in addition to the interaction between the sub-lattices, a triangular arrangement shown in fig-2.10 (e) will have a lower energy than the uniaxial Neel type arrangements may also occur. Such type of arrangements can be extended to a large number of variants, involving various three-dimensional multi-spin-axis arrangements.

Another type of multi-spin-axis arrangement, which does not seem to have been considered before, might arise when there are strong local anisotropy forces tending to hold each spin in a particular direction relative to the crystal sub-lattice. As per example, the simple case of a cubic crystal in which one sub-lattice consists of three types of moment, each of which is bound by some anisotropy forces to one of the three cube axes and interaction with a second sub-lattice produces a compromise arrangement shown in fig-2.10 (f). Though there is no direct experimental evidence for such type of arrangement, but it seems very likely that some ferrimagnetic rare-earth compounds have this type of arrangement.

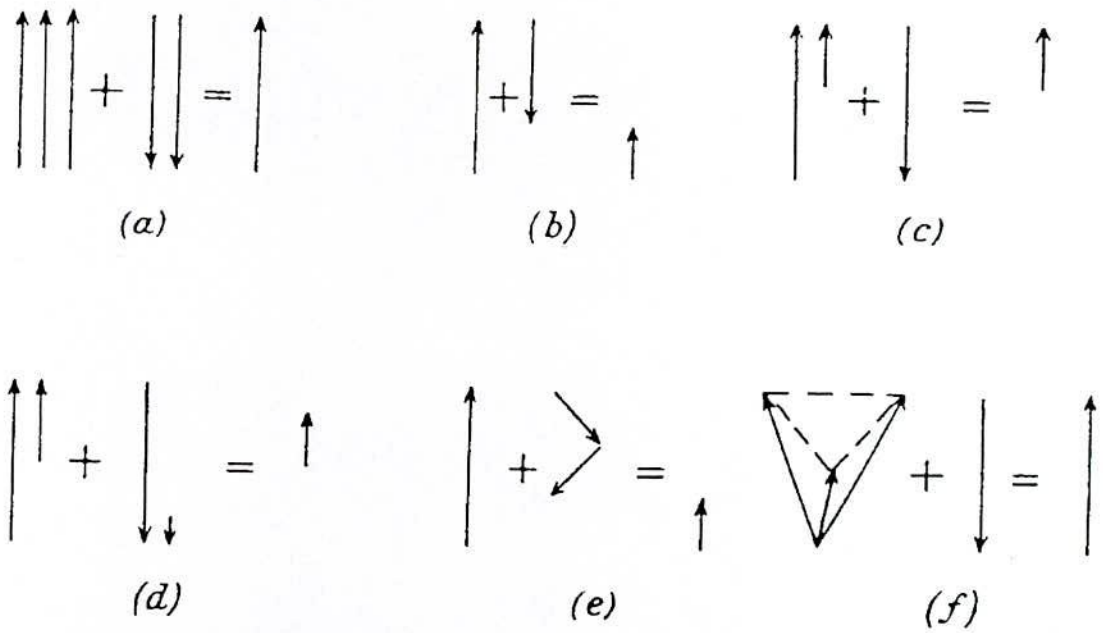

Fig-2.10: Illustrations of six simple sub-lattice arrangements, which can give rise to a spontaneous ferrimagnetic moment.

Crystallographic studies of ferrites have provided the clue that the cations in a crystal occupy two crystallographically different kinds of positions called A- sites and B-sites. Neel made the fundamental assumption that the exchange interaction between these two sites is negative, meaning that the spin orientation is opposite to each other which may also takes place in antiferromagnetic substances. The difference is that, in the case of ferrimagnetism magnitudes of the A and B sub-lattices are not equal which results in a net spontaneous magnetization.

Exchange interaction taking place in ferrites is of different kind. According to Neel, the cations are mutually separated by bigger anions (oxygen ions), which practically exclude a direct contact between the cation orbital, making any direct exchange at least very weak. Instead, we encounter *Supper Exchange* i.e. indirect exchange via oxygen p orbital that may be strong enough to order the magnetic moments. The strength of the exchange interaction depends on the degree of orbital overlap of oxygen p orbital and transition metal d orbital. As the metal ions move apart and the angle between them decreases from 180^0 to 90^0 the strength of interaction decreases. Neel's report, the interaction are taken as effective inter and intra-sublattice interactions A-A, B-B and A-B. The type of magnetic order depending upon the relative strength of the sub-lattices. The theory of super exchange and the semi empirical rules yields some predictions concerning the sign and strength of this interaction [16]. It has been observed that A-A interaction is weaker comparing to B-B interaction. But angle between B-B interaction is 90^0 thus making it weak compared to A-B interaction where angle is 125^0. Thus antiparallel spin alignment takes in two sublattices.

The interaction energy density may be written as

$$U = -2J\,(S_i \cdot S_j) \qquad (2.1)$$

If the exchange integral, J is positive, we will get ferromagnetism. A negative J may give rise to anti-ferromagnetism or ferri-magnetism. The mean exchange field acting on A and B sites may be written as

$$B_A = \lambda M_A - \mu M_B$$

$$B_B = \mu M_A - \nu M_B \qquad (2.2)$$

All constants λ, μ, v are taken to be positive. The minus sign responsible for the anti-parallel interaction. The interaction energy density then becomes

$$U = -\frac{1}{2}(B_A . M_A + B_B . M_B)$$

$$= \frac{1}{2}\lambda M_A^2 + \mu M_A M + \frac{1}{2} V M_B^2 \qquad (2.3)$$

The interaction energy density is lower when M_A is anti-parallel to M_B than when M_A is parallel to M_B. The energy of anti-parallel alignment should be compared with zero, because a possible solution is $M_A = M_B = 0$. Thus when

$$\mu M_A M_B > \tfrac{1}{2}(\lambda M_A^2 + v M_B^2)$$

the ground state will have M_A directed opposite to M_B. Under certain conditions there may be non-collinear spin arrays of still lower energy.

CHAPTER THREE

Specimen Preparation Techniques

3.1.1. Methodology of Ferrite Preparation

In the present research work for the preparation of M-type hexaferrites we are using magnetite as the raw materials, which are abundantly found in the beach sand of Cox's bazar. In Bangladesh, in 1961 during a geological survey for the radioactive minerals from Cox's bazar beach sand potentially valuable heavy minerals like magnetite, hematite, rotile, zircon etc was found. Magnetite has been separated magnetic separator of Beach Sand Minerals Exploitation Centre, Cox's bazar under Bangladesh Atomic Energy Commission (BAEC). An upgradation of the quality of magnetite was performed up to the purity level 97-97.3%. Previously it was difficult to determine the actual concentration of each mineral present in the beach sand. Chemical method has been employed to get the chemical concentration of the minerals. To get the elemental concentration of each constituent element present on the sand methods like PIXE and XRF have been used. But it was difficult to determine the concentration of the minerals in crystalline form or compound, which has three or four constituent elements using the above mentioned methods.

Krishna [3.1] has been demonstrated that X-ray diffraction (XRD) is a versatile non-destructive analytical method for the qualitative identification and quantitative estimation of the various crystalline forms present in powdered or solid samples. The author report that a given substance always produces a characteristic diffraction pattern, whether that substance is present in the pure state or as one constituent of a mixture of substance. This is the basis for the diffraction method of chemical analysis. Qualitative analysis for a particular substance is accomplished by identification of the pattern of that substance. Quantitative analysis is also possible, because the intensities of the diffraction lines due to one constituent of a mixture depend on the proportion of that constituent in the specimen [3.2].

The main advantage lies on the diffraction analysis is that it discloses the presence of a substance, as that substance actually exists in the sample or not in terms of its constituent chemical elements. To know the state of chemical combination of the elements involved or the particular phases in which they are present diffraction analysis of the specimen is very important. The XRD method has been widely used for the analysis of such substances as mineral, ore, clay, soil, alloy, industrial dust etc. Compared with the ordinary chemical analysis, the XRD method has the additional advantages that it is usually much faster, requires only very small amount of sample and non-destructive. The concentration of magnetite along with the impurities present investigated by Saha [3.3] by XRD method is furnished in the table 3.1.

Table 3.1

Concentration of Magnetite of Cox's bazar beach sand along with the impurity level

Minerals	Chemical Formula	Concentration (wt%) range (± 2%)
Magnetite	Fe_3O_4	97.00 - 97.30
Hematite	Fe_2O_3	1.70 – 2.20
Akdalatite	Al_2O_3	0.40 – 0.60
Quartz	SiO_2	0.30 – 0.40

The XRD data shown in table 3.1 indicates that the "magnetite" collected from Cox's Bazar beach sand has a very good purity level. In this connection it may be mentioned that in a previous BAEC Report [3.4] it has been found that the level of magnetite was shown in a different way, i. e., as hematite and iron oxide. In that report hematite has been shown as 73.58% and iron oxide as 22.01%. By using the chemical method the data was extracted. Actually, the magnetite is formed from hematite and iron oxide under certain temperature and pressure conditions. It is again very easy to convert magnetite into hematite and iron oxide in the heating process. During the chemical process, probably

magnetite has been converted into hematite and into iron oxide. For this reason, in the chemical method, hematite and iron oxide was observed. That is why, to find the actual mineralogical concentration of the sand XRD method is much more preferable.

3.2 Method of Preparation

The preparation of hard ferrites with optimum magnetic properties is a complex and difficult job to do. Knowledge and control of the chemical composition, homogeneity and microstructure are very crucial. The preparation of hard ferrites with desired magnetic properties has always demanded delicate handling and cautious approach. As the most of the properties needed for ferrite applications are not intrinsic but extrinsic, preparation of samples has to encounter added complexity. The ferrite is not completely defined by its chemistry and crystal structure but also requires knowledge and control of parameters of its microstructure such as density, lattice parameter, porosity and their intra- and intergranular distribution. It is well known that almost all ferrites decompose at the elevated temperature if we want to melt them under normal conditions. This happens because the oxygen splits off at higher temperature reducing Fe^{3+} to Fe^{2+}. This necessarily implies that ferrite preparation by melting, as in case of metals, is not possible.

Now a days different synthesis techniques are used with various doopants to produce ferrites with enhanced structural, electrical and magnetic properties suitable for magnetic, high-density magneto-optical recording media and microwave applications [3.5-3.6]. There are several processes of preparing M-type hexaferrites such as chemical co-precipitation method [3.7], hydrothermal precipitation-calcination technique [3.8], sol-gel method [3.9], microemulsion synthesis [3.10], glass crystallization method [3.11], sputtering technique [3.12], liquid mix technique/ the organic resin method [3.13], salt-melt technique [3.14], aerosol pyrolysis [3.15] and organometallic precursor

technique [3.16]. Recently a simple route to produce ferrite powders of very small particles and morphology have been widely used known as ball milling by using conventional ceramic method [3.17-3.19]. In the meantime, the researches on improving the structural, physical and magnetic properties have never been stopped [3.20-3.22]. In our present research work conventional ceramic method has been employed for the preparation of Ba-hexaferrite and Sr-hexaferrite for its relative simplicity and availability. The powder preparation process and sintering facility available at the Materials Science Division, Atomic Energy Centre, Dhaka, has been utilized for the preparation of samples.

The compositions employed for preparation of ferrites are given in below:

i) $(SrO)_{1-x}(La_2O_3)_x$ 5.7 Fe_2O_3, where x = 0.00, 0.04, 0.08

ii) SrO 5.7 Fe_2O_3 + [0.7wt% CaO + 0.3wt% SiO_2]

iii) $(BaO)_{1-x}(La_2O_3)_x$ 5.7 Fe_2O_3, where x = 0.00, 0.04, 0.08

iv) BaO 5.7 Fe_2O_3 + [0.7wt% CaO + 0.3wt% SiO_2]

The following table 3.2 shows the compositional details for the preparation of 100 gm of Sr-hexaferrite of chemical formula $(SrO)_{1-x}(La_2O_3)_x$ 5.7 Fe_2O_3, where x = 0.00, 0.04, 0.08.

Table 3.2

Compositional details of $(SrO)_{1-x}(La_2O_3)_x$ 5.7 Fe_2O_3, where x = 0.00, 0.04, 0.08

x	1-x	Weight of SrO gm	Weight of La_2O_3 gm	Weight of Fe_2O_3 gm
0.00	1	10.220	0.00	89.779
0.04	0.96	9.726	1.274	88.999
0.08	0.92	9.241	2.527	88.233

Table 3.3 represents the compositional details for the preparation of 100 gm of Ba-hexaferrite of chemical formula $(BaO)_{1-x}$ $(La_2O_3)_x$ 5.7 Fe_2O_3, where x = 0.00, 0.04, 0.08

Table 3.3

Compositional details of $(BaO)_{1-x}$ $(La_2O_3)_x$ 5.7 Fe_2O_3, where x = 0.00, 0.04, 0.08

x	1-x	Weight of BaO gm	Weight of La_2O_3 gm	Weight of Fe_2O_3 gm
0.00	1	14.416	0.00	85.584
0.04	0.96	13.751	1.217	85.031
0.08	0.92	13.093	2.419	84.487

As SrO, BaO and Fe_2O_3 were not available in our laboratory we have used $SrCO_3$, $BaCO_3$ and Fe_3O_4 magnetite as the raw materials for the preparation of the hexaferrite samples. The compositional details for the preparation of 100 gm of Sr-hexaferrite powders by using $SrCO_3$, and Fe_3O_4 having chemical formula $(SrO)_{1-x}$ $(La_2O_3)_x$ 5.7 Fe_2O_3, where x = 0.00, 0.04, 0.08 are given in the following table 3.4.

Table 3.4

Compositional details of $(SrO)_{1-x}$ $(La_2O_3)_x$ 5.7 Fe_2O_3, where x = 0.00, 0.04, 0.08 by using $SrCO_3$, and Fe_3O_4

x	1-x	Weight of $SrCO_3$ gm	Weight of La_2O_3 gm	Weight of Fe_3O_4 gm
0.00	1	14.559	0.00	88.552
0.04	0.96	13.856	1.274	87.783
0.08	0.92	13.164	2.527	87.027

The compositional details for the preparation of 100 gm of Ba-hexaferrite powders by using $BaCO_3$, and Fe_3O_4 having chemical formula $(BaO)_{1-x}$ $(La_2O_3)_x$ 5.7 Fe_2O_3, where x = 0.00, 0.04, 0.08 are given in the following table 3.5.

Table 3.5

Compositional details of $(BaO)_{1-x}$ $(La_2O_3)_x$ 5.7 Fe_2O_3, where x = 0.00, 0.04, 0.08 by using $BaCO_3$, and Fe_3O_4

x	1-x	Weight of $BaCO_3$ gm	Weight of La_2O_3 gm	Weight of Fe_3O_4 gm
0.00	1	18.553	0.00	84.414
0.04	0.96	17.696	1.217	83.869
0.08	0.92	16.850	2.419	83.332

In addition to the above six compositions we have also prepared hexaferrite samples with the simultaneous addition of CaO and SiO_2. With 100 gm of pure Sr- and Ba-hexaferrite powders 1 gm of (CaO + SiO_2) was added simultaneously.

The following table 3.6 shows the compositional details for the Sr- and Ba-hexaferrite powders with the simultaneous addition of CaO and SiO_2.

Table 3.6

Compositional details of SrO 5.7 Fe_2O_3 + [0.7 wt%CaO + 0.3wt% SiO_2] and BaO 5.7 Fe_2O_3 + [0.7 wt%CaO + 0.3wt% SiO_2] hexaferrite powders

Composition	Weight of $SrCO_3/BaCO_3$ gm	Weight of Fe_3O_4 gm	Amount of (CaO + SiO_2) gm
SrO 5.7 Fe_2O_3 + [0.7 wt%CaO + 0.3wt% SiO_2]	14.559	88.552	1
BaO 5.7 Fe_2O_3 + [0.7 wt%CaO + 0.3wt% SiO_2]	18.553	84.414	1

The following block diagram shown in fig- 3.1 represents the method employed for the M-type Ba- and Sr- hexaferrites:

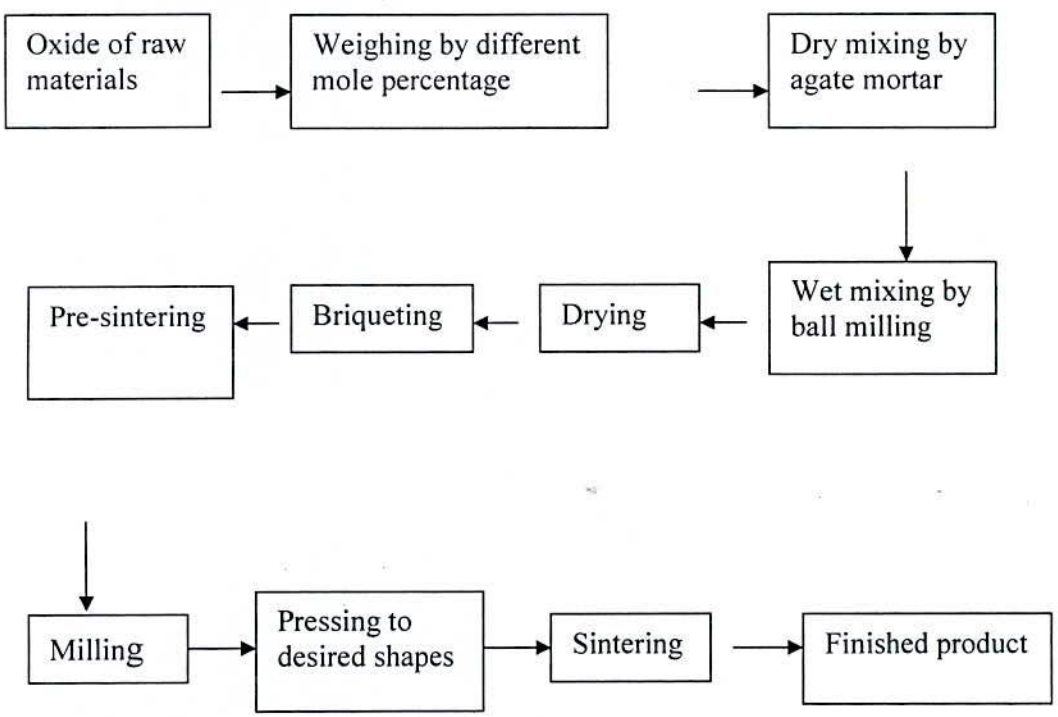

Fig-3.1: Block diagram for the ferrite preparation

The overall preparation process generally comprised of the following four major steps [3.23]:

i) Preparing a homogeneous mixture of the materials with the cations more or less in the ratio corresponding to that in the final product

ii) Prefiring the mixture to form ferrites

iii) Conversion of the raw ferrite into powder and pressing the powder into the desired shapes

iv) Sintering to produce the final ferrite samples

It might have been strictly remembered that the sintering process is irreversible in terms of microstructure so that constant care could be maintained to keep conditions constant prior to and during sintering. A brief discussion given bellow will give us the idea about the above-mentioned four major steps.

3.2.1 Preparing a Homogeneous Mixture of Materials

The extend of this work in this step varies greatly, depending on the starting materials. When component oxides are used, the corresponding step involves a mere mixing of the oxides by wet milling. To avoid iron contamination, mixing is done with stainless steel balls in a steel ball-milling machine and a fluid such as distilled water is used to prepare the mixture into slurry.

The raw materials for the preparation of Sr- and Ba-hexaferrite were oxides of iron, strontium carbonate, barium carbonate and lanthanum oxide. The constituents in required off-stoichiometric proportions as given in table 3.2 and 3.3 were weighed first and then were thoroughly mixed using ceramic mortar and pestle. The resultant powders were then ball milled for $9\frac{1}{2}$ hours using steel ball (in the ratio 1: 6 powder to ball) in distilled water to produce a homogeneous mixture of the constituents and to reduce the particle size as well.

3.2.2 Presintering the Mixtures to form Ferrite

The slurry prepared in step 1 is dried, palletized and then transferred to a porcelin crucible for presintering in a constant temperature of 1200°C for 4 hours. Presintering of the materials were performed in a furnace named Gallen Camp at AECD. As far as the final composition of the ferrite is concerned step-2 is most crucial because subsequent steps would not change the composition substantially. For this reason, it is important to understand how a ferrite is formed from its component oxides.

The mechanism just described for the formation of ferrites justifies the separate presintering and sintering steps taken in the preparation procedures. The raw ferrite thus formed in step 2 has poor qualities. In order to produce chemically homogeneous and magnetically better material the presintered lump material was crushed. The mixtures were then milled thoroughly using ceramic mortar and pestle for 3-4 hours to obtain homogenous mixture. It is to be mentioned that the particle size can be reduced to 1-5 micron by normal ball milling.

3.2.3 Converting the Raw Ferrite into Powder and Pressing the Powder

To promote successful sintering in the next step, the powder must be well characterized after grinding with respect to such factors as particles size and distribution, particle shape, homogeneity, absorbed gases, impurities and intraparticle porosity. Iron contamination due to continuous wear of the mill wall and still ball need to be closely watched and minimized. Now to the ground homogeneous powder polyvinyl alcohol is added as a binder. Pressing the powder into compacts of desired shapes is done either by conventional method in a die-punch assembly or by hydrostatic or isostatic compaction.

By conventional method in a die-punch assembly a uniformly dense body is difficult owing to the friction gradient of the powder at the walls of the die and between the particles themselves. This problems is somewhat overcome by the

addition of external and internal lubricant to the powder such as stearic acid. Mainly, we made two types of samples- cylindrical and toroidal. Specimen was prepared by a hydraulic press with a pressure of 60 bar. The die was designed and made in the workshop of AECD. This is made of nonmagnetic stainless steel.

3.2.4 Sintering

Sintering commonly refers to processes involved in the heat treatment of powder compacts at elevated temperatures where diffusional mass transport is appreciable. Sintering is traditionally used for manufacturing ceramic objects, and has also found uses in such fields as powder metallurgy. Successful sintering usually results in a dense polycrystalline solid. However, sintering can proceed only locally (i.e. at contact point of grains), without any appreciable change in the average overall density of a powder compact.

Ceramic processing is based on the sintering of powder compacts rather than melting/solidification/cold working (characteristic for metals), because:

i) Ceramics melt at high temperatures
ii) As-solidified microstructures cannot be modified through additional plastic deformation and recrystallisation due to brittleness of ceramics
iii) The resulting coarse grains would act as fracture initiation sites
iv) Low thermal conductivities of ceramics (<30-50 W/mK), in contrast to high thermal conductivity of metals (in the range 50-300 W/mK) cause large temperature gradients, and thus thermal stress and shock in melting-solidification of ceramics.

3.3 Why do we need Sintering?

The principal goal of sintering is the reduction of compact porosity. Sometimes the initial spaces between compacted grains of ceramics are called

"voids", to differentiate them from the isolated spaces = pores, which occur in the final stages of sintering. The sintering process is usually accompanied by other changes within the material, some desirable and some undesirable. The largest changes occur in:

i) To bind the particles together so as to impart sufficient strength to the products
ii) To densify the green compacts by eliminating the pores and
iii) To homogenize the materials by completing the reactions left unfinished in the presintering step [3.24]
iv) To make strength of elastic modulus
v) To make hardness and fracture toughness
vi) To make homogenous distribution of grain number, grain size and shape
vii) To improve the average pore size and shape
viii) To get a stable chemical composition and crystal structure

Sintering is a widely used but very complex phenomenon. The fundamental mechanisms of sintering are still a matter of controversy. Experimental quantification of changes in pore fraction and geometry during sintering can be attempted by several techniques, such as: dilatometry, buoyancy, gas absorption, porosimetry, indirect methods (e.g. hardness) and quantitative microscopy etc.

The description of the sintering process has been derived from model experiments (e.g., sintering of a few spheres) and by observing powdered compact behavior at elevated temperatures. The following phenomena were observed:

i) Increase of inter-particle contact area with time
ii) Rounding-off of sharp angles and points of contact

iii) In most cases, the approach of particle centres and overall densification

iv) Decrease in volume of interconnected pores

v) Continuing isolation of pores

vi) Grain growth and decrease in volume of isolated pores

Since certain mechanisms of mass transport can be dominant in some systems, two broad categories of sintering are recognized: Solid-state sintering where all densification is achieved through changes in particle shape, without particle rearrangement or the presence of liquid. And liquid-phase sintering, where some liquid that is present at sintering temperatures aids compaction. Grain rearrangement occurs in the initial stage followed by a solution-reprecipitation stage. Usually, the liquid amount is not sufficient to fill the green-state porosity in normal liquid-assisted sintering of ceramics. In many instances, supposedly Solid State Sintering proceeds in the presence of previously undetected (or transient) small amounts of liquid (perhaps introduced as impurities during the powder preparation stage, such as silicates in oxide ceramics Al_2O_3, ZrO_2).

During sintering, if the only material transport mechanism originates on the surface of particles, no compact shrinkage takes place. In such a case a change of the shape and size of pores and particles is observed and commonly defined as grain growth or coarsening. Grain growth/coarsening depletes the system of surface energy and effectively STOPS the densification of the compact, even if mass transport mechanisms other than evaporation/condensation or surface diffusion become operational. At best, the coarsening process decreases the driving force for sintering and therefore the sintering rate, expressed as shrinkage versus time, decreases in the intermediate stage. Densification in the intermediate stage takes place only if: mass is transported from the particle volume or, mass is transported from the grain boundary and Proceeds through

the solid as volume diffusion or along a boundary as grain boundary diffusion towards the neck forming between the sintering particles.

The origin of mass transport during sintering determines the ability of the compact to shrink and eliminate porosity. There are systems where sintering proceeds vigorously through evaporation/condensation or through surface diffusion, without any shrinkage of the compact. In most cases this is an undesirable phenomenon, whenever residual porosity is undesirable. In some systems (e.g. recrystallised SiC) this technique of bonding ceramic particles is acceptable.

A remarkable feature of most of these equations is that, using curve-fitting procedures, a nearly perfect fit can be obtained with experimental data on sintering. However, little or no insight into sintering mechanisms is obtained and incorrect conclusions are drawn when physical meanings are attributed to the fitted constants. This is because real systems deviate significantly from idealized models: particles are irregular in size and shape, particles are non-uniformly distributed in space and rearrange during sintering, necks grow asymmetrically and different sintering stages (neck formation, neck growth, rearrangement, grain growth with or without shrinkage, closed porosity sintering) are controlled by different mechanisms, which interact and overlap in a complex way.

The formation of necks is also a key process leading to the shrinkage of pores. Precisely how pores disappear during sintering has long been a subject of intensive investigation. The theory has been changed from the traditional, but now obsolete, theory based on the reduction of surface energy as the driving force for eliminating the pores, through the microcreep diffusion theory of Naborro and Herring to the current theory of Kuczynski [3.25]. On the basis of

volume diffusion induced under surface tension, an important equation for the initial stage of the sintering process is given by

$$\Delta L/L = [(AD^* \gamma\Omega/\bar{r}^{-3} kT)t]^{-\frac{1}{2}} \quad , \qquad (3.1)$$

where $\Delta L/L$ is the shrinkage of the compact, Ω the volume of a single vacancy, D^* the coefficient of self-diffusion for the slowest moving species, γ the surface energy, $\bar{r}$ the average radius of the particles, t the sintering time and A is a constant, of the approximate value of unity.

The above equation indicates that sintering fulfills the first two requirements more efficiently when the compact features high surface energy and self diffusivity and the particles are fine. For densification, Burke [3.26] made two important observations. One is that the formation of necks only marks the initial stage of sintering; an intermediate stage beings when grain growth occurs with the compact density at around 60% of the theoretical value and ends when the pore phase becomes discontinuous and the density reaches a value of $\approx$ 95%. Another observation of Burke deals with the final stage of sintering. If discontinuous grain growth occurs after the intermediate stage, migration of grain boundaries will leave the remaining isolated pores trapped inside the grains, thus preventing further shrinkage of these intra particle pores and practically stopping the sintering process.

In this operation, the cooling rate plays an important role on which the structural modification is mainly based. Sintering of crystalline solids follows the following empirical relationship regarding rate of grain growth [3.27]

$$\bar{d} = kt^n \, , \qquad (3.2)$$

where $\bar{d}$ is the mean grain diameter, t is sintering time, n is about $\frac{1}{3}$ and k is a temperature dependent parameter.

Presintered samples were hand milled for about three hours to make the mixture homogeneous. The powder materials were again wet milled in steel ball extensively for 6 hours to get fine ferrite powder with acetone. The powder was then dried and mixing with polyvinyl alcohol pressed into pressed into desired shapes using metal dies. Different shapes of dies were used for the finished products. The finished products were sintered at constant temperatures of 1210, 1225, 1235, 1245 and 1260^0C in air for 2 hours.

CHAPTER FOUR

Experimental Details

4.1 Density of Hexaferrites

The density, ρ of the samples are measured by using the following mathematical relation

$$\rho = \frac{m}{V} \text{ g/cc} \qquad (4.1)$$

where

ρ is the density of the substance, measured in g/cc

m is the mass of the substance, measured in g

V is the volume of the substance, measured in cm^3

Mass is the property of a physical object that quantifies the amount of matter and energy it is equivalent. Mass is a central concept of classical mechanics and related subjects, and there are several forms of mass within the framework of relativistic kinematics. The volume of a solid object is the three-dimension vaginaal concept of how much space it occupies, often quantified numerically. Volumes of straight-edged and circular shapes are calculated using arithmetic formulas. Volumes of other curved shapes are calculated using integral calculus, by approximating the given body with a large amount of small cubes or concentric cylindrical shells, and adding the individual volumes of those shapes. The generalization of volume to arbitrarily many dimensions is called content . In differential geometry, volume is expressed by means of the volume form.

4.2 Porosity Measurement

Porosity, P of the samples prepared by standard ceramic method in percentage were calculated using the following equation [4.1]:

$$P = (1 - \frac{\rho}{\rho_X}) \times 100\% \qquad (4.2)$$

where ρ is the density of the samples and ρ_x is the X-ray density calculated by the following method

$$\rho_X = \frac{Weight\ of\ atoms\ in\ unit\ cell}{Volume\ of\ unit\ cell} = \frac{\sum A}{NV} \quad (4.3)$$

where ΣA represents the sum of the atomic weights of the atoms in the unit cell

N is the Avogadro's number

V is the volume of unit cell given by the following formula

$$V = \frac{\sqrt{3}\, a^2 c}{2} \quad (4.4)$$

where a and c are the lattice parameters of the hexagonal ferrites.

In our present case of hexagonal ferrite each unit cell contains two atoms. Inserting the value of Avogadro's number we get the formula for the X-ray density as follows

$$\rho_X = \frac{1.66020 \times 2 \sum A}{V} \quad (4.5)$$

4.3 Lattice Parameter Calculation from XRD Data

X-ray diffraction technique is widely used in order to investigate the various properties of matter and it is also a unique powerful method for the structural analysis of the matter. The crystal structure of a substance produces the diffraction pattern (of X-rays): the shape and size of the unit cell are determined from the angular positions of the diffraction peaks (lines), and the arrangements of the atoms within the unit cell are determined from the relative intensities of the lines. The lattice parameters of the unit cell are deduced from the angular position of the diffraction lines. To indexing the pattern, the lattice parameters are want to be calculable from the position and the Miller indices of the diffraction lines by using the Bragg's law of X-ray diffraction. In work of the highest precision, a small correction for refraction is sometimes applied. The index of refraction for X-rays in matter differs very slightly from unity, so that an X-ray has slightly different

wavelengths in air and in a crystal. The correction to a lattice parameter is less than $1x10^{-6}$Å.

The lattice parameter a and c are calculated from the value of d_{hkl} corresponding to the different peaks of the neighboring planes according to the following equation

$$d_{hkl} = \left(\frac{4}{3} \frac{h^2 + hk + k^2}{a^2} + \frac{l^2}{c^2} \right)^{-\frac{1}{2}} \qquad (4.6)$$

where $\mathbf{d}_{hkl}$ is the spacing between the neighboring planes of a unit cell of the hexagonal ferrites calculated from Bragg's X-ray diffraction formula, (hkl) representing the indices of the different reflection planes and a and c are the lattice parameters of the corresponding hexaferrites [4.2].

4.4 X-Ray Diffraction (XRD) Technique

X-rays are the electromagnetic waves whose wavelengths are in the neighborhood of 1 Å. The wavelength of an X-ray is thus of the same order of magnitude as the lattice constant of crystals, and it is this which makes X-rays so useful in structural analysis of crystals.

X-rays are produced in a device called an X-ray tube. When the target material of the X-ray tube is bombarded with electrons accelerated from the cathode filament, two types of X-ray spectra are produced. The first is called the continuous spectra. The continuous spectra consist of a range of wavelengths of X-rays with minimum wavelength and intensity (measured in counts per second) dependent on the target material and the voltage across the X-ray tube. The minimum wavelength decreases and the intensity increases as voltage increases. The second type of spectra, called the characteristic spectra, is produced at high voltage as a result of specific electronic transitions that take place within individual atoms of the target material. Figs- 4.1 and 4.2 show the continuous and the characteristic spectra of X-rays.

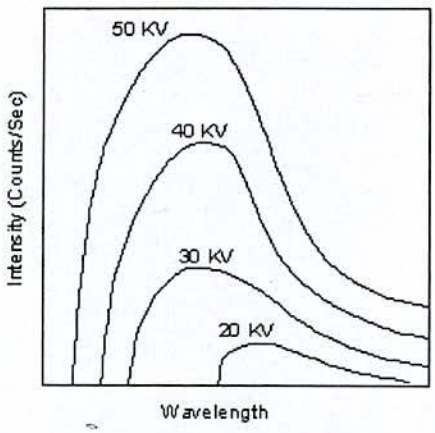

Fig-4.1: Continuous X-ray spectra

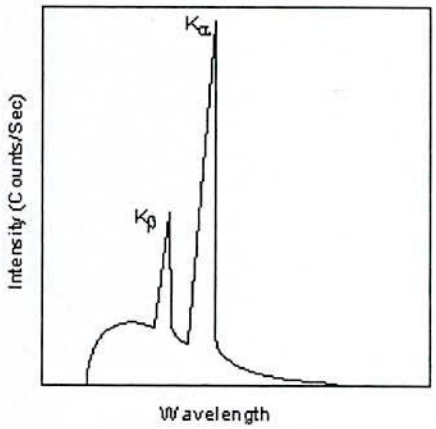

Fig-4.2: Characteristic X-ray spectra

For commonly used target materials in X-ray tubes, the X-rays have the following well-known experimentally determined wavelengths as shown in table 4.1

Table 4.1

X-ray wavelengths of different target materials

Element	Wavelength (λ)Å
Mo	0.711
Cu	1.542
Co	1.790
Fe	1.937
Cr	2.291

The Bragg formulation of X-ray diffraction also referred to as Bragg diffraction shows that crystalline solids produced surprising patterns of reflected X-rays (in contrast to that of, say, a liquid). They found that in these crystals, for certain specific wavelengths and incident angles, intense peaks of reflected radiation (known as *Bragg peaks*) were produced. The concept of Bragg diffraction applies equally to neutron diffraction and electron diffraction processes. W. L. Bragg explained this result by modeling the crystal as a set of discrete parallel planes

separated by a constant parameter *d*. It was proposed that the incident X-ray radiation would produce a Bragg peak if their reflections off the various planes interfered constructively.

Bragg expressed this in an equation now known as Bragg's Law:

$$2d\sin\theta = n\lambda \qquad (4.7)$$

where d is the spacing between crystal planes, θ is the angle between the incident rays and the surface of the crystal and n is positive integer.

Bragg's diffraction method also suggests that the diffraction is only possible when $\lambda < 2d$ [4.3]. X-ray diffraction (XRD) is a versatile non-destructive analytical technique for identification and quantitative determination of various crystalline phases of powder or solid samples of any compound. A PHILIPS X Pert PRO X-ray diffraction system was used to get X-ray data for the samples at the Materials Science Division, Atomic Energy Center, Dhaka, which is a sophisticated X-ray diffractometer installed very recently, shown in fig-4.3.

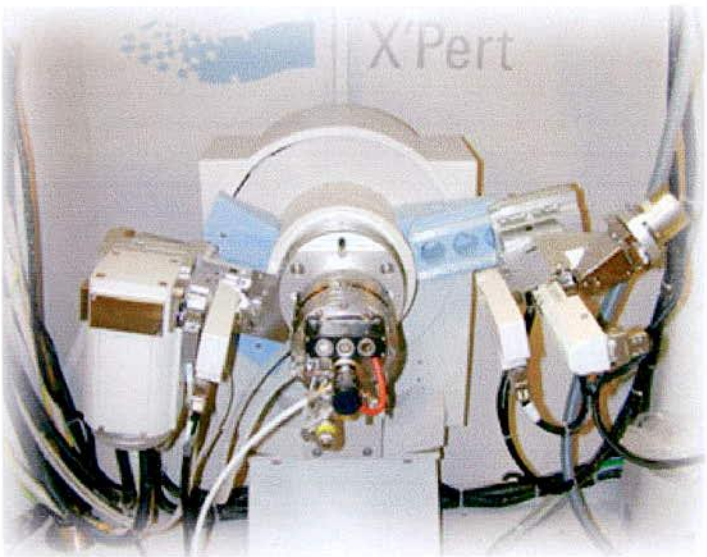

Fig-4.3: Internal arrangement of a PHILIPS X' Pert PRO X-ray diffractometer

4.4.1. Different Parts of the PHILIPS X' Pert PRO XRD System

A complex of instruments for X-ray diffraction analysis has been established for both materials research and specimen characterization. These include facilities for studying single-crystal defects, and a variety of other materials problems. A PHILLIPS X'Pert PRO X-ray diffractometer was used for the lattice parameter determination in the Materials Science Division, Atomic Energy Center, Dhaka. The PHILIPS X' Pert PRO XRD system comprised of the following parts

i) "Cu-Tube" with maximum input power of 60 kv and 55mA
ii) "Ni-Filter" to remove Cu-K_α component
iii) "Solar Slit" to pass parallel beams only
iv) "Programmable Divergent Slit" (PDS) to reduce divergence of beam and control irradiated beam area
v) "Mask" to get desired beam area
vi) "Sample holder" for powder sample
vii) "Anti Scatter Slit" (ASS) to reduce air scattering background
viii) "Programmable Receiving Slit" (PRS) to control the diffracted beam intensity and
ix) "Solar Slit" to stop scattered beam and pass parallel diffracted beam only

4.4.2. Measurement System of the PHILIPS X' Pert PRO XRD System

A new state-of-the-art modular "X'pert" XRD system from Philips has multi modular primary and secondary optics in order to account for the various requirements of primary X-ray beam divergence and detector angular acceptance. A Cu source with possibilities of line or point focus is used. In the high-resolution mode, a 12 arc-sec angular divergence of the primary beam can be achieved by using a four-crystal Ge monochromator, allowing for the investigation of thin films and multilayered systems with high crystalline quality. A Guttman mirror is also available in the primary optics increasing the efficiency of primary beam, making it ideal for the investigation of diffuse scattering arising from defects in

thin films. In addition, a three-bounce analyzer crystal can be placed between the sample and the detector in order to limit the detector acceptance to ~ 12 arc-sec. This configuration is ideal composition and lattice parameter variations within 10-5 can be determined. The system is also well suited for reflectivity measurements by probing diffraction intensities at glancing angles of incidence in order to quantify thin film thickness and interface abruptness.

The following fig- 4.4 demonstrates the block diagram of the X' Pert PRO XRD System. The powder diffraction technique was used with a primary beam power of 40kV and 30 mA for Cu-K_α radiation. A nickel filter was used to reduce Cu-K_β radiation and finally Cu-K_α radiation was only used as the primary beam.

The experiment has been performed at room temperature. A 2θ scan was taken from 20^0 to 80^0 to get all possible fundamental peaks of the sample with the sampling pitch of 0.02^0 and time for each step date collection was 1.0 sec. Both the programmable divergence and receiving slits were used to control the irradiated beam area and output intensity from the sample, respectively. An anti scatter slit was used just after the sample holder to reduce air scattering. Two solar slits were used just after the tube and in front of the detector to get parallel beam only. All the data of the samples were stored in the computer memory and later on analyzed them using computer "Software "X' PERT HIGHSCORE". For XRD experiment each sample was set on a glass slide and fixed the sample by putting adhesive type at the two ends of the sample.

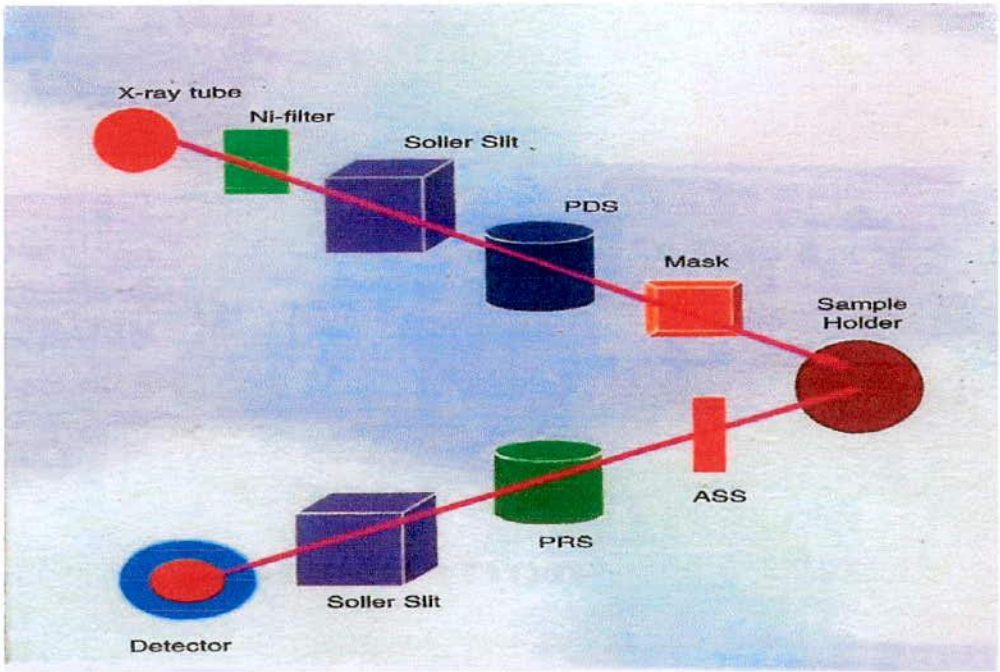

Fig-4.4: Block diagram of the PHILIPS X' Pert PRO XRD

4.4.3 Analysis of X-Ray Diffraction Data

The XRD data consisting of 2θ and d_{hkl} values corresponding to the different crystallographic planes are used to determine the crystallographic parameters of the samples viz., lattice parameter. Lattice parameters of Sr- and Ba-hexaferrites were determined by using the equation (4.6) for different neighboring reflection planes. Using these reflections the lattice spacing (inter planer spacing), d was calculated from the Bragg's diffraction equation.

4.5 Microstructure Study

Magnetic properties of the hexaferrite samples are strongly dependent upon the sensitive control of the microstructure. Permeability is directly proportional to the grain size of the samples. At least up to a critical diameter of the grains causes the permeability to increase monotonically. Resistivity and density of the ferrite

samples are also dependent on the porosity of the samples. Resistivity of the samples increases with the trapped intra-granular pores. Hence the microstructural studies of the samples are required for making prediction about the result of permeability and resistivity of the ferrite samples. For microstructure study the ferrite samples were polished step by step. Primarily the samples were polished by using Metaserv Universal Polisher, Model No. C 200/5V, Volts 240, Amp. 0.75. Secondly, using another polishing machine 99 Phoenix Ave, Enfield, CT06082 USA, Model No. LABPOL 8/12, keeping a speed of 300-450 rev/sec for about 1 hour using different grades of Al_2O_3 fine powders mixing with water. In the tertiary stage the polished samples were cleaned ultrasonically for $\frac{1}{2}$ hour using an ultrasonic cleaner FRITSCH @ Laboratte, Model: 17.202, No. 1030. After the fine polishing and ultrasonic cleaning the samples were etched thermally under suitable temperature for the different samples down below 150 to 100°C of the sintering temperature for 2 minutes in air for every sample. As the thermal etching was finished the samples were ready for the microstructure study. The microstructure measurement of the samples were done by using a Scanning Electron Microscope (SEM), Model No. S-3400 N, Hitachi installed at Industrial Physics Division, Bangladesh Council for Scientific and Industrial Research (BCSIR), Dhaka, Bangladesh.

4.5.1 The Scanning Electron Microscope (SEM)

Scanning electron microscopy (SEM) or electron probe microanalysis (EPMA) are generally considered micro-analytical techniques which are able to *image* or *analyze* materials we can not generally observe with the resolution offered by visible techniques. By *image* we mean photograph of an object much smaller than we can see, even with the aid of an optical microscope. The SEM has a unique capability of giving view of a flea the same perspective as the Chevy driveway. By *analyze* we mean identify the elements (e.g., silicon, iron, etc) of which the specimen is composed. Elemental analysis can also be accomplished at a micro-

scale; for example, EPMA can probe a specimen as small as 5 thousands of a millimeter (5 microns), and not only identify the elements present but measure them with a small degree of error. These instruments represent two if the greatest advances in scientific instrumentation; however they do have their limits. For example, not all specimens can be exposed to the high vacuum within the specimen chamber. Also, elements lighter than atomic number 8 (oxygen) can not be measured without reservations, and EPMA is not sensitive to many elements below 100ppm. Still, this instrumentation has proved invaluable, especially for mineralogists and petrologists, and a good operator can vary one parameter or another to circumvent instrumental weaknesses.

These instruments belong to a broad category of particle beam instruments. In this case we bombard materials with electrons which have high energies because they have mass and because they have been accelerated with thousands of volts. SEM has been historically used as cameras and microanalyzers for elemental analysis, modern electron probes offer both capabilities while optimizing for one or the other. For example, SEM can quantify X-rays with its *energy dispersive x-ray detector* (EDX), but it is designed for ease of use and for a variety of specimens. Scanning electron microscopes have been generally used as cameras, that is, for photographing specimens beyond the capabilities of ordinary optical microscopes. While the images obtained appear very real and as if they were photographed by ordinary means, the apparent illumination is a function of particle emission rather than radiation we're familiar with. These particles emitted are termed *secondary electrons*, and their detection via a SE detector is displayed on a scanning TV display. A bright image will be the result of high secondary electron emission, while the primary influence on high emission is the surface structure of the specimen. The end result is therefore brightness associated with surface characteristics and an image which looks very much like a normally illuminated subject.

The usefulness of quantifying elemental compositions is invaluable in the sciences of mineralogy, petrology and materials research. Students and investigators can measure the composition of several mineral phases which are, apparently or assumed, in equilibrium with each other. This information can be used to estimate the temperature and pressure at the time of crystallization. It is also able to measure the composition of a rock-forming mineral relative to its growth history; for example, its core and rim compositions.. Material science applications are even more varied, from thin film semi-conductors to photonics materials to super conductors. In the case of thin-films, by measuring various X-ray intensities at a number of different accelerating voltages, both the composition and thickness of various films deposited on a substrate may be determined with excellent accuracy. Single crystal grown for various purposes can have their formula stoichiometry measured and compared with X-ray diffraction data. The following figure 4.5 show the pictorial diagram of SEM Model No. S-3700 N by Hitachi, Japan.

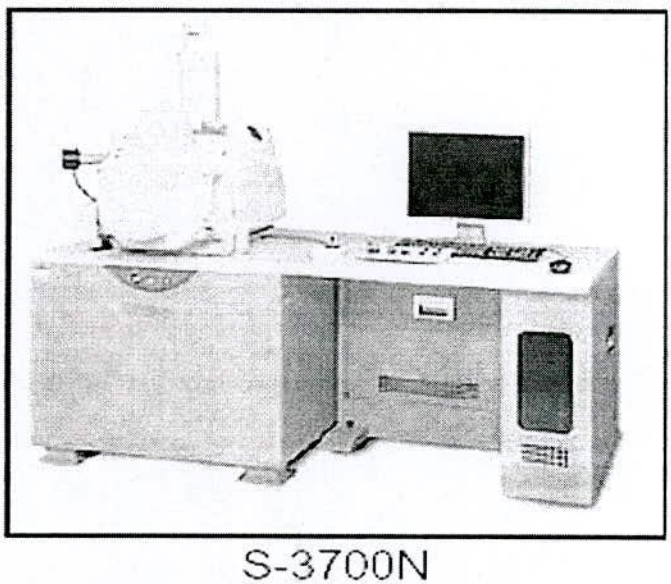

Fig-4.5 Scanning Electron Microscope

4.6 Curie Temperature Measurement

Curie temperature measurement is one of the most important measurements regarding magnetism. Curie temperature provides substantial information on magnetic status of substance in respect of the strength of exchange interaction. So, the determination of Curie temperature accurately is of great importance. The temperature dependence properties of ferrite materials depend upon its sublattice distribution and spin orientations of the metal ions and we can predict about the sublattice magnetization by measuring the Curie temperature. Hence the determination of Curie temperature accurately is of great importance.

There are several processes of measuring the Curie temperature;

i) By measuring susceptibility against temperature

ii) By measuring variation of initial permeability with temperature

iii) By observing the temperature dependence of magnetization

iv) By measuring the variation of resistivity of the samples with temperature

In our present research work, we measured the Curie temperature of the samples by observing the variation of real part of the initial complex permeability of the hexaferrites with temperature.

4.6.1 Measurement of Curie Temperature by Observing the Variation of Initial Permeability with Temperature

For ferrimagnetic materials in particular, for ferrite it is customary to determine the Curie temperature by measuring the permeability as a function of temperature. According to Hopkinson effect [4.4] which arises mainly from the intrinsic anisotropy of the material has been utilized to determine the Curie temperature of the samples. According to this phenomenon, the permeability increases gradually with temperature and reaching to a maximum value just before the Curie temperature. At Curie temperature, the value of permeability falls sharply with temperature. Therefore Curie temperature was determined as that temperature

where the first derivative of the permeability with respect to temperature ($\frac{d\mu}{dT}$) attains its maximum. In other words, where the rate of change of permeability with respect to temperature is maximum.

The initial permeability of the prepared samples was performed by using WAYNE KERR IDUCTANCE ANALYZER 3255B, a small oven and a thermocouple-based thermometer. We made use of the excellent experimental facilities available at Materials Science Division, AECD. The temperature dependent permeability was measured by using induction method. The specimen formed the core of the coil. We used a 100 kHz AC signal of 100 mV. By varying temperature, inductance of the coil as a function of temperature was measured. Dividing this value by L_0 (inductance of the coil without core material), we got the permeability of the core i.e. the sample. When the magnetic state inside the ferrite sample changes from ferromagnetic to paramagnetic, the permeability falls sharply. From this sharp fall at specific temperature the Curie temperature is determined. This is the basic principle used in our experimental set up.

The real part of permeability was measured by using impedance analyzer. The permeability μ' is calculated by using the following formula

$$\mu' = \frac{L_s}{L_0} \qquad (4.8)$$

where L_s is the self inductance of the sample core and

$$L_0 = \frac{\mu_0 N^2 s}{\bar{d}} \qquad (4.9)$$

where L_0 is the inductance of the winding coil without the sample core and N is the number of turns of coil (here N=5), s is the area of cross section as given below and N is the number of turns of coil (here N=5), s is the area of cross section as given below s=dh, where, $d=(d_1 \sim d_2)/2$, h=height

and $\bar{d}$ is the mean diameter of the sample given as follows: $\bar{d} = \frac{d_1 + d_2}{2}$

The number of turns in each coil is 5. The sample thus wound is kept in a little oven with a thermocouple placed at the middle. The thermocouple measures the temperature inside oven and also of the sample. The sample is kept just in the middle part of the cylindrical oven so that gradient is minimized. The temperature of the oven is raised slowly. If the heating rate is very fast then temperature of the sample may not follow the temperature inside the oven and there can be misleading information on the temperature of the samples. The thermocouple showing the temperature in that case will be erroneous. Due to the closed winding of wires the sample may not receive the heat at once. So, a slow heating rate can eliminate this problem. Also a slow heating ensures accuracy in the determination of Curie temperature. The oven was kept thermally insulated from the surroundings. Actually Curie temperature was measured from the temperature dependence of initial permeability. The temperature was measured with a digital thermometer attached close to the sample and put inside the furnace where the temperature fluctuation is almost negligible. Then the permeability versus temperature curve was plotted from which the Curie temperature was calculated.

4.7 Measurement of Permeability

For high frequency application, the desirable property of a ferrite is the high permeability with low loss. The present goal of most of the recent ferrite researches is to fulfill this requirement. Before going into the complexity of permeability measurement, we take a detour through the theories and mechanisms involved in permeability.

4.7.1 Theory of Permeability

Permeability is namely defined as the proportional constant between the magnetic field induction B and applied intensity H:

$$B=\mu H \qquad (4.10)$$

This naïve definition needs further sophistications. If a magnetic material is subjected to an AC magnetic field as given bellow:

$$H = H_0 e^{i\omega t} \tag{4.11}$$

then it is observed that the magnetic flux density B experiences a delay. The delay is caused due to presence of various losses and is thus expressed as

$$B = B_0 e^{i(\omega t - \delta)} \tag{4.12}$$

where δ is the phase angle and marks the delay of B with respect to H. The permeability is then given by

$$\mu = \frac{B}{H} = \frac{B_0 e^{i(\omega t - \delta)}}{H_0 e^{i\omega t}}$$

$$= \frac{B_0 e^{-i\delta}}{H_0}$$

$$= \mu' - i\mu'' \tag{4.13}$$

$$\text{where } \mu' = \frac{B_0}{H_0}\cos\delta,\ \mu'' = \frac{B_0}{H_0}\sin\delta \tag{4.14}$$

The real part μ' of complex permeability μ as expressed in equation (4.12) represents the component of B, which is in phase with H, so it corresponds to the normal permeability. If there are no losses, we should have $\mu = \mu'$. The imaginary part μ'' corresponds to that part of B, which is delayed by phase angle 90^0 from H. The presence of such a component requires a supply of energy to maintain the alternating magnetization, regardless of the origin of delay.

The ratio of μ'' to μ', as is evident from equation (4.12) gives

$$\frac{\mu''}{\mu'} = \frac{(B_0/H_0)\sin\delta}{(B_0/H_0)\cos\delta} = \tan\delta \tag{4.15}$$

This tanδ is called the Loss Factor or Loss tangent. The Q-factor or quality factor is defined as the reciprocal of this loss factor, i.e.

$$Q = \frac{1}{\tan\delta} \tag{4.16}$$

4.7.2 Mechanisms of Permeability

Mechanisms of permeability can be explained as the following way: a demagnetized magnetic material is divided into number of Weiss domains separated by block walls. In each domain all the magnetic moments are oriented in

parallel and the magnetization has its saturation value M_s. In the walls the magnetization direction changes gradually from the direction of magnetization in one domain to that in the next. The equilibrium positions of the walls result from the interactions with the magnetization in neighboring domains and from the influence of pores; crystal boundaries and chemical inhomogeneities which tend to favor certain wall positions.

4.7.3 Techniques of Measurements of Permeability

Measurements of permeability normally involve the measurements of the change in self-inductance of a coil in presence of the magnetic core. The behavior of a self-inductance can now be described as follows. Suppose we have an ideal lossless air coil of inductance L_0. On insertion of magnetic core with permeability μ, the inductance will be μL_0. The complex impedance Z of this coil can be expressed as

$$Z = R + jX = j\omega L_0\mu = j\omega L_0(\mu' - j\mu'') \qquad (4.17)$$

where the resistive part is

$$R = \omega L_0\mu' \qquad (4.18)$$

and the reactive part is

$$X = \omega L_0\mu' \qquad (4.19)$$

The radio frequency (RF) permeability can be derived from the complex impedance of a coil Z (equation 4.17). The core is usually toroidal to avoid demagnetizating effects. The quantity L_0 is derived geometrically.

4.7.4 Frequency Characteristics of Ferrite Samples

The frequency characteristics of the hexaferrite samples i.e. the permeability spectra were investigated using a Hewlett Packard Impedance Analyzer of model No. 4192A. The measurements of inductances were taken in the frequency range of 1 kHz to 13MHz. The values of measured parameters obtained as a function of

frequency and the real and imaginary part of permeability and the loss factor are calculated. μ′ is calculated by using the following formula

$$\mu' = \frac{L_s}{L_0} \tag{4.20}$$

$$\text{and } \tan\delta = \frac{\mu''}{\mu'} \tag{4.21}$$

Where L_s is the self-inductance of the sample core

$$\text{and } L_0 = \frac{\mu_0 N^2 s}{\bar{d}} \tag{4.22}$$

where L_0 is the inductance of the winding coil without the sample core and N is the number of turns of coil (here N=5), s is the area of cross section as given below and N is the number of turns of coil (here N=5), s is the area of cross section as given below s=dh, where, $d=(d_1 \sim d_2)/2$, h=height

and $\bar{d}$ is the mean diameter of the sample given as follows: $\bar{d} = \frac{d_1 + d_2}{2}$

4.8 Resistivity Measurement

Resistivity is an intrinsic property of a magnetic material. Ferrites materials are technically very important because of their high resistivity and low eddy current losses. Eddy current losses are inversely proportional to resistivity of the ferrite samples. Therefore, the measurement of resistivity is very crucial for the ferrite materials.

For the resistivity measurement the samples were sintered at 1245°C for 2 hours in air. The samples were polished using metallurgical polishing machine with the help of silicon carbide MRE papers with grid size 600, 800 and 1200 successively. After that the samples were clean with acetone and then again polished with special velvet type polishing cloth named as alphagam for finer polishing using fine alumina powder dispersed in a liquid. Samples are then cleaned in a ultrasonic cleaner and dried in furnace at 150°C for several hours. Then the samples are again cleaned with acetone and silver paste was added to both the sides of the

polished pellet samples together with two thin copper wires of 100-micron diameter for conduction. Again the samples are dried at 150°C to eliminate any absorbed moisture. DC resistivity was measured using an electrometer Keithley model 6514, USA at room temperature. The resistivity has been calculated using the formula,

$$\rho = \frac{R\,A}{l} \text{ ohm-meter} \qquad (4.23)$$

Where l is the length and A is the cross-sectional area of the samples. The conduction electrons are responsible for the current flow. The electron undergoes a collision only because the lattice is not perfectly regular. We group the derivations from a perfect lattice into two classes: lattice vibrations (phonons) of the ions around their equilibrium position due to thermal excitation of the ions and all static imperfections, such as foreign impurities or crystal defects. Now we can write

$$\rho = \rho_{ph} + \rho_i \qquad (4.24)$$

It is seen that ρ has split into two terms: a term ρ_i is due to scattering by impurities, which is independent of T, called residual resistivity. Another term added to this is ρ_{ph} arises from the scattering by phonons and therefore temperature dependent. This is called ideal resistivity.

At low temperature T, the scattering by phonons is negligible because the amplitudes of oscillations are very small; in that region $\rho_{ph} \rightarrow 0$, is a constant. As T increases, scattering by phonons becomes more effective and ρ_{ph} (T) increases; this is why ρ increases. When T becomes significantly large, scattering by phonons dominates and $\rho \approx \rho_{ph}$ (T). In the high temperature region ρ_{ph} (T) increases linearly with T. Resistivity linearly increases with T up to the melting point for the case of pure element. On the other hand, the electrical resistivity of metallic glass is measured to be very high due to the disorder arrangement of the atoms. The electrons suffer enormous scattering as they pass through the disorder matrix of ions. Thus the mean free paths of the conduction electrons are very short

and hence the drift velocities of the electrons are very low giving the material a property of high electrical resistivity. This resistivity may drop quite abruptly at a certain temperature as the temperature of the sample is increased. The increase in temperature give rise to the information of small regions of ordered phases at the onset of segregation and thus attaining the crystalline phase when the resistivity falls simply as the crystallization temperature. This unique property of the metallic glass is of very interesting of the people who are working with the commercial applications of metallic glasses e.g., the power supplies, transformers, magnetic heads, magnetic shielding etc. Ferrites are semiconductors, and their resistivity decreases with increasing temperature according to the relation:

$$\rho = \rho_0 e^{-\frac{E_a}{K_B T}} \tag{4.25}$$

The temperature dependence of chemical reactions can be expressed by defining the activation energy

$$E_a = K_B T^2 \frac{d \ln \rho}{dT} \tag{4.26}$$

By using $d\left(\frac{1}{T}\right) = -\frac{dT}{T^2}$ and rearranging equation (4.32) we obtain

$$E_a = -R \frac{d \ln \rho}{d\left(\frac{1}{T}\right)} \tag{4.27}$$

E_a is the energy needed to release an electron from the ion for a jump to the neighboring ion giving rise to electrical conductivity known as the activation energy [4.5-4.6].

4.9 Magnetization Measurement

Magnetization is defined as the magnetic moment per unit volume. There are various ways of measuring magnetization of a substance. In our present study, magnetization measurements have been carried out by quantum design physical property measurement system (PPMS) vibrating system magnetometer (VSM).

Fig- 4.6 shows the diagram of quantum design physical property measurement system (PPMS) vibrating system magnetometer (VSM).

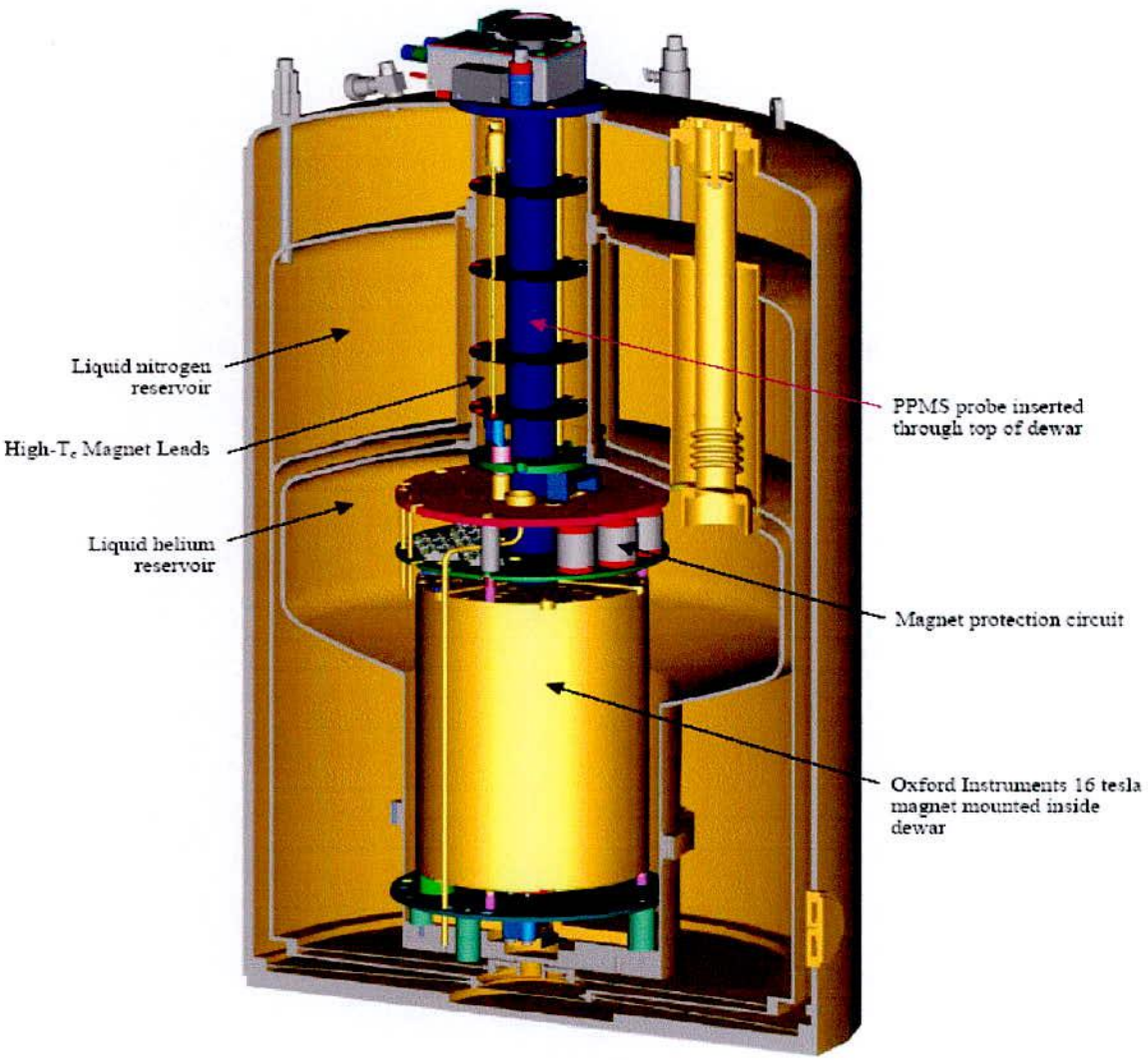

Fig- 4.6: Quantum design physical property measurement system (PPMS) vibrating sample magnetometer (VSM)

4.9.1 Quantum Design Physical Property Measurement System (PPMS) Vibrating Sample Magnetometer (VSM)

Quantum design physical property measurement system (PPMS) by Oxford Instruments provides the widest range of performance. This system has been designed primarily for performing high field magnetometry, electromagnetic and

thermal transport property measurements. PPMS represents a unique concept in laboratory equipment. It is an open architecture, variable temperature-field system that is optimized to perform a variety of automated measurements. The PPMS works like a dedicated system, but its tremendous flexibility lets us perform different types of measurements. However, any of the capabilities can be combined to configure a system suitable for your particular research needs. In its continuing effort to offer advanced measurement capabilities for the physical property measurement system (PPMS), quantum design announces the introduction of the P525 PPMS vibrating sample magnetometer (VSM) application. The addition of the VSM to the automated PPMS measurement applications makes this exceptionally versatile material characterization. Vibrating Sample Magnetometer (VSM) measurement system for the Physical Property Measurement System (PPMS) is a fast, sensitive and fully automated DC magnetometer. The PPMS sample-mounting system is the most interesting and unique feature of this instrument. At the bottom of the sample chamber is a 12-pin connector pre-wired to the system electronics. This connector allows to plug in a removable sample insert or sample "puck" and offers convenient access to electrical leads for application hardware and electronics. This connector provides the foundation for all of the PPMS measurement inserts.

4.9.2 Advantages of the VSM System

The VSM linear motor transport uses a uniquely designed linear motor to vibrate the sample. Unlike other vibrating sample magnetometers that use a short-throw resonant voice-coil design, the PPMS VSM linear motor is designed to operate at 40 Hz, with rapid slewing possible over about 6.5 cm of travel. The large range of motion enables the PPMS VSM system to perform rapid, completely automated centering operations which does not require the manual adjustments to center the sample. The sensitivity of the VSM detection coils is not significantly affected by large magnetic fields, so the PPMS VSM can perform sensitive measurements up to the maximum field available from PPMS magnet. The VSM detection coil is

inserted into the PPMS sample chamber by using the standard PPMS sample interface design. This procedure makes it easy to reconfigure the VSM option with alternate pickup coil designs in the future. The pickup coil configuration can easily be changed as easily as we can change a sample puck. It is easy to activate and deactivate the VSM option on your PPMS, just like the other PPMS options. The modularity of the design enables to perform successive types of measurements with little additional effort.

4.9.3 The Measurement Technique

The basic measurement is accomplished by oscillating the sample near a detection (pickup) coil and synchronously detecting the voltage induced. By using a compact gradiometer pickup coil configuration, relatively large oscillation amplitude (1-3 mm peak) and a frequency of 40 Hz, the system is able to resolve magnetization changes of less than 10-6 emu at a data rate of 1 Hz. The VSM option for the PPMS consists primarily of a VSM linear motor transport (head) for vibrating the sample, a coilset puck for detection, electronics for driving the linear motor transport and detecting the response from the pickup coils, and a copy of the Multi Vu software application for automation and control. The sample is attached to the end of a sample rod that is driven sinusoidally. The center of oscillation is positioned at the vertical center of a gradiometer pickup coil. The precise position and amplitude of oscillation is controlled from the VSM motor module using an optical linear encoder signal read back from the VSM linear motor transport. The voltage induced in the pickup coil is amplified and lock-in detected in the VSM detection module. The VSM detection module uses the position encoder signal as a reference for the synchronous detection. The system is designed to be user-installable and compatible with existing PPMS systems.

4.9.4 System Requirements

The VSM requires a PPMS computer system running Microsoft Windows XP software. If upgrading installed PPMS, it may be necessary to upgrade the

computer to Windows XP. Systems with VSM require a minimum clearance height of 3m (10 ft) for sample exchange.

Power Requirements: 200-240V/50 or 60 Hz, 20 A

Temperature range: 1.9 K - 400 K

Magnetic field: up to16 tesla

Coil-set bore: 6.3 mm

Sample holders: Brass half tube-inner diameter = 3.3 mm; outer diameter = 3.6 mm

Sample Mass < 1 gram

VSM oscillation frequency (calibrated): 40 Hz

VSM oscillation amplitude (typical): 2 mm peak - Range of 0.1 mm - 5mm

4.9.5 Hysteresis Loop in Hard Ferrites

Hysteresis is a subject, which covers a wide range of behavior in materials, both in magnetism and other disciplines. The response of a magnetic substance to an applied magnetic field and its magnetic hysteresis is an essential tool of magnetism. Paramagnetic and diamagnetic materials can easily be recognized, soft and hard ferromagnetic materials give different types of hysteresis curves and from these curves parameters such as saturation magnetization, remanent induction and coercivity are readily calculated. Detailed study of hysteresis curves can give indications of the type of magnetic interactions occurring within the sample.

When a ferromagnetic material is magnetized in one direction, it will not relax back to zero magnetization when the imposed magnetizing field is brought to zero in the opposite direction. If an alternating magnetic field is applied to the material, its magnetization will trace out a loop called a hysteresis loop. The lack of retraceability of the magnetization curve is the property called hysteresis and it is related to the existence of magnetic domains in the material. Once the magnetic domains are reoriented, it takes some energy to turn them back again. This

property of ferromagnetic materials is useful as a magnetic memory. Some compositions of ferromagnetic materials will retain an imposed magnetization indefinitely and are useful as permanent magnets. The magnetic memory aspects of iron and chromium oxides make them useful in audio tape recording and for the magnetic storage of data on computer disks. Ferrimagnetic materials have non-linear initial magnetization curves as the changing magnetization with applied field is due to a change in the magnetic domain structure. These materials show hysteresis and the magnetization does not return to zero after the application of a magnetic field. The following fig-4.6 shows a typical hysteresis loop.

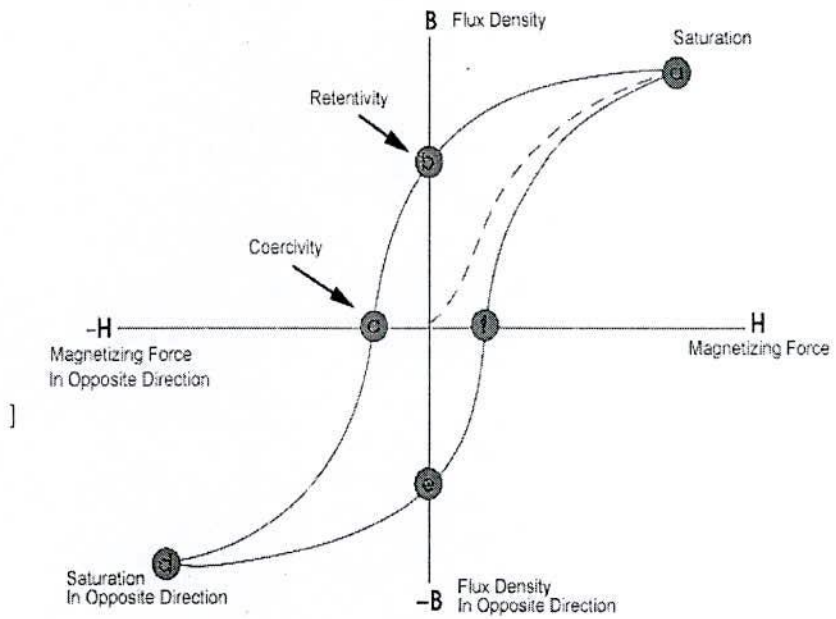

Fig-4.7 Hysteresis Loop

In the first quadrant of the loop is the initial magnetization curve (dotted line), which shows the increase in magnetization on the application of a field to an unmagnified sample. In the first quadrant the magnetization and applied field are both positive, i.e. they are in the same direction. The magnetization increases initially by the growth of favorably oriented domains, which will be magnetized in the easy direction of the crystal. When the magnetization can increase no further by the growth of domains, the direction of magnetization of the domains then

rotates away from the easy axis to align with the field. When all of the domains have fully aligned with the applied field saturation is reached and the magnetization can increase no further.

If the field is removed the magnetization returns to the Y-axis i.e. H=0, and the domains will return to their easy direction of magnetization, resulting in a decrease in magnetization. As seen in figure, the line from the saturation point to the Y-axis is horizontal, which is representative of a well-aligned material, where the domains are magnetized in the easy direction of the crystal at the saturation point. If the direction of applied field is reversed i.e. to the negative direction, the magnetization will follow the line into the second quadrant. The hysteresis means that the magnetization lags behind the applied field and will not immediately switch direction into the third quadrant i.e. negative magnetization. The magnetization will only decrease after a sufficiently high field is applied to:

i) Nucleate and grow domains favorably oriented with respect to the applied field or

ii) Rotate the direction of magnetization of the domains towards the applied field

Whenever a high field in the reverse direction is applied saturation magnetization will be achieved in the negative direction. If the applied field is then decreased and again applied in the positive direction then the full hysteresis loop is obtained. If the field is repeatedly switched from positive to negative directions and is of sufficient magnitude then the magnetization and induction will cycle around the hysteresis loop in an anti-clockwise direction. The area contained within the loop indicates the amount of energy absorbed by the material during each cycle of the hysteresis loop. The shape of the hysteresis loop tells a great deal about the material being magnetized. Relative to other materials, a material with a wider hysteresis loop has: lower value of permeability, higher remanent magnetization and higher value of coercivity. In a similar fashion comparing to other materials, a

material with the narrower hysteresis loop has: higher value of permeability, lower remanent magnetization and lower coercive field.

A great deal of information can be learned about the magnetic properties of a material by studying its hysteresis loop. As the hysteresis loop shows the relationship between the induced magnetic flux density (B) and the magnetizing force (H), it is often referred to as the B-H loop or M-H loop. From the hysteresis loop, a number of primary magnetic parameters of a material can be determined. From the first quadrant the saturation magnetization, M_s can be measured.

4.9.6 Saturation Magnetization, M_s

The fundamental experimental quantity in magnetic materials is the magnetization, defined as the magnetic moment per unit volume. Saturation magnetization, M_s can easily be measured in the laboratory. The saturation magnetization is the maximum induced magnetic moment that can be obtained in a magnetic field beyond which no further increase in magnetization occurs. The difference between spontaneous magnetization and the saturation magnetization has to do with magnetic domains. Saturation magnetization is an intrinsic property, independent of particle size but dependent on temperature. When the volume of the sample may change, as with temperature, it is convenient to measure the moment per unit mass rather than per unit volume, this quantity is usually equal to the magnetization per unit volume multiplied by the density.

Magnetization is in general a strongly nonlinear function of the applied field H and, in sufficiently high field, reaches a limiting value called the saturation magnetization, M_s. The saturation magnetization is temperature dependent, in general decreasing from a maximum value at 0K to a zero value at the Curie temperature. At fixed temperature, magnetization versus field is both nonlinear and hysteretic: a plot of M vs H for a cycle of field from $+H \rightarrow 0 \rightarrow -H \rightarrow 0 \rightarrow +H$ is called a magnetic hysteresis loop and contains much of the information needed

to characterize a magnetic material. Magnetization is a structure sensitive static (intrinsic) property, the magnetic field required to produce the saturation value varies according to the relative geometry of the field to the easy axes and other metallurgical conditions of the material. In other words, the approach to saturation is a structure sensitive process. The value of M_s can be calculated from a well established empirical relation between M and H [4.7-4.10]. Using numerical analysis of the magnetization curve based on the law of approach to saturation (LAS) the value of M_s can be calculated from the following equation:

$$M(H)=M_s(1-\frac{a}{H}-\frac{b}{H^2}-\frac{c}{H^3})+\chi_0 H \qquad (4.28)$$

where a, b, c.....χ_0 are constants. The term $\chi_0 H$ is inserted in the above relation to indicate an increase in spontaneous magnetization when a high field is applied to reduce the misalignments of spins caused by thermal agitation. In the fields over a few thousands the term $\frac{a}{H}$ is usually dominant, so that the above expression reduces to

$$M(H)=M_s(1-\frac{a}{H}) \qquad (4.29)$$

High field measurements of M can therefore be plotted against H and extrapolated to $\frac{1}{H}=0$ in order to find the value of saturation magnetization.

4.9.7 Remanent Magnetization, M_r

A good permanent magnet should produce a high magnetic field with a low mass, and should be stable against the influences, which would demagnetize it. The desirable properties of such magnets are typically stated in terms of the remanent magnetization of the magnet materials. The field that retained by the magnet after the magnetizing field has been removed is called the remanence, M_r. The alloys from which permanent magnets are made are often very difficult to handle metallurgically. They are mechanically hard and brittle. They may be cast and then ground into shape, or even ground to a powder and formed. From powders, they

may be mixed with resin binders and then compressed and heat-treated. Maximum anisotropy of the material is desirable, so to that end the materials are often heat treated in the presence of a strong magnetic field. Materials with high remanent magnetization and high coercivity from which permanent magnets are made are sometimes said to be "*magnetically hard*" to contrast them with the "magnetically soft" materials from which transformer cores and coils for electronics are made.

4.9.8 Coercivity, H_c

The reverse field required to bring the magnetization to zero is called the intrinsic coercivity, H_c. The reversal of magnetization can come about as a rotation of the magnetization in a large volume or through the movement of domain walls under the pressure of the applied field. In general materials with few or no domains have a high coercivity whilst those with many domains have a low coercivity. However, domain wall pinning by physical defects such as vacancies, dislocations and grain boundaries can increase the coercivity. Magnetic hardening in general is based on two types of magnetization processes:

i) Reversal of magnetization by a rotation process or a nucleation mechanism, and

ii) Reversal of magnetization by domain wall displacements

The first one of these two processes is connected with the existence of a small isolated particle or grains which are magnetically saturated and consist of one single domain (e. g., in sintered magnets). The second case is realized in as cast bulk materials optimized by special pretreatments. Recently, hard magnetic materials have also been produced by rapid quenching and mechanical alloying where the hardening mechanism may consist of a combined mechanism suppression of the expansion of a reversed nucleus by a pinning process of the domain wall boundaries of the nuclei.

The absolute upper bound of H_c is given by the so called nucleation field for homogeneous relation

$$\mu_0 H_N = \frac{2K_1}{M_s} - N_{eff}\,\mu_0 M_s \qquad (4.30)$$

where the first term represents the magnetocrystalline filed and the second term s takes care of demagnetizing fields characterized by an effective demagnetization factor N_{eff}.

In hard magnetic materials the cohesive field can be satisfactorily described by a modification of equation [4.11]:

$$\mu_0 H_c = \frac{2K_1}{M_s}\alpha - N_{eff}\,\mu_0 M_s \qquad (4.31)$$

where α takes care of the effects of the microstructure on H_c. In the case of nucleation hardened ferromagnets, α results from regions where the magnetocrystalline anisotropy is reduced. For pinning hardened magnets, α describes the strength of domain wall pinning centers.

4.9.9 Coercivity Mechanisms

There are various methods of increasing or decreasing the coercivity of magnetic materials, all of which involve the controlling the magnetic domains within the material. For a hard magnetic material it is desirable that the domains cannot easily rotate its direction of magnetization and that the domain walls do not move easily and / or nucleation of domains is difficult. To prevent easy rotation of domains the material could have strong uniaxial magnetocrystalline anisotropy. Alternatively, shape anisotropy can occur in needle-like particles, where the magnetostatic energy is less when the magnetization is in the long axis of the needle compared to the short axis.

If the size of a magnetic particle decreases then there is a critical size below which the decrease in magnetostatic energy by splitting into two domains is less than the increase in energy due to the introduction of the domain wall. Particles that are below this critical size are known as "single domain particles", and if they have sufficiently high anisotropy to prevent the easy rotation of the direction of

magnetization then the particles will be permanently magnetic and difficult to demagnetize. This type of coercivity mechanism can be observed in melt-spun NdFeB magnets where the crystal size is ~50nm, compared to the critical size for single domain particles of ~300nm.

Permanent magnets can also achieve coercivity by making the nucleation of new domains difficult. This mechanism can be found in sintered NdFeB permanent magnets where a non-magnetic grain boundary phase acts to smooth the grain boundaries, removing domain nucleation sites. Nucleation controlled permanent magnets are easily magnetized as the initial state has several domains in each crystal, but are difficult to demagnetize because this would require the nucleation of new reverse domains.

CHAPTER FIVE

Results and Discussion

5.1 Density of the Hexaferrites

Density is of ferrite samples play a vital role in the determination of magnetic as well as electrical properties. Higher value of the permeability of the soft ferrite and higher value of coercivity of the hard magnetic materials could be achieved by controlling the density. In general density can be changed by changing either the pressure or the temperature. The effect of pressure and temperature on the densities of liquids and solids is small because the typical compressibility for a liquid or solid is 10^{-6} bar^{-1} (1 bar = 0.1 MPa) and a typical thermal expansivity is 10^{-5} K^{-1}. In contrast, the density of gases is strongly affected by pressure. Boyle's law says that the density of a perfect gas is given by

$$\rho = \frac{mP}{RT} \qquad (5.1)$$

where R is the universal gas constant, P is the pressure, m is the molar mass, and T the absolute temperature.

The density of the samples in pure states and with some additives at different sintering temperature was measured by using the usual mathematical formula

$$\rho = \frac{m}{V} \qquad (5.2)$$

where ρ is the density, m is the mass and V is the volume of the hexaferrites.

The following tables 5.1 and 5.2 shows the variation of density of Sr- hexaferrites and Ba-hexaferrites in pure state and with the addition of La_2O_3, [0.7 wt% CaO + 0.3 wt% SiO_2] and sintering temperature. Synthesis and characterization of Ba-Sr hexaferrite has been prepared following conventional ceramic method using magnetite from Cox's Bazar beach sand and reported by Hoque [5.1]. It was found the average density as 4.72 gm/cc. In our research the value of density of Sr-hexaferrite with and without small additives has been found to vary between 4.58 to 4.91 gm/cc dependent on sintering temperature and additives. Density is an important parameter for the magnetic materials so that the materials are compact, hard and stress effective and not be deformed for any kind of mechanical ill

treatment. In our study, we have noted that the density of Sr-hexaferrite samples increases monotonically with the increase of sintering temperature as well as increase amount of La_2O_3 content. But the density of Sr-hexaferrite with controlled amount of addition of CaO + SiO_2 does not change significantly with sintering temperature with values ranging from 4.77 to 4.87 gm/cc. The higher value density for the Sr-hexaferrites with CaO and SiO_2 addition when compared without additives and sintered at T_s = 1210°C indicates that the additives has beneficial effect on the classification of the ferrites.

Table5.1

Density of Sr-hexaferrite samples with additives and sintering temperatures

Composition	x	Sintering Temperature, T_s (^{0}C)	Density, ρ (gm/cc)
$(SrO)_{1-x}(La_2O_3)_x$ 5.7 Fe_2O_3	0.00	1210	4.58
		1225	4.84
		1235	4.85
		1245	4.89
		1260	4.88
	0.04	1210	4.64
		1225	4.86
		1235	4.87
		1245	4.89
		1260	4.90
	0.08	1210	4.79
		1225	4.90
		1235	4.91
		1245	4.90
		1260	4.83
SrO 5.7 Fe_2O_3 + [0.7wt% CaO + 0.3wt% SiO_2]	--------	1210	4.77
		1225	4.85
		1235	4.83
		1245	4.87
		1260	4.80

The limiting density of Ba-hexaferrite after additions of various oxides is observed 4.4 gm/cc by Gadala [5.2]. In our investigation, the density of Ba-hexaferrite with and without additives has been observed to vary between 4.89 to 5.09 gm/cc. With

the addition of La_2O_3 the density of Ba-hexaferrites was found to be increased up to 5.09 gm/cc depending upon the sintering temperature. This means that the La_2O_3 has a densification effect even on the Ba-hexaferrites. In our study it has been found that the density of the hexaferrites increases remarkably with the simultaneous addition of [CaO + SiO_2].

Table5.2

Density of Ba-hexaferrite samples with additives and sintering temperatures

Composition	x	Sintering Temperature, T_s (^{0}C)	Density, ρ (gm/cc)
$(BaO)_{1-x}(La_2O_3)_x$ 5.7 Fe_2O_3	0.00	1210	4.89
		1225	5.01
		1235	5.02
		1245	5.04
		1260	4.99
	0.04	1210	5.09
		1225	4.98
		1235	5.00
		1245	5.07
		1260	5.03
	0.08	1210	4.90
		1225	5.06
		1235	5.07
		1245	5.08
		1260	4.96
BaO 5.7 Fe_2O_3 + [0.7wt% CaO + 0.3wt% SiO_2]	--------	1210	5.03
		1225	5.02
		1235	5.06
		1245	5.05
		1260	5.01

At the same time it has also been observed that the increase in sintering temperature does not have significant change on the density of the Ba-hexaferrite samples. This means that the additives work as the sintering aid i.e., reducing the sintering temperature. Throughout the research it has been found that the density of the Sr- and Ba-hexaferrite samples increases with the increase in sintering temperature.

5.2 Porosity of the Ferrites

Solid ferrites and rocks are often not so solid. Porosity measures how much open space is there in ferrite or in a rock. If we look at a sponge we can see many open spaces. Ferrites are like that; only the spaces are generally much smaller, so that they cannot be seen without a microscope. Porosity (p) of the samples is calculated by using the formula,

$$p = \frac{\rho_x - \rho}{\rho_x} \qquad (5.3)$$

where ρ_x is the X-ray density and ρ is the apparent density. Tables 5.3 and 5.4 display the porosity of the Sr-hexaferrite and Ba-hexaferrite samples.

Table 5.3
X-ray density and porosity of Sr-hexaferrites sintered at 1245°C

Composition	x	X-ray density, ρ_x (gm/cc)	Apparent density, ρ (gm/cc)	Porosity, $\mathbf{p} = \frac{\rho_x - \rho}{\rho_x} \times 100\%$
$(SrO)_{1-X}$ $(La_2O_3)_X$ 5.7 Fe_2O_3	0.00	4.90	4.83	1.43
	0.04	4.95	4.85	2.02
	0.08	4.99	4.87	2.40
SrO5.7 Fe_2O_3 +[0.7wt%CaO + 0.3wt% SiO_2]	-----	5.17	4.79	7.35

It is known that the porosity of ceramic samples results from the two sources: intra-granular porosity and intergranular porosity [5.3].

The total porosity can be written as

$$P = P_{intra} + P_{inter} \qquad (5.4)$$

The intra-granular porosity mainly depends on the grain size. The porosity of the investigated samples has been determined from the X-ray density and the measured bulk density using equation (5.2) and demonstrated in tables 5.3 and 5.4.

Table 5.4
X-ray density and porosity of Ba-hexaferrites sintered at 1245°C

Composition	x	X-ray density, ρ_x (g/cc)	Apparent density, ρ (g/cc)	Porosity, $p = \frac{\rho_x - \rho}{\rho_x} \times 100\%$
$(BaO)_{1-x}$ $(La_2O_3)_x$ 5.7 Fe_2O_3	0.00	5.09	5.04	1.96
	0.04	5.17	5.07	2.71
	0.08	5.15	5.02	2.30
BaO5.7 Fe_2O_3 +[0.7wt%CaO + SiO_2]	-----	5.43	5.05	7.31

It is understood from the data that the X-ray density increases linearly with the increase of La_2O_3 concentration and with the addition of [CaO + SiO_2]. The apparent density increases monotonically with addition of La_2O_3 content. This signifies that La_2O_3 and [CaO + SiO_2] have a pronounced effect on the densification of the Sr- and Ba-hexaferrites when it is substituted by La_2O_3 and [CaO + SiO_2]. The synthesis and characterization of Ba-Sr hexaferrite prepared by conventional ceramic method using magnetite from Cox's Bazar beach sand and reported that the average porosity has been observed 7.23% by Hoque [5.1] et al. In our investigation the average value of the porosity was found as 3.82%. During our investigation it has been found that the porosity of the experimental samples increases linearly with the increase of La_2O_3-content. The higher porosity has been found whenever CaO and SiO_2 has been added simultaneously to the samples.

5.3 X-Ray Diffraction (XRD) Analysis

For the study of ferrite properties crystallographic characterization and identification of phases is obvious. X-ray diffraction (XRD), neutron diffraction and electron diffraction are useful techniques to identify the various phases of the synthesized ferrites as well as their unit cell parameters. In the present study XRD technique has been employed to discern these parameters. X-ray diffraction (XRD) studies of the samples were performed by using Philips X'PERT PRO X-ray Diffractometer using Cu-K_α radiation in the range of 2θ = 20° to 80° in steps of 0.02°. XRD patterns of the sintered samples (sintering temperature 1245°C) $(SrO)_{1-x}$ $(La_2O_3)_x$ 5.7 Fe_2O_3, where x = 0.00, 0.04, 0.08 and SrO 5.7 Fe_2O_3 + [0.7%CaO + 0.3% SiO_2] are presented in figs-5.1 and 5.2. As is seen in fig-5.1 (a), without additive for Sr-hexaferrites the peaks appeared at 30.45, 31.11, 32.43, 34.31, 37.26, 40.56, 44.70, 55.31, 56.98 and 63.27^0 attributed to (110), (008), (107), (114), (203), (205), (207), (217), (2011) and (220) reflections. Sr-hexaferrites including the doped samples are identified to be M-type hexaferrite structure. The results are in good agreement with JCPDS data of PDF # 720739 [5.4]. No impurity peaks were detected indicating that the samples are of single phase and quite homogeneous. For all the samples the XRD patterns the fundamental peak of maximum intensity for Sr-hexaferrites were found at 2θ = 32.4341° corresponding to the 2θ = 33.45° with the reported value [5.4-5.5]. The relative intensities of the samples exhibit a strong dependency on the doping content. As seen from the figures the relative intensities of Sr-hexaferrites peaks increases with the La doping, while decreased with (CaO + SiO_2) addition. According to the XRD analysis of the strontium hexaferrite samples the different Bragg positions, d-spacings, the relative intensities and the corresponding indices of the planes are presented in table-5.5 to table-5. 8.

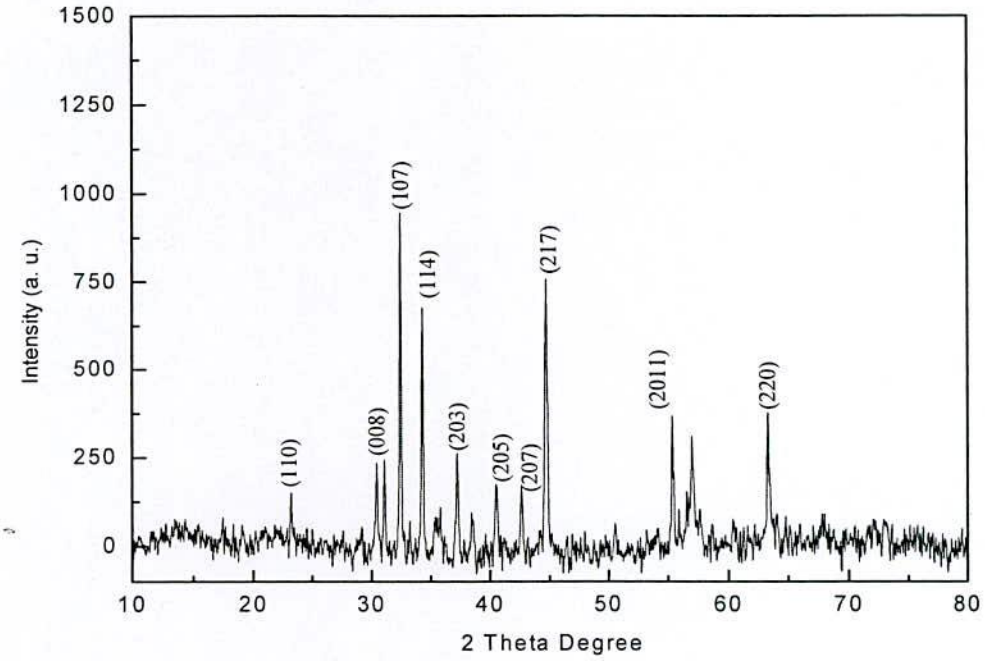

(a)

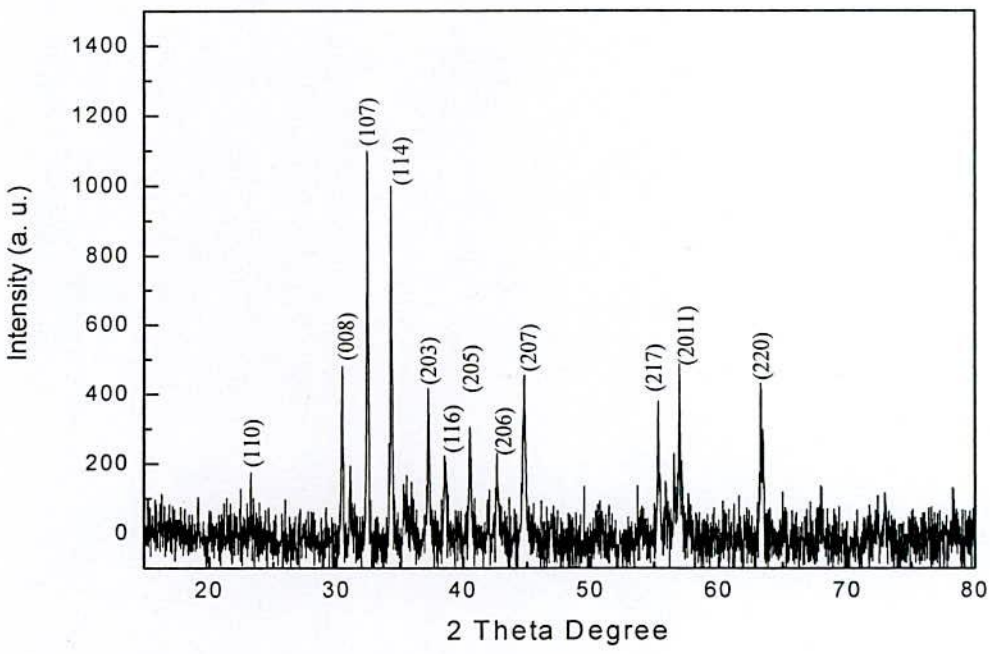

(b)

Fig- 5.1: X-ray diffraction (XRD) pattern of $(SrO)_{1-x}$ $(La_2O_3)_x$ 5.7 Fe_2O_3, where (a) x = 0.00, (b) x = 0.04

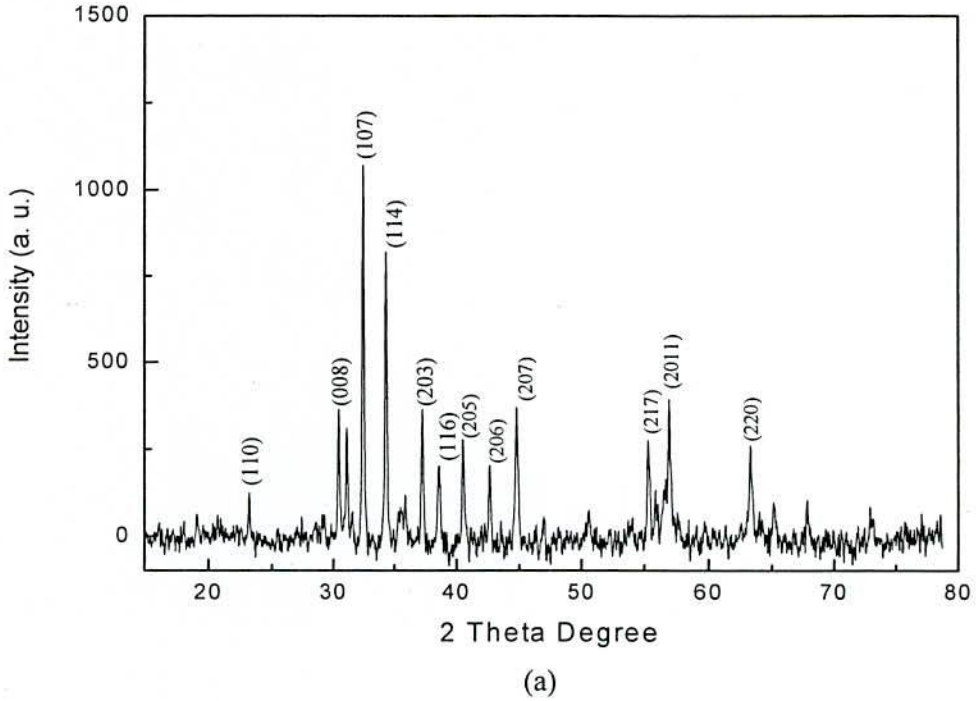

(a)

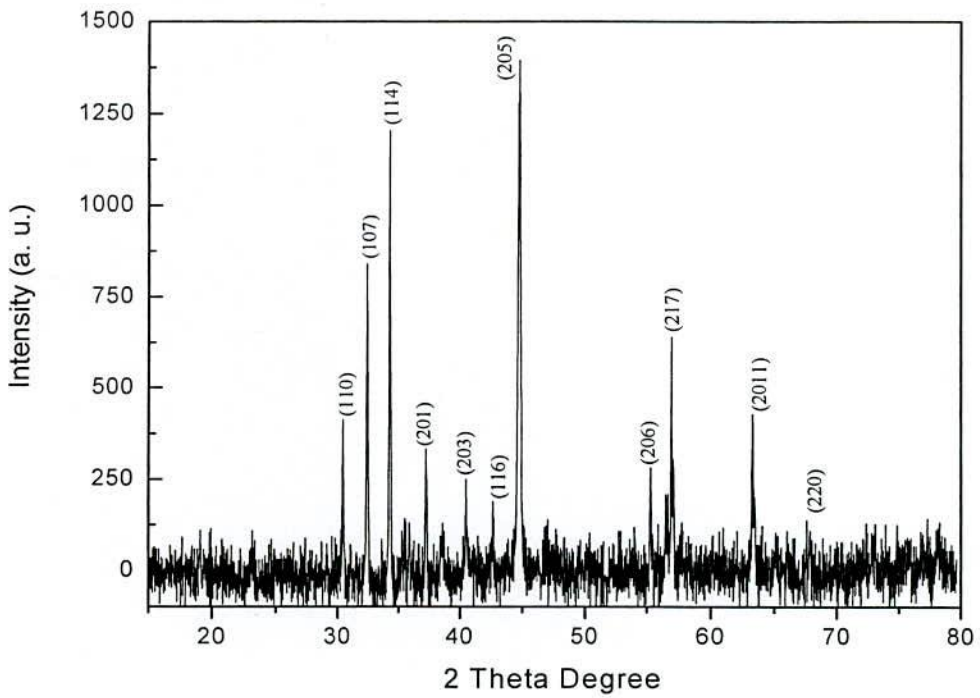

(b)

Fig- 5.2: X-ray diffraction (XRD) pattern of $(SrO)_{1-x}$ $(La_2O_3)_x$ 5.7 Fe_2O_3, where (a) x = 0.08 and (b) SrO 5.7 Fe_2O_3 + [0.7 wt% CaO + 0.3wt% SiO_2]

Table 5.5

XRD data of $(SrO)_{1-x}(La_2O_3)_x$ 5.7 Fe_2O_3 with x = 0.00

Position [2θ°]	Height [cps]	FWHM [2θ°]	d-spacing [Å]	Relative intensities [%]	Reflection planes (hkl)
30.45	161.00	0.1574	2.9354	26.39	(110)
31.11	175.22	0.1378	2.8753	28.72	(008)
32.43	610.10	0.1574	2.7605	100.00	(107)
34.31	430.17	0.1574	2.6135	70.51	(114)
37.26	179.22	0.1574	2.4131	29.37	(203)
40.56	120.52	0.2362	2.2244	19.75	(205)
44.70	464.81	0.1771	2.0275	76.19	(207)
55.31	206.82	0.1378	1.6609	33.90	(217)
56.98	174.29	0.2362	1.6162	28.57	(2011)
63.27	213.92	0.1440	1.4686	35.06	(220)

Table 5.6

XRD data of $(SrO)_{1-x}(La_2O_3)_x$ 5.7 Fe_2O_3 with x = 0.04

Position [2θ°]	Height [cps]	FWHM [2θ°]	d-spacing [Å]	Relative intensities [%]	Reflection planes (hkl)
30.46	302.19	0.1378	2.9352	43.40	(110)
32.24	98.01	0.2362	2.8756	14.08	(008)
31.10	696.30	0.0787	2.7605	100.00	(107)
32.43	634.28	0.0590	2.6165	91.09	(114)
34.27	242.82	0.1181	2.4140	34.87	(203)
37.25	123.95	0.2362	2.3347	17.80	(116)
38.56	178.32	0.1574	2.2263	25.61	(205)
40.52	90.54	0.4723	2.1191	13.00	(206)
42.67	272.89	0.1968	2.0240	39.19	(207)
55.31	190.44	0.1574	1.6610	27.35	(217)
56.98	262.52	0.0960	1.6148	37.70	(2011)
63.28	253.81	0.0960	1.4684	36.45	(220)

Table 5.7

XRD data of $(SrO)_{1-x}$ $(La_2O_3)_x$ 5.7 Fe_2O_3 with x = 0.08

Position [2θ°]	Height [cps]	FWHM [2θ°]	d-spacing [Å]	Relative intensities [%]	Reflection planes (hkl)
30.44	252.19	0.1574	2.9364	34.41	(110)
31.10	219.25	0.1181	2.8755	29.92	(008)
32.43	732.88	0.1378	2.7612	100.00	(107)
34.28	633.98	0.0787	2.6163	86.51	(114)
37.25	276.44	0.1574	2.4139	37.72	(203)
38.57	151.90	0.2362	2.3341	20.73	(116)
40.51	202.80	0.1181	2.2268	27.67	(205)
42.62	155.78	0.1181	2.1215	21.26	(206)
44.77	258.99	0.1968	2.0243	35.34	(207)
55.31	183.34	0.1574	1.6611	25.02	(217)
56.94	235.39	0.1181	1.6173	32.12	(2011)
63.31	146.31	0.3840	1.4677	19.96	(220)

Table 5.8

XRD data of SrO 5.7 Fe_2O_3 + [0.7wt% CaO + 0.3wt% SiO_2]

Position [2θ°]	Height [cps]	FWHM [2θ°]	d-spacing [Å]	Relative intensities [%]	Reflection planes (hkl)
30.44	264.43	0.0787	2.9367	34.49	(110)
32.42	530.93	0.1181	2.7620	69.24	(107)
34.26	750.96	0.0590	2.6172	97.94	(114)
35.58	37.72	0.9446	2.5231	4.92	(201)
37.26	194.14	0.1574	2.4135	25.32	(203)
38.58	57.33	0.4723	2.3339	7.48	(116)
40.53	93.72	0.2362	2.2258	12.22	(205)
42.55	44.99	0.4723	2.1246	5.87	(206)
55.30	157.87	0.1181	1.6613	20.59	(217)
56.94	321.26	0.1181	1.6173	41.90	(2011)
63.27	263.32	0.0960	1.4687	34.34	(220)

XRD studies of the Ba-hexaferrite samples have also been performed by using Philips X'PERT PRO X-ray Diffractometer using Cu-K_α radiation of wavelength λ = 1.542 Å in the range of 2θ = 20° to 80° in steps of 0.02°. The phase and purity level of the hexaferrite samples of compositions $(BaO)_{1-x}$ $(La_2O_3)_x$ 5.7 Fe_2O_3, where x = 0.00, 0.04, 0.08 and BaO 5.7 Fe_2O_3 + [0.7wt% CaO + 0.3wt% SiO_2] sintered at 1245°C in air for 2 hours have been determined from the XRD patterns are shown in figs-5.3-5.4. As observed from the XRD patterns of fig-5.3 and fig-5.4, all the peaks are identified to be single-phase magnetoplumbite structure with hexagonal symmetry (JCPDS data of PDF # 84-0757) [5.6] without having any other intermediate phases. This also demonstrates the homogeneity and purity level of the prepared samples. For pure Ba-hexaferrite samples the peaks appeared at 23.05, 30.40, 32.24, 34.18, 37.15, 40.41, 42.55, 55.12, 56.62, 63.17 and 72.79^0 attributed to (006), (110), (107), (114), (203), (205), (206), (207), (217), (2011), (220) and (1116) reflections. The fundamental peak with maximum intensity for Ba-hexaferrites has been found to vary between 2θ = 32.24 to 32.27° with a reflection (107). The corresponding d-spacing for the fundamental peak of maximum intensity has been found to vary from 2.7741 to 2.7766 Å. Such confirmation of XRD study is supported by the earlier analysis of Liu [10]. The relative intensities of the hexaferrites have been found to be strongly depending on the amount of additives. The XRD patterns also show that the relative intensities of Ba-hexaferrites peaks decreases with the increase in La-content. But the amount of decrease of relative intensities of the ferrite samples has been found to be lower with the simultaneous addition of (CaO + SiO_2). From the XRD analysis of the

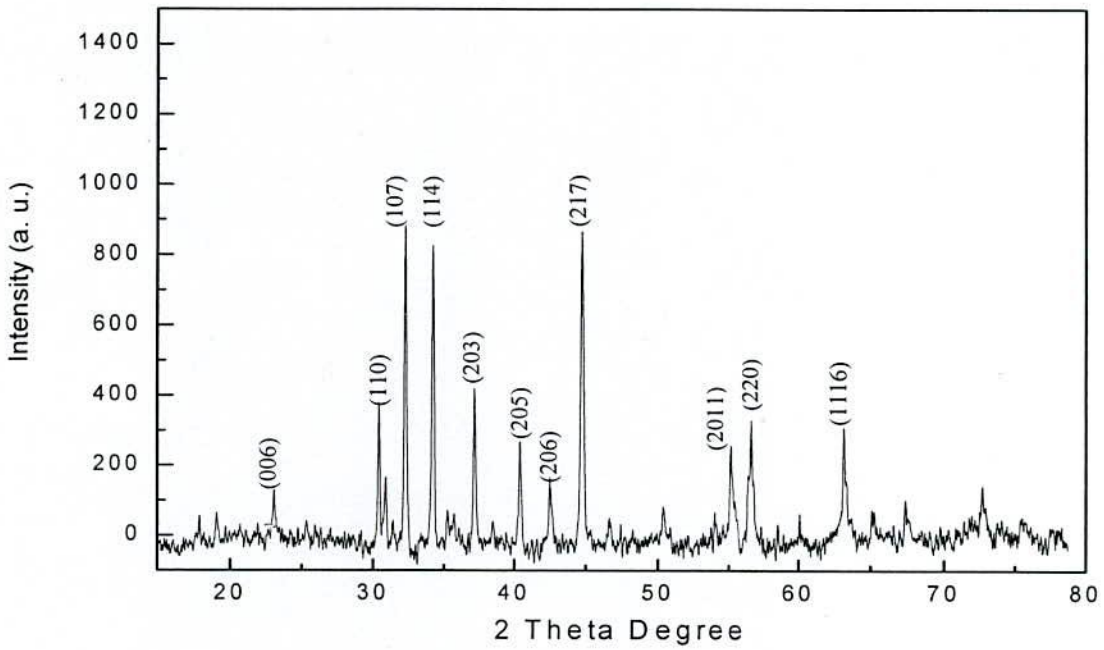

(a)

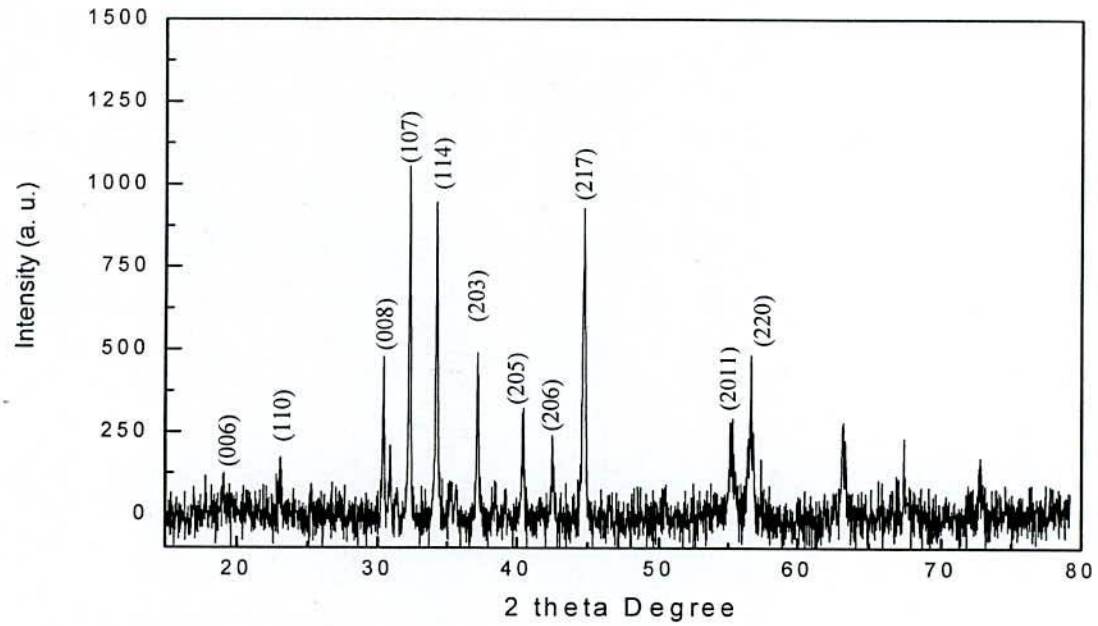

(b)

Fig-5.3: X-ray diffraction (XRD) pattern of $(BaO)_{1-x}$ $(La_2O_3)_x$ 5.7 Fe_2O_3, where (a) x = 0.00, (b) x = 0.04

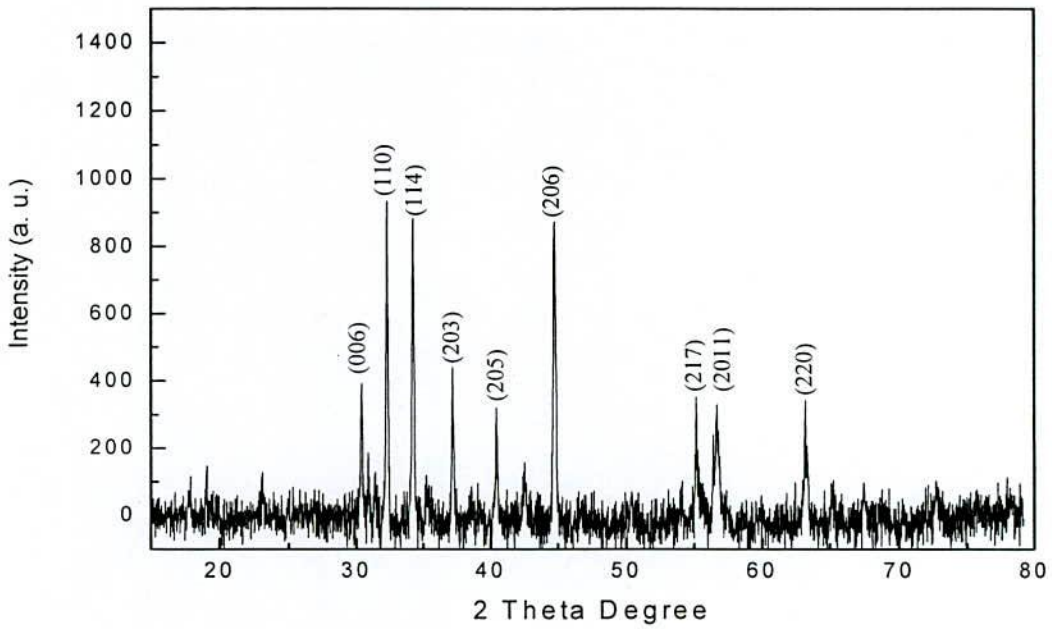

(a)

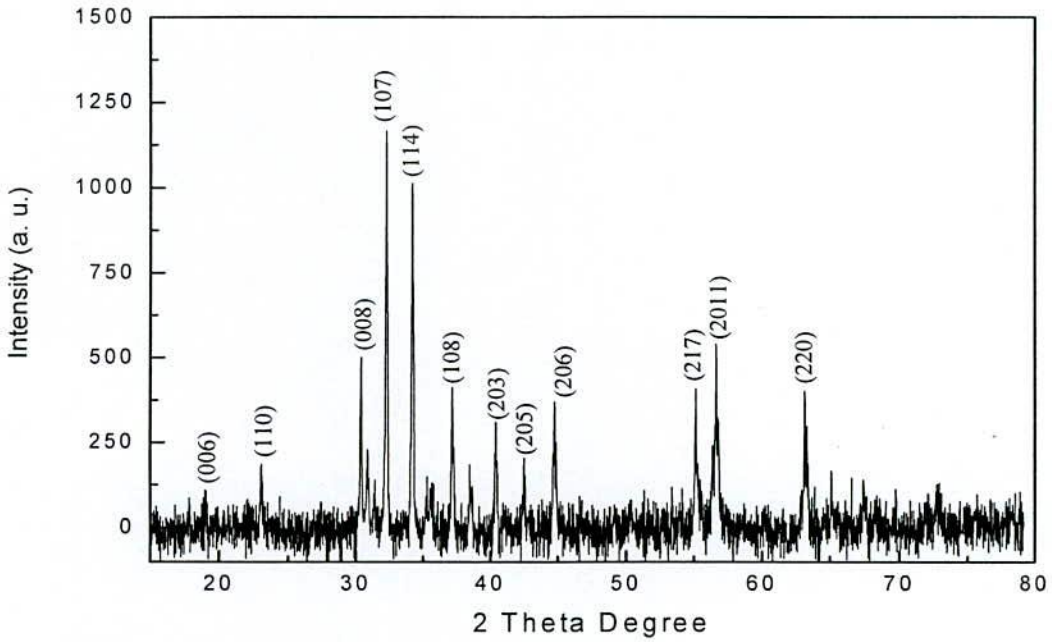

(b)

Fig-5.4: X-ray diffraction (XRD) pattern of $(BaO)_{1-x}$ $(La_2O_3)_x$ 5.7 Fe_2O_3, where (a) x = 0.08 and (b) BaO 5.7 Fe_2O_3 + [0.7 wt% CaO + 0.3wt% SiO_2]

Ba-hexaferrite samples the different Bragg positions, d-spacings, the relative intensities and the corresponding indices of the planes are displayed in table-5.9 to table-5. 12.

Table 5.9

XRD data of $(BaO)_{1-x}$ $(La_2O_3)_x$ 5.7 Fe_2O_3, where x = 0.00

Position [2θ°]	Height [cps]	FWHM [2θ°]	d-spacing [Å]	Relative intensities [%]	Reflection planes (hkl)
23.05	58.80	0.4723	3.8579	9.02	(006)
30.40	270.94	0.0787	2.9407	41.55	(110)
32.24	652.09	0.0787	2.7766	100.00	(107)
34.18	562.78	0.0787	2.6232	86.30	(114)
37.15	297.49	0.0720	2.4179	45.62	(203)
40.41	195.21	0.1574	2.2319	29.94	(205)
42.55	99.14	0.2362	2.1249	15.20	(206)
55.12	172.40	0.1181	1.6661	26.44	(217)
56.63	215.10	0.1181	1.6254	32.99	(2011)
63.17	212.38	0.1200	1.4707	32.57	(220)
72.79	57.29	0.5760	1.2982	8.79	(1116)

Table 5.10

XRD data of $(BaO)_{1-x}(La_2O_3)_x$ 5.7 Fe_2O_3, where x = 0.04

Position [2θ°]	Height [cps]	FWHM [2θ°]	d-spacing [Å]	Relative intensities [%]	Reflection planes (hkl)
23.07	80.76	0.2362	3.8561	12.23	(006)
30.41	303.70	0.0984	2.9399	46.00	(110)
30.89	138.60	0.1574	2.8948	20.99	(008)
32.25	660.27	0.0984	2.7755	100.00	(107)
34.19	594.17	0.0984	2.6228	89.99	(114)
37.17	282.98	0.1181	2.4190	42.86	(203)
40.43	176.24	0.1574	2.2308	26.69	(205)
42.52	101.21	0.2362	2.1262	15.33	(206)
55.19	127.48	0.3149	1.6643	19.31	(217)
56.67	295.63	0.0720	1.6230	44.77	(2011)
63.22	143.15	0.3840	1.4697	21.68	(220)

Table 5.11

XRD data of $(BaO)_{1-x}(La_2O_3)_x$ 5.7 Fe_2O_3, where x = 0.08

Position [2θ°]	Height [cps]	FWHM [2θ°]	d-spacing [Å]	Relative intensities [%]	Reflection planes (hkl)
30.38	226.41	0.0984	2.9425	39.18	(110)
32.27	577.92	0.1378	2.7741	100.00	(107)
34.21	550.44	0.1181	2.6214	95.25	(114)
37.15	282.86	0.0720	2.4179	48.94	(203)
40.43	179.79	0.1181	2.2313	31.11	(205)
42.51	83.70	0.2362	2.1267	14.48	(206)
55.15	201.26	0.1181	1.6654	34.83	(217)
56.75	172.02	0.3936	1.6221	29.77	(2011)
63.18	200.00	0.1440	1.4706	34.61	(220)

Table 5.12

XRD data of BaO 5.7 Fe_2O_3 + [0.7wt% CaO + 0.3wt% SiO_2]

Position [$2\theta°$]	Height [cps]	FWHM [$2\theta°$]	d-spacing [Å]	Relative intensities [%]	Reflection planes (hkl)
23.07	83.77	0.2362	3.8559	12.43	(006)
30.38	246.91	0.0984	2.9425	36.63	(110)
30.91	125.89	0.1574	2.8934	18.68	(008)
32.25	674.07	0.1181	2.7754	100.00	(107)
34.18	632.12	0.0787	2.6236	93.78	(114)
35.44	48.78	0.4723	2.5333	7.24	(108)
37.16	247.41	0.1574	2.4198	36.70	(203)
40.40	183.19	0.1574	2.2328	27.18	(205)
42.57	45.24	0.6298	2.1236	6.71	(206)
55.13	218.44	0.1181	1.6659	32.41	(217)
56.66	331.00	0.0720	1.6231	49.10	(2011)
63.14	215.00	0.1440	1.4712	31.90	(220)

5.4 Determination of Lattice Parameters from XRD Data

The lattice parameter a and c of the prepared samples has been calculated from the values of d-spacings corresponding to the different peaks of the neighboring planes according to the relation

$$d_{hkl} = [\frac{4(h^2+hk+k^2)}{3a^2} + \frac{l^2}{c^2}]^{-\frac{1}{2}} \qquad (5.5)$$

The values of lattice parameters a and c, unit cell volume and the ratio $\frac{c}{a}$ as calculated for strontium and barium hexaferrite samples are displayed in table 5.13 to table 5.14.

Table 5.13
Lattice parameter and unit cell volume of Sr-hexaferrites sintered at 1245°C

Composition	x	Unit cell volume ($Å^3$)	Molar weight	a (Å)	c (Å)	c/a
$(SrO)_{1-X}$ $(La_2O_3)_X$ 5.7 Fe_2O_3	0.00	686.60	1013.86	5.8742	23.0025	3.916
	0.04	686.51	1022.76	5.8703	23.0044	3.919
	0.08	687.08	1031.63	5.8708	23.0038	3.918
SrO5.7 Fe_2O_3 +[0.7wt%CaO + 0.3wt% SiO_2]	-----	687.83	1071.14	5.8734	23.0243	3.920

Table 5.14
Lattice parameter and unit cell volume of Ba-hexaferrites sintered at 1245°C

Composition	x	Unit cell volume ($Å^3$)	Molar weight	a (Å)	c (Å)	c/a
$(BaO)_{1-X}$ $(La_2O_3)_X$ 5.7 Fe_2O_3	0.00	1063.57	1063.57	5.8815	23.1479	3.94
	0.04	1070.47	1070.47	5.8735	23.0044	3.92
	0.08	1077.37	1077.367	5.8851	23.1475	3.93
BaO5.7 Fe_2O_3 +[0.7wt%CaO +0.3wt% SiO_2]	-----	1134.67	1120.87	5.8850	23.1473	3.93

As calculated from the X-ray diffraction data lattice parameter a and c of Sr-hexaferrites are presented in table 5.13 are somewhat fluctuating with increasing La_2O_3 content. The slight changes in lattice parameters may have been caused by the difference between the ionic radii of La^{3+} (1.22 Å) and Sr^{2+} (1.32 Å) and, between Fe^{3+} (0.67 Å) and Fe^{2+} (0.80 Å). Similar results are reported by Liu [5.7]. Whenever (CaO + SiO_2) is added with Sr-hexaferrite both the lattice parameters were found to be decreased. This is because addition of (CaO + SiO_2) significantly reduces the grain size as well as the density of the samples. The results displayed in table 5.13 show that the unit cell volume of Sr-hexaferrites is decreased with the

increase in La_2O_3-content. This variation in unit cell volume might have been associated with the larger ionic radii of La^{3+} (1.22 Å) and Sr^{2+} (1.32 Å) compared with that of Fe^{3+} (0.67 Å) and Fe^{2+} (0.80 Å) [5.8]. These results suggest that most of the La ions are dissolved both in the SrM grains and the grain boundaries, which lead to deviation of the unit cell volume comparing with the undoped one. The lattice parameters of the Sr-hexaferrite samples found in our study correlates well with literature values [5.8]. The influence the La doping on the properties of SrBa hexagonal ferrites prepared by vibrating ball milling following ceramic technique sintered at 1250-1260°C for 1-1.5 hour in air and showed that lattice parameter c slightly increases whereas the parameter a is somewhat fluctuating as was observed by Niem [5.9]. This is because the particles are reduced in dimension with increasing La_2O_3 doping in the sample during ball milling.

According to the values of the lattice parameters displayed in table 5.14, it is seen that both the lattice parameter a and c of the pure barium hexaferrite samples are higher a little compared to that of the doped samples due higher Ba^{2+} (0.7455 Å) ionic radii compared to those of La^{3+} (0.575 Å) ionic radii. With increasing La-contents both the lattice parameters systematically decreased because the crystal structures of Ba-hexaferrites were contracted after being doped with La ions. Investigation of the magnetic properties of Zn-Ti substituted barium hexaferrites prepared by mechanical milling and for pure barium hexaferrite samples by Angels et al. [5.8] found the value of lattice parameters a = 5.8950 Å and c = 23.2410 Å respectively. Author also reported

that the lattice parameter a increases slowly first with the substitution, while c remains almost constant.

The effect of doping of MnO_2 on the magnetic properties of M-type barium ferrites by Zhang [5.10] having different wt% of MnO_2 0.00, 0.25, 0.50, 0.75, 1.00, 1.50, 2.00 found that the values of lattice parameters are almost constant. The value of a and c are maximum at x = 0.25 and the parameters a = 5.8830 Å and c = 23.1810 Å of BaM doped with MnO_2 of 0.75 wt% are smaller then those of the others, which is probably because that more Mn ions entry the BaM grains and lead to transformation of the crystal lattice. Hoque et. al. [5.1] calculated the lattice parameters a and c for BaSr hexaferrite samples as 5.8856 Å and 23.1710 Å respectively, which reflects the accuracy of our measurements. Study of magnetic properties of Zn-Ti substituted barium hexaferrites prepared by mechanical milling [5.3] and for pure barium hexaferrite is 0.6994 nm^3 and increases up to a certain level of the substitution amount then decreases again. This slight increase in unit cell volume can be related to the longer ionic radii of Zn^{2+} (0.74 Å) and Ti^{4+} (0.68 Å) compared to that of Fe^{3+} (0.64 Å). In our investigation it has been found that the unit cell volume of the barium hexaferrite increases linearly with the increases in La-substitution. This increase in cell volume is related to the longer ionic radii of La^{3+} (1.22 Å) compared to that of Fe^{3+} (0.67 Å).

5.5 Microstructure Analyses

Microstructure refers of the microscopic description of the individual constituents of a material. Microstructure significantly affects the magnetic and electrical properties of ferrites. Domain behavior and its relation to microstructure of magnetic materials and the critical grain size, necessary to maintain a single domain can be obtained from microstructure study of the ferrite samples. Microstructure study of hexagonal ferrites show the relations among grain size, coercive force, permeability and dielectric losses.

The micrographs of Sr- and Ba-hexaferrites sintered at 1210, 1225, 1245 and 1260°C have been given in figs- 5.5-5.10 show the variation of grain size with the sintering temperature and additives. The grain size of the hexaferrites has been found to be increased with increasing sintering temperature [5.11]. During our investigation it has also been noticed that the grain size of the samples increases with the increase in sintering temperature. During the early stage of sintering the volume fraction of pores is very large and no grain growth occurs at all. As the sintering proceeds, the porosity decreases and many of the small pores disappear. The grains that grow consume their neighbors, grow larger and add more sides. As the grain size increases it is expected that the permeability of the samples also will be increased due to the domain wall motion. Resistivity of the samples depends upon the porosity and high resistivity is needed for low losses. Considering the entire factors, we can select an optimum sintering temperature for each sample from the microstructure study. For the samples with small grains, pores are found at the grain boundaries whereas samples with large grains, the majority of pores are trapped inside the grains at large distance from the grain boundaries, which might affect the permeability, density and resistivity of the hexaferrites. The size and morphology investigation of $SrFe_{12}O_{19}$ /SiO_2 prepared by citrate precursor technique with uniform silica layer by Fu [5.4] was done using (JEM 1200 EX) transmission electron microscope (TEM). Authors shown that a SiO_2 coating is enwrapped on the $SrFe_{12}O_{19}$ surface forming a core-shell structure of $SrFe_{12}O_{19}$ /SiO_2 nanocomposites. The $SrFe_{12}O_{19}$ is a kind of magnetic material that has more scattered electrons than that of SiO_2 which is a kind of non-magnetic oxides, so the core region is dark, while the shell region was found to be bright. The core of strontium ferrite is spherical or elliptical and the diameter of the core is in the range of 40-65 nm having a thickness of the shell of about 9 nm.

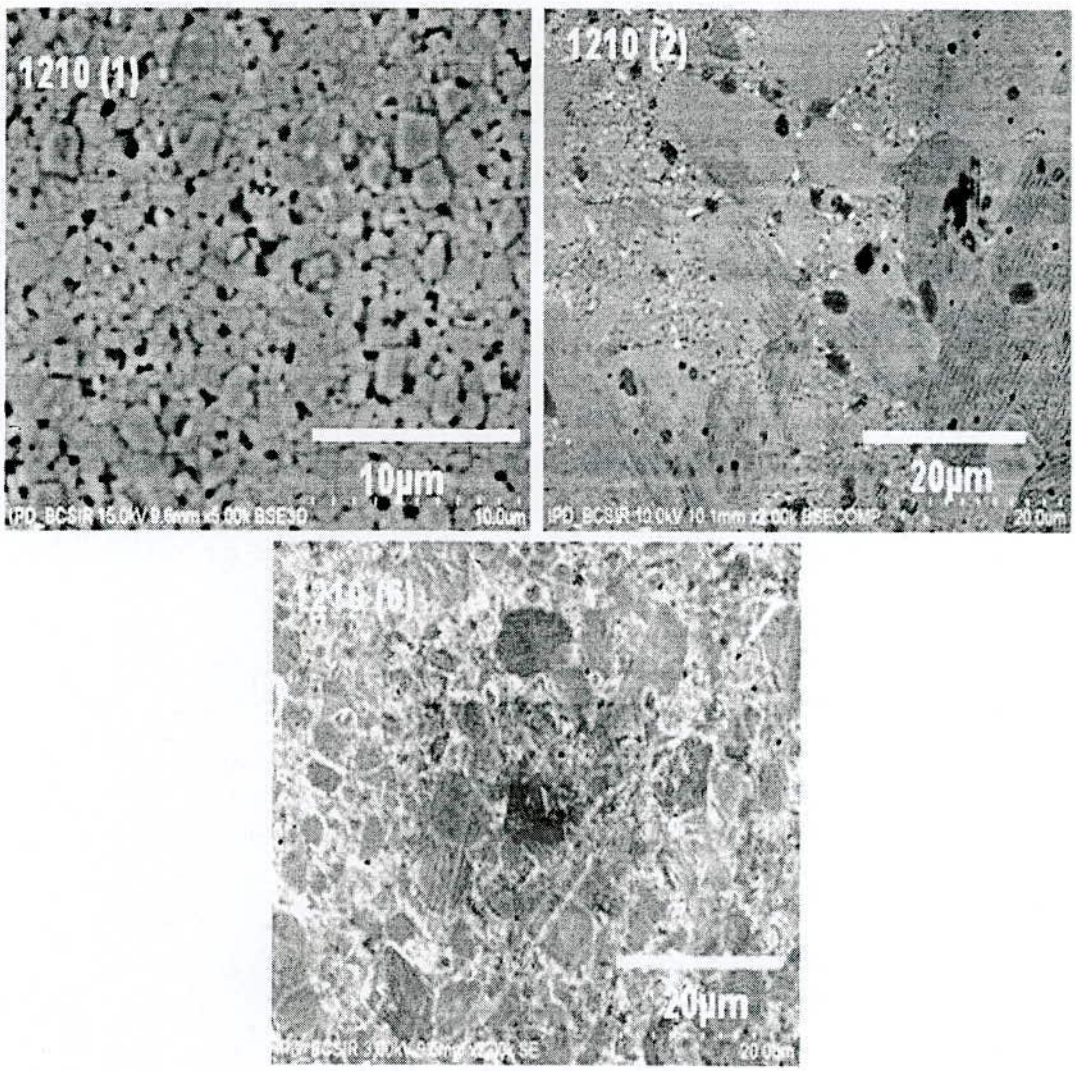

Fig-5.5: SEM micrographs of the samples (1) SrO 5.7 Fe_2O_3 (2) BaO 5.7 Fe_2O_3 and (6) $(BaO)_{1-x}$ $(La_2O_3)_x$ 5.7 Fe_2O_3 where x = 0.08 sintered at 1210°C

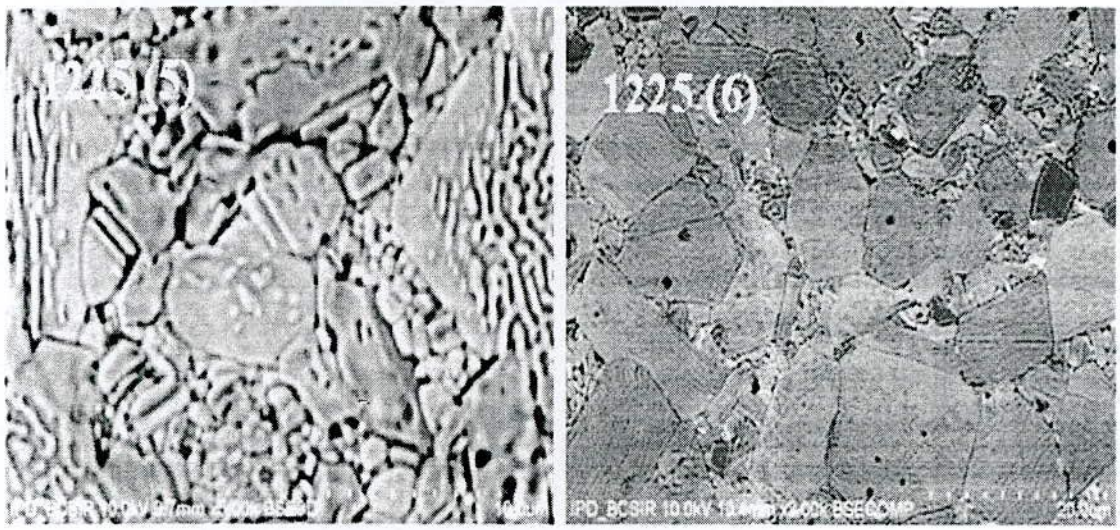

Fig-5.6:SEM micrographs of the sample (5) $(SrO)_{1-x}$ $(La_2O_3)_x$ 5.7 Fe_2O_3 (6) $(BaO)_{1-x}$ $(La_2O_3)_x$ 5.7 Fe_2O_3 where x = 0.08 sintered at 1225°C

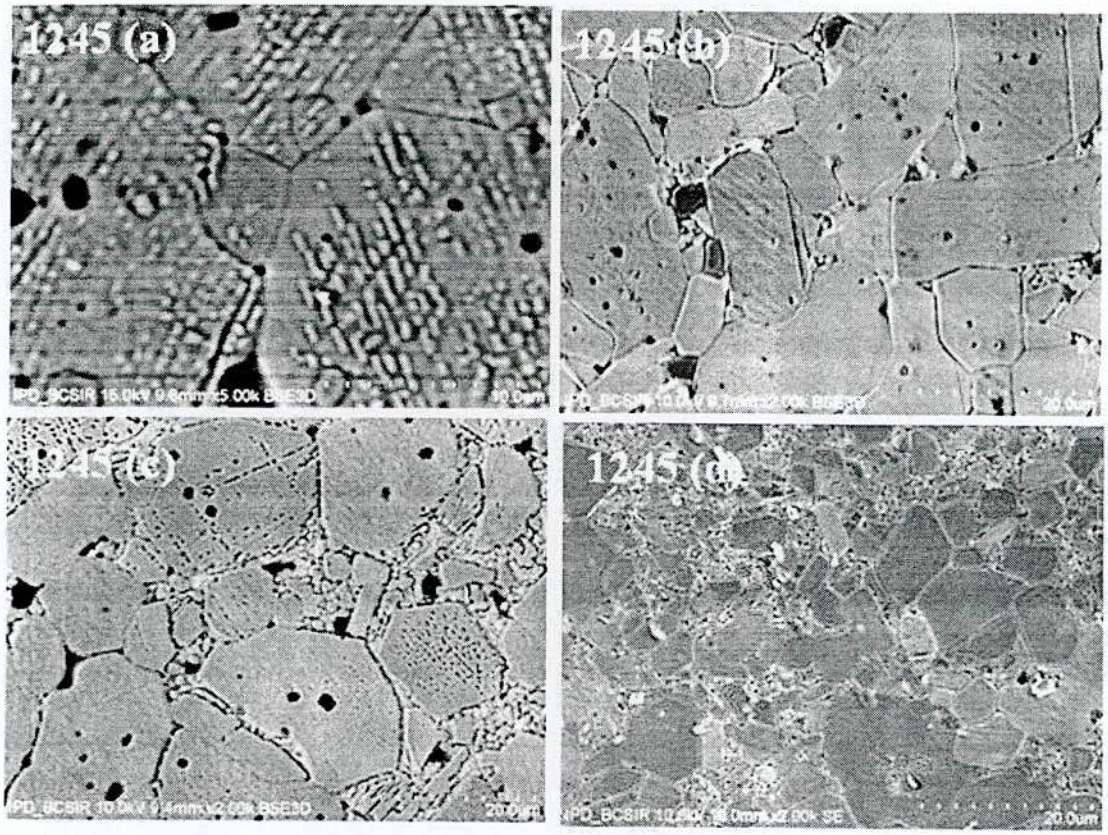

Fig-5.7:SEM micrographs of the samples (a) SrO 5.7 Fe_2O_3 (b) BaO 5.7 Fe_2O_3 (c) $(SrO)_{1-x}$ $(La_2O_3)_x$ 5.7 Fe_2O_3 and (d) $(BaO)_{1-x}$ $(La_2O_3)_x$ 5.7 Fe_2O_3 where x = 0.04 sintered at 1245°C

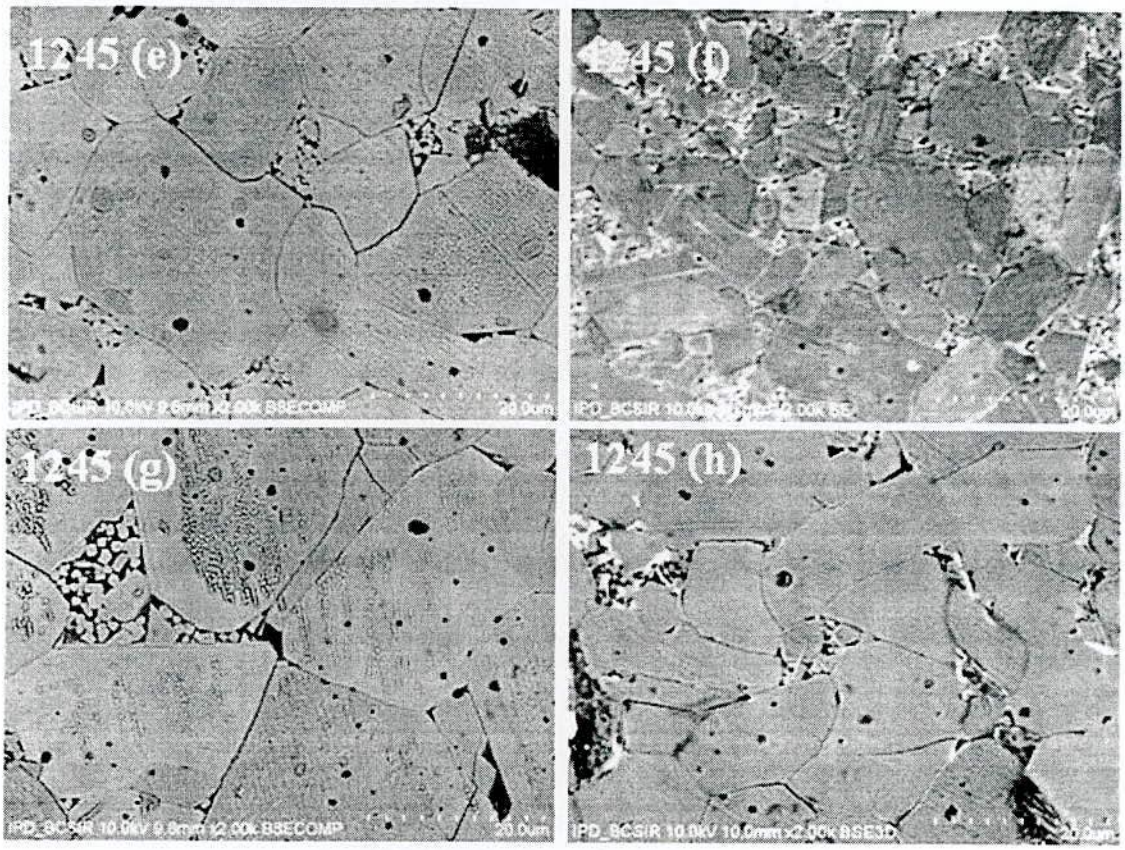

Fig-5.8: SEM micrographs of the samples (e) $(SrO)_{1-x}$ $(La_2O_3)_x$ 5.7 Fe_2O_3 (f) $(BaO)_{1-x}$ $(La_2O_3)_x$ 5.7 Fe_2O_3, where x = 0.08 (g) BaO 5.7 Fe_2O_3 + [0.7wt% CaO + 0.3wt% SiO_2] and (h) BaO 5.7 Fe_2O_3 + [0.7wt% CaO + 0.3wt% SiO_2] sintered at 1245°C

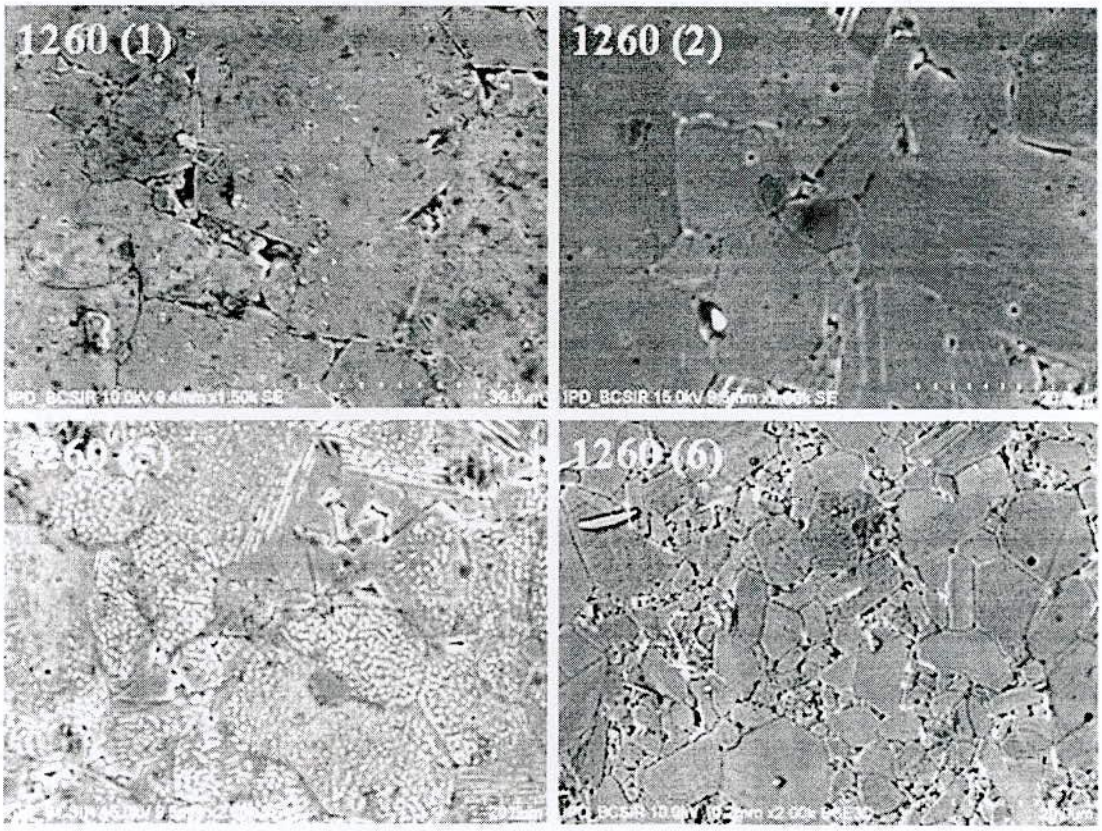

Fig-5.9: SEM micrographs of the samples (1) SrO 5.7 Fe_2O_3 (2) BaO 5.7 Fe_2O_3 (5) $(SrO)_{1-x}$ $(La_2O_3)_x$ 5.7 Fe_2O_3 and (6) $(BaO)_{1-x}$ $(La_2O_3)_x$ 5.7 Fe_2O_3 where x = 0.08 sintered at 1260°C

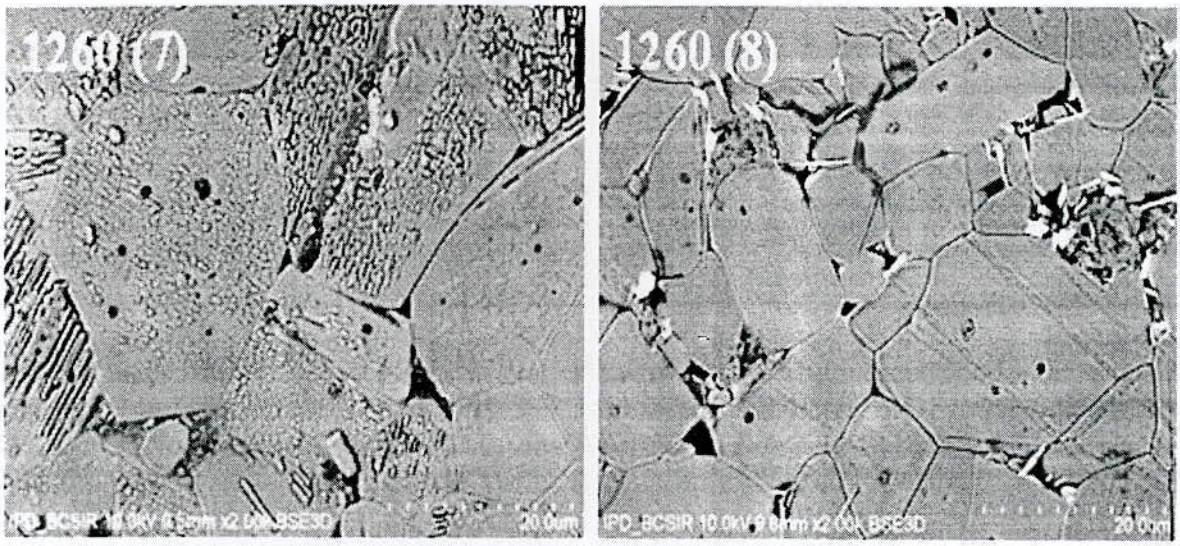

Fig-5.10:SEM micrographs of the samples (7) SrO 5.7 Fe_2O_3 + [0.7wt% CaO + 0.3wt% SiO_2] (8) BaO 5.7 Fe_2O_3 + [0.7wt% CaO + 0.3wt% SiO_2] sintered at 1260°C

If we observe the micrographs of the composition SrO 5.7 Fe_2O_3 at sintering temperatures T_s = 1210°, 1245° and 1260°C shown in fig- 5.5(1), 5.7(a) and 5.9 (1) demonstrate that the average grain size of the hexaferrites increases from a value of 1.5- 2μ at T_s = 1210°C to a value of 15μ at T_s = 1245°C and at T_s = 1260°C grains of big sizes varying from 16 to19μ. This indicates that for the same composition the grain size of the hexaferrites are strongly dependent upon the sintering temperature. As the sintering temperature increases the grains size has been found to be increased. It has also been observed that at higher sintering temperature some small particles have been trapped in between the bigger grains. This may happen due to the inhomogeneity in mixing by hand milling by agate motor or in the case of ball milling imperfection.

The micrographs of Ba-hexaferrite samples without additives presented in fig-5.5(2), 5.7(b) and 5.9(2) at the same sintering temperatures mentioned above for Sr-hexaferrites it has been observed that the average grain size increases from a value of 3-4μ to a value of 8-10μ with the increase in sintering temperature from 1210° to 1260°C. At low temperature sintering a large number of small particles has been found to be trapped at different regions of the hexaferrite samples. With rise in sintering temperature the grain size has been found to be clear with a trapping of small number of particles whereas at T_s = 1260°C almost no trapping was observed with increased grain size.

Now if we investigate the effect of La_2O_3 and [CaO + SiO_2] addition on the Sr-hexaferrite samples sintered at a constant temperature 1245°C shown in fig-5.7 (a), (b), (c) and (d), we see that the grain size of the hexaferrite samples decreases with increase of La_2O_3 content. At the same time whenever controlled amount of [CaO + SiO_2] has been added with the Sr-hexaferrites it has been found that the average grain size of the samples being increased compared to the undoped one. These results obtained from the microstructure analyses of the Sr-hexaferrite samples to be well agreement with the hysteresis parameters measurements.

Almost identical results have been noted in the case of Ba-hexaferrite samples sintered at 1245°C when La_2O_3 has been used as additives. But in the case of [CaO + SiO_2] addition with the pure BaM it has been observed that the average grain size of the hexaferrites decreases from a value of 5-6μ to a value of 4.5μ. Throughout the microstructure study of the hexaferrites it has been found that at a constant sintering temperature La_2O_3 acts as a grain refiner in either cases of the hexaferrite samples.

Let us now see the simultaneous effect of additives and sintering temperature on the microstructures of the Sr-hexaferrites. For this observation, we consider the micrographs 5.5(1), 5.6(5), 5.7(a), 5.7(c), 5.8(e), 5.9(5). From the micrographs it is clearly found that the average grain size increases as the increase in sintering temperature. But when sintering temperature was increased with the simultaneous addition of the La_2O_3 it has been seen that for the same composition sintered at T_s = 1210°, 1245° and 1260°C the grain size was to be 2-2.5μ, 10μ and 16-20μ respectively indicating increments of the grain size with the increase in sintering temperature and additives. Simultaneous effect of additives and increase in sintering temperature causes a smaller increase of the grain size comparing with the only increase in sintering temperature. Similar effect has also been observed in the case of microstructure analyses of the Ba-hexaferrites.

Again if we observe the simultaneous effect of addition of [CaO + SiO_2] and increase in sintering temperature on the microstructure of Sr-hexaferrite samples we see at T_s = 1210° and 1245°C without [CaO + SiO_2] addition the average grain size is 2-2.5μ and 15 μ respectively, which increases up to 20μ as the sintering temperature becomes T_s = 1260°C. But at T_s = 1245°C with [CaO + SiO_2] addition the grain size has been found to 16μ and at T_s = 1260°C the grain size of the Sr-hexaferrite samples found to be reduced up to 12-13μ. This means that at higher sintering temperature with simultaneous addition of [CaO + SiO_2] the grain size

has been found to be decreased. That is improved magnetic properties of permanent magnets may be achievable for samples at higher T_s.

But in the case of BaM without [CaO + SiO_2] addition at T_s = 1210°C and T_s = 1245°C the average grain size has been found to 3-4μ and 5-6μ respectively. At T_s = 1245°C whenever [CaO + SiO_2] has been added the average grain size of the hexaferrites has been noted to 4-5μ. When T_s = 1260°C the addition of [CaO + SiO_2] giving rise as increase in the grain size of the Ba-hexaferrite samples thus indicating that with [CaO + SiO_2] addition optimum magnetic qualities of the Ba-hexaferrite samples may be achieved at lower sintering temperature.

Influence of La-doping on the magnetic properties of SrBa hexagonal ferrites with composition $(Sr_{0.25}Ba_{0.75})_{1-x}$ $(La_2O_3)_{x/2}$ 5.3 Fe_2O_3 was investigated by Niem et. al.[5.9]. Authors performed the microstructure analysis of the samples by SEM. During their investigation it has been reported that sample with x =0.02 along the plane perpendicular to the preferred direction shows that after ball milling for 48 hours the particles are reduced in dimension with the increase in La-doping in the sample. It has also been observed that almost all the grains have the size of a single domain (<1.3 μm). The sintering materials SiO_2 is used as to limit the grain growth.

Investigation on the influence of SiO_2 and CaO additions on the microstructure and magnetic properties of sintered Sr-hexaferrites by Tofper [5.12] using TEM, Philips CM 20FEG a gradual increase in density and grain size with decreasing ratio SiO_2/CaO (S/C) has been found. To optimize the microstructure formation, i.e., to obtain sintered samples with high density and only little grain growth several sintering regimes were tested. A serious problem was appearance of abnormal grain growth. The tendency to form huge grains with size of about 100 μm in a matrix of grains of the size of about 2-5 μm also increases with decreasing S/C ratio. The best results were observed with sintering at a peak temperature of

1280°C. Without the additives a dense and anisotropic microstructure with platelet-shaped grains of 1-2 μm in height and about 3-5 μm in length is observed. Similar results have been found with only CaO addition. Addition of 0.5wt% SiO_2 remarkably reduced the grain size as well as the density. The dense microstructure of the samples is transformed into high remanence, but due to the relatively large platelet-shaped grains the coercivity is low. But as the grain size decreased coercivity is increased resulting in a decrease of remanence. With simultaneous addition of CaO and SiO_2 having various S/C ratio, the microstructure of the samples show significant changes in the size of the grains. The samples with large C/S ratio small grains with 2-3 μm in length are observed, samples with smaller C/S ratio show longer grains of up to 5 μm. Grain growth along hexagonal c-axis hardly occurs, whereas perpendicular to this axis the grains grow, i.e., the aspect ratio tends to increase if S/C ratio becomes smaller.

The magnetic and microstructural properties of both polycrystalline and single crystal samples of BaM have been studied to elucidate the relationship between the coercivity and grain boundary pinning effect [5.13]. With the increasing sintering temperature of the polycrystalline sample from 1100 to 1300°C, the grain size gradually increases. Large grains which are about a few microns and have better inter-grain connectivity are observed in the sample sintered at 1300°C. A notable feature in grain morphologies is that large plate-like grains appear to grow perpendicular to the c-axis. The samples sintered at 1100°C displays lots of small grains with poor connectivity in which the grain size is about 0.5 μm.

The particle morphology of the barium hexaferrite powders with and without La_2O_3 was investigated for the sintered samples using SEM [5.14]. The micrographs show that the La_2O_3 has significant effect on the particle size and morphology. The grain sizes were found to be smaller in the later samples. The average pore size in the sintered samples was 6.1 μm, whereas that of the La_2O_3 added sample decreased to about 3.8 μm. So the addition of La_2O_3 has the effect of

not only reducing grain size but also forming very dense microstructure. The addition of La_2O_3 as a grain refiner improves the magnetic properties by refinement of microstructure. In our investigation it has been observed that with addition of La_2O_3 the particle size of the hexaferrite samples was found to be reduced remarkably which causes the coercivity to increase. With the addition of CaO and SiO_2 in the Ba-hexaferrite samples the grain size was found to be enhanced which in turn causes the coercivity in increase as seen from the hysteresis parameters presented in table 5.23. It has also been noticed that the sintering temperature has significant effect on the microstructure. As the sintering temperature increases the density and the grain size of the hexaferrites increases which in turn causes to a decrease in coercivity. It is, however, reasonable to suggest that the low temperature sintering plays an important role for the formation of dense microstructure as well as higher value of coercivity which concomitant with the previous results [5.13]. The large value of coercivity suggests that the coercivity is attributed to the pinning of magnetization at the grain boundaries. That is the coercivity of the Ba-hexaferrite samples can also be controlled by the grain morphology.

5.6 Curie Temperature Measurements

The Curie temperature, T_c study is very important because it predicts the substantial information about nature of interaction in ferrites. Curie temperature also signifies the strength of the exchange interaction between the magnetic atoms. In Curie temperature thermal energy overcome exchange energy and material is changed into paramagnetic material from ferrimagnetic material i.e., a magnetically ordered substance becomes magnetically disordered. It can also be added that above the Curie temperature spontaneous magnetization of the samples vanishes and ferrimagnetic materials behaves like a paramagnetic one.

5.6.1 Curie Temperature Measurement by using the Variation of Initial Permeability with Temperature

T_c of all the Sr- and Ba-hexaferrite samples has been determined from the temperature dependence of initial permeability. Fig-5.11(a, b, c and d) and fig-5.12 (a, b, c and d) show the temperature dependence of the initial permeability, μ' of the Sr- and Ba- hexaferrite samples. T_c has been taken as the temperature at which a sharp fall of the permeability is observed. T_c may also be determined as that temperature where the first derivative of the permeability with respect to temperature $(\frac{d\mu}{dT})$ attains its maximum. In other words, where the rate of change of permeability with respect to temperature is maximum. Temperature dependence of a. c. initial permeability of the hexaferrite samples subjected to a constant frequency of 100 kHz and 100 mV using a signal generator. The calculated numerical values of all the T_c's of the hexaferrite samples are shown in tables 5.15 and 5.16.

The literature value of Curie temperature for pure Sr-ferrite is 450^0C [5.15]. Liu et. al. [5.16] studied the La^{3+} substituted Sr-hexaferrite and measured the Curie temperature of the pure Sr-hexaferrite is 457.5^0C and also showed that the value of Curie temperatures decrease with the increase in La^{3+} substituted amount. In our study we have reported, the value of Curie temperature of Sr-hexaferrites with and without La_2O_3 addition is exactly same as the standard published literature value of the Curie temperature of pure Sr-hexaferrite 450^0C, a constant value. Whenever a small amount of ($CaO + SiO_2$) is added the Curie temperature has been found to be increased up to 455^0C. This small variation of T_c is quite expected considering the temperature range in which the material is applied and off-stoichiometric composition of the hexaferrites.

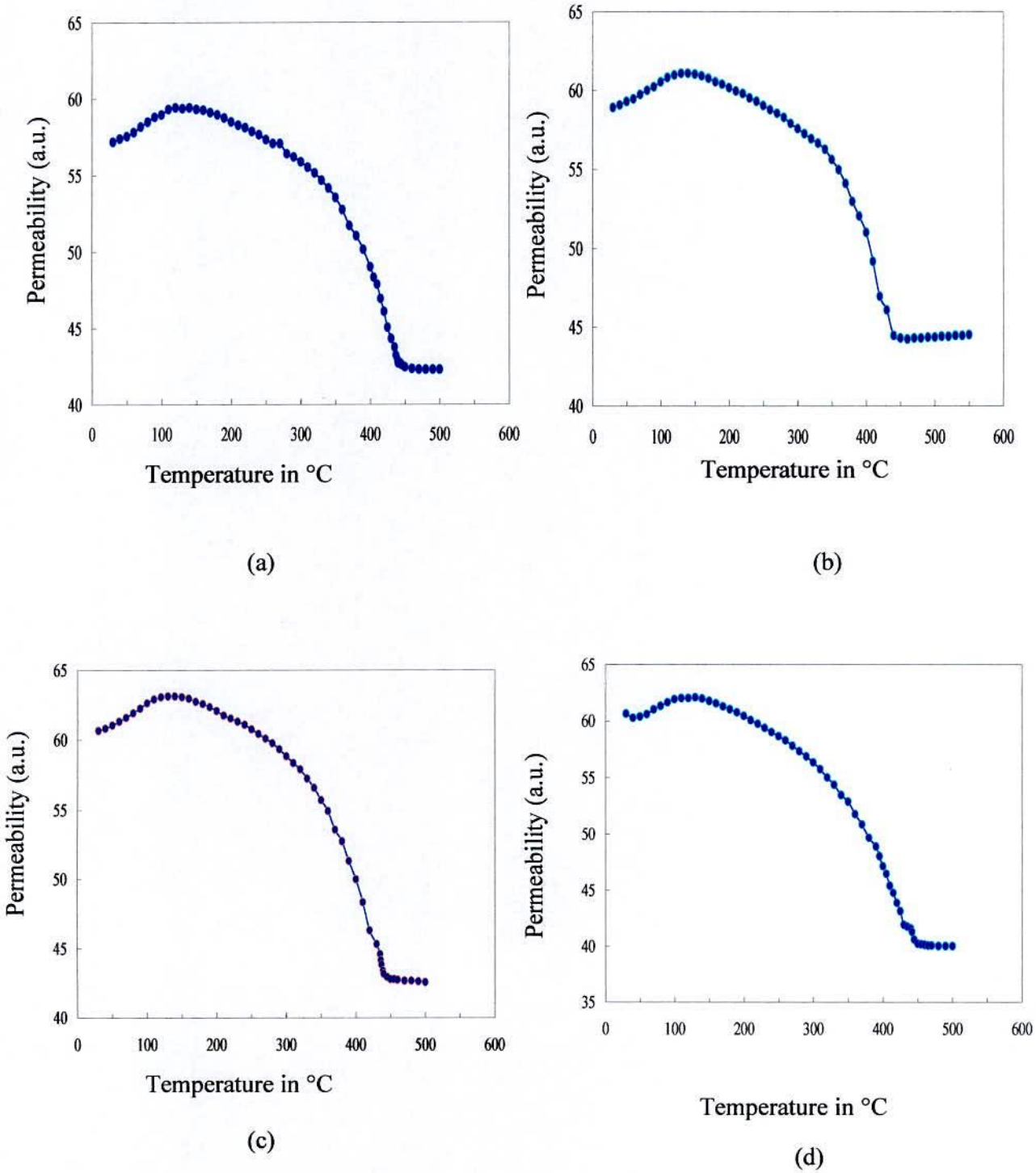

Fig-5.11: T_c determination from the temperature dependence of a. c. initial permeability of $(SrO)_{1-x}(La_2O_3)_x 5.7\ Fe_2O_3$ where (a) x = 0.00, (b) x = 0.04 (c) x = 0.08 and (d) SrO 5.7 Fe_2O_3 [0.7wt% CaO + 0.3wt% SiO_2]

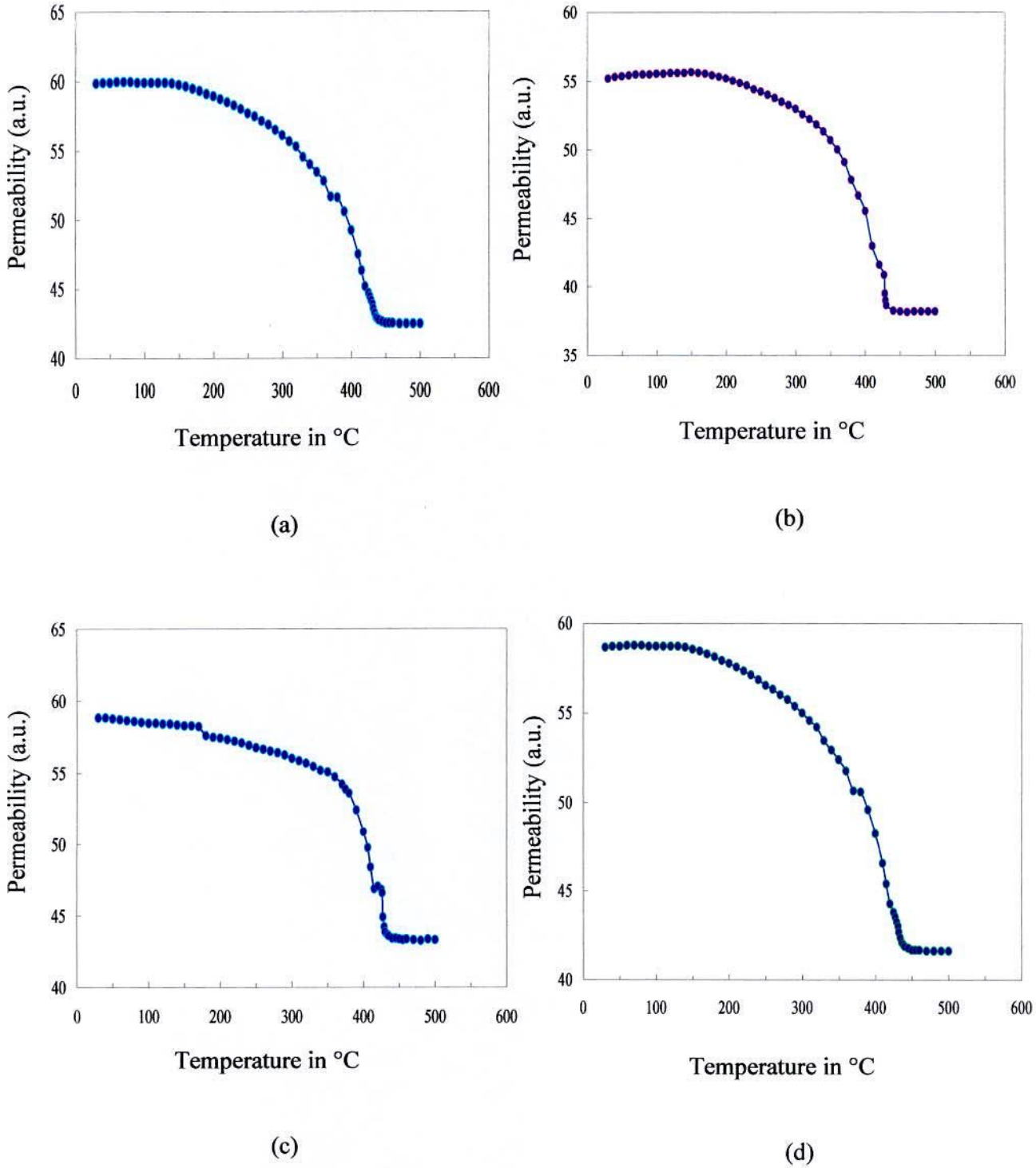

Fig-5.12: T_c determination from the temperature dependence of a. c. initial permeability of $(BaO)_{1-x}(La_2O_3)_x 5.7\ Fe_2O_3$ where (a) x = 0.00, (b) x = 0.04 (c) x = 0.08 and (d) BaO 5.7 Fe_2O_3 [0.7wt% CaO + 0.3wt% SiO_2]

Table 5.15

Curie temperature for Sr-hexaferrites

Composition	x	Curie Temperature, T_c (°C)
$(SrO)_{1-x}$ $(La_2O_3)_x$ 5.7 Fe_2O_3	0.00	450
	0.04	450
	0.08	450
SrO 5.7 Fe_2O_3 [0.7wt% CaO + 0.3wt% SiO_2]	-------	455

Table 5.16

Curie temperature for Ba-hexaferrites

Composition	x	Curie Temperature, T_c (°C)
$(BaO)_{1-x}$ $(La_2O_3)_x$ 5.7 Fe_2O_3	0.00	455
	0.04	450
	0.08	445
BaO 5.7 Fe_2O_3 [0.7wt% CaO + 0.3wt% SiO_2]	-------	460

Fang [5.5] studied the doping effect on the crystal structure and magnetic properties of chromium substituted strontium hexaferrite nanoparticles and showed that Curie temperature of the prepared samples decreases linearly with the doping content from 480°C to 427°C for x = 0.00 to x = 0.60. Ca and La-Co concentrations have a small effect on the magnetic properties of Ba- and Sr-hexaferrites as reported by Grossinger et al. [5.17].

The standard value of T_c for pure Ba-hexaferrite is 450^0C. Kim [5.18] studied the magnetic properties of La^{3+} substituted Ba-ferrite and reported that the value of Curie temperatures decrease with the increase in La-amount. Hoque [5.1] reported that Curie temperature of BaSr-hexaferrites prepared from magnetite of Cox's

bazar beach sand is around 430 to 435^{0}C. Angels [5.13] thoroughly investigated the magnetic properties of Zn-Ti substituted barium hexaferrites prepared by mechanical milling and found that Curie temperature for pure barium hexaferrite is 442°C and decreases linearly with the substitution of Zn-Ti. In our study, we have measured the Curie temperature of pure barium hexaferrite samples to be 455°C and with the addition of La_2O_3 Curie temperature was decreased linearly to 445°C. A small variation between the measurements of the Curie temperatures has been found due to the off-stoichiometric composition of the samples and over the range of the temperature through which the samples was considered because the preparation of the samples at higher sintering temperature in fact leads to the formation of grains with larger size and fewer defects. At the same time whenever controlled amount of CaO and SiO_2 were added simultaneously to the hexaferrite samples the value of T_c was found to be increased up to 460°C.

5.7 Permeability of Hexaferrites

Permeability is very important parameter in magnetism distinguishing the magnetic materials into soft and hard one. It indicates how much magnetic induction the material in a given magnetic field generates. In addition it can also be mentioned that permeability is a measure of degree of penetration of magnetic field through the substance or in other words it measures the capacity of the substance to take magnetization. For a magnetic material the dependence of permeability with frequency and temperature is an important aspect for their application as insulator. Hence, the study of initial permeability has been a subject of great interest from both the theoretical and practical points of view. The optimization of the dynamic properties such as complex permeability in the high frequency range requires a precise knowledge of the magnetization mechanisms involved. Permeability ranges from 100000 H/m in materials such as paramalloy down to as 1.1 in some permanent magnets [5.19]. Permeability and coercivity are reciprocal to each other.

5.7.1 Frequency Dependence of Initial Permeability of Sr-hexaferrite Samples with Additives

The magnetization mechanisms contributing to the complex permeability, $\mu = \mu' - i\mu''$, in soft polycrystalline ferrites have been a controversial subject for a long time and remain unsolved satisfactorily. Figs-5.13 (a) and (b) show the real part of the complex initial permeability of the Sr-hexaferrites of compositions $(SrO)_{1-x}(La_2O_3)_x$ 5.7 Fe_2O_3, where x = 0.00, 0.04, 0.08 and SrO 5.7 Fe_2O_3 + [0.7wt% CaO + 0.3wt% SiO_2] as a function of frequency sintered at 1260°C in air for 2 hours. Complex permeability has been calculated using low frequency Impedance Analyzer (Hewlett Packard) Model No. 4192A in the frequency range of 1kHz to 13 MHz at room temperature using conventional technique based on the determination of complex impedance of circuit located with toroid shaped sample. It is clearly evident from the permeability curves that with increase in La_2O_3 content the value of the permeability does not show significant change in magnitude whereas with the simultaneous addition of 0.7wt% CaO + 0.3wt% SiO_2 the permeability of the Sr-hexaferrite sample shows a little higher value comparing to the undoped one. The general characteristic of the curves is that the real part of the initial permeability remains fairly independent on frequency throughout the frequency range considered for the observation. It is well known that the permeability of polycrystalline ferrites is determined by the superposition of two magnetization mechanisms, i.e., spin rotation and domain wall motion. As the density of the materials increases with the increase in sintering temperature the grain size as well as the permeability of the samples might have been increased, which appears to be connected with an increase in the contribution from the domain wall displacement.

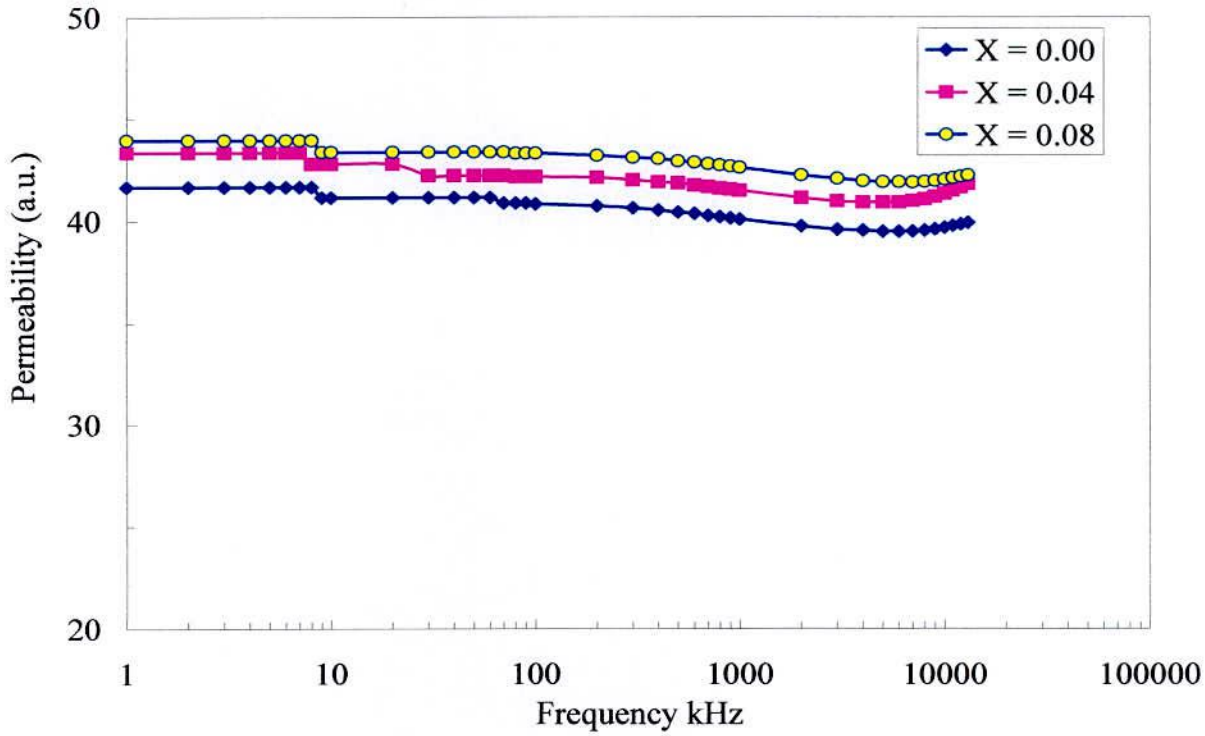

(a)

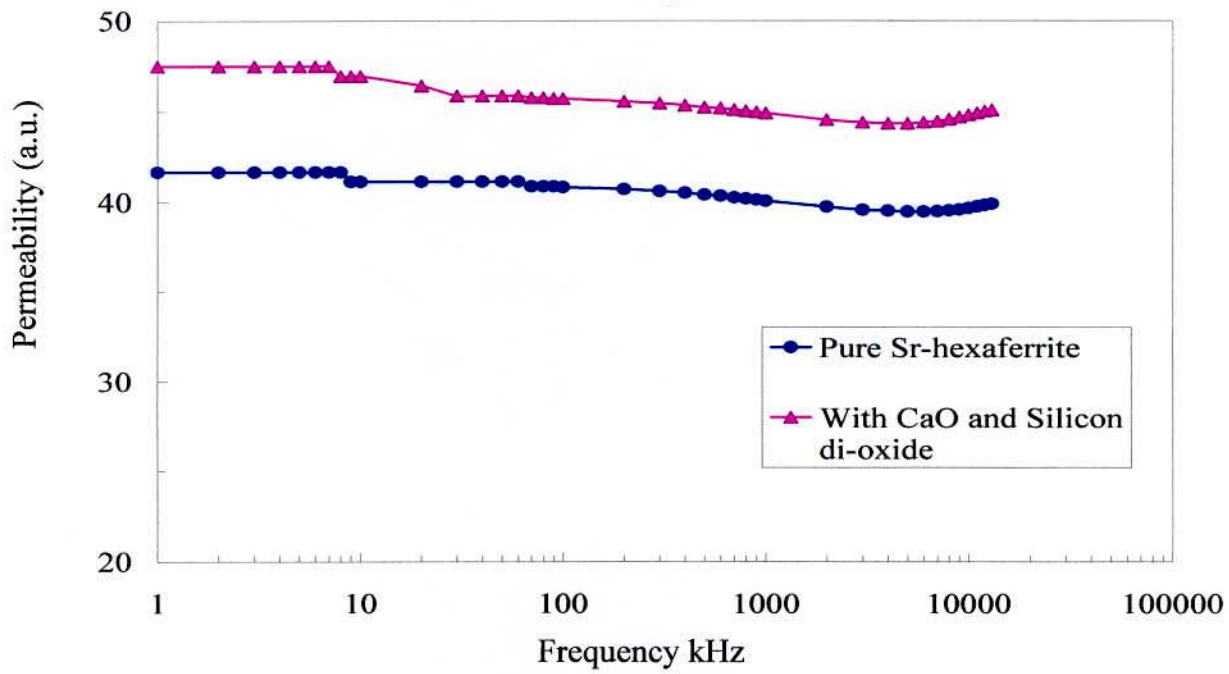

(b)

Fig-5.13: (a) Initial complex permeability Vs frequency curves of $(SrO)_{1-x}(La_2O_3)_x$ $5.7Fe_2O_3$

Fig- 5.13 (b) Initial complex permeability Vs frequency curves of SrO $5.7Fe_2O_3$ and SrO $5.7Fe_2O_3$ [0.7wt% CaO + 0.3wt% SiO_2]

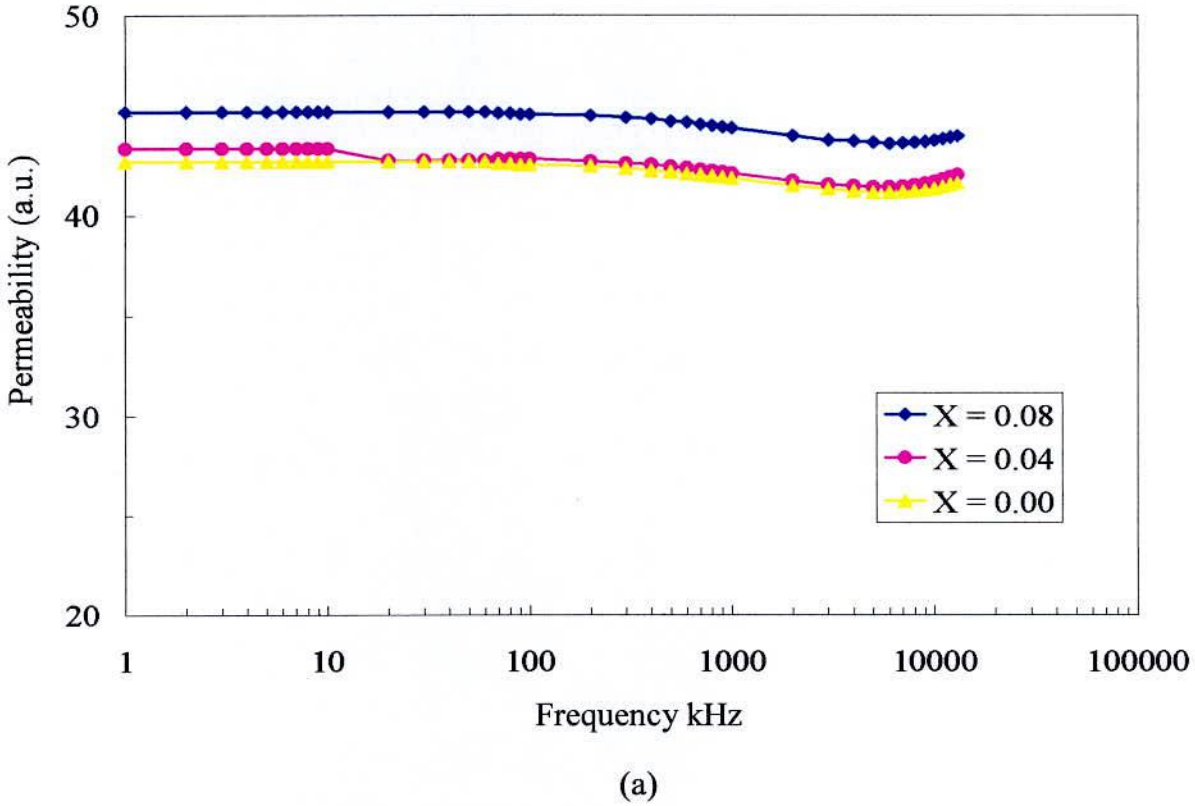

(a)

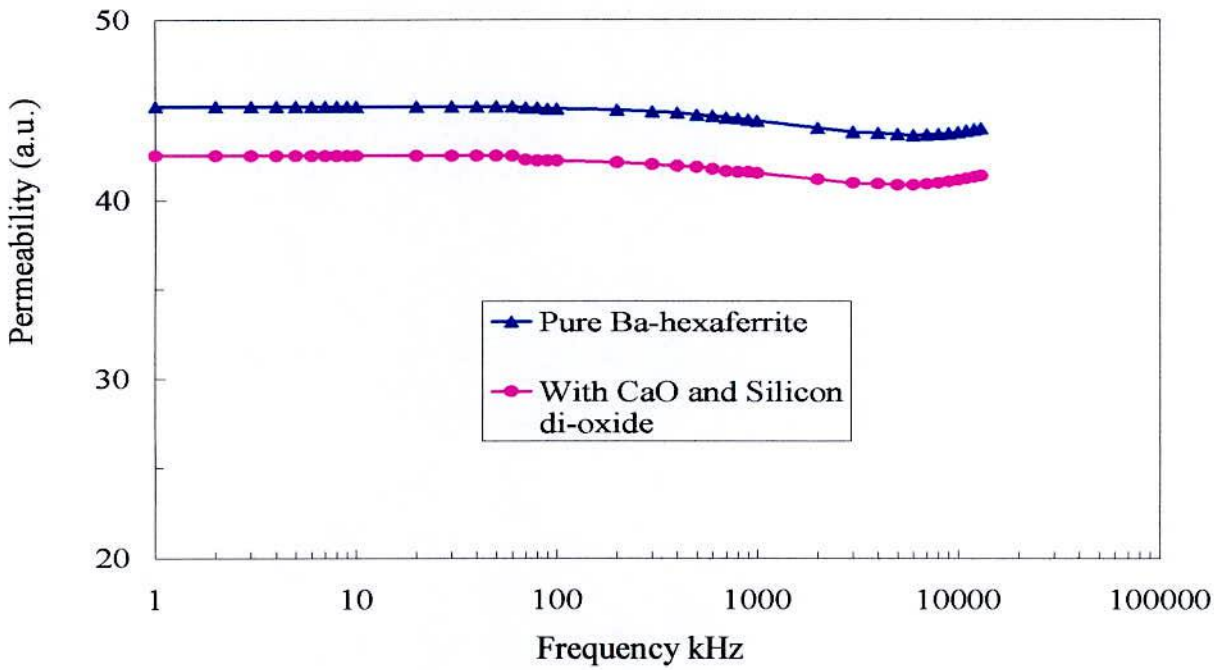

(b)

Fig-5.14: (a) Initial complex permeability Vs frequency curves of $(BaO)_{1-x}(La_2O_3)_x\ 5.7Fe_2O_3$

Fig-5.14: (b) Initial complex permeability Vs frequency curves of BaO $5.7Fe_2O_3$ and BaO $5.7Fe_2O_3$ [0.7wt% CaO + 0.3wt% SiO_2]

5.7.2 Frequency Dependence of Initial Permeability of Ba-hexaferrite Samples with Additives

Figs-5.14 (a) and (b) demonstrate the real part of the complex initial permeability of the Ba-hexaferrite samples of compositions $(BaO)_{1-x}(La_2O_3)_x$ 5.7 Fe_2O_3, where x = 0.00, 0.04, 0.08 and BaO 5.7 Fe_2O_3 + [0.7wt% CaO + 0.3wt% SiO_2] as a function of frequency sintered at 1245°C in air for 2 hours. From the permeability curves it is observed that the real part of the initial permeability decreases with the La_2O_3-content first and as the amount of La_2O_3-content increases the permeability does not show significant change. It may be summarized that with a small addition of La_2O_3 on the Ba-hexaferrites the density might have been increased which leads to an increase in the permeability. Our result is in agreement with the previous standard results, ferrites with higher density and larger average grain size posses a higher initial permeability [5.20]. In comparison with the Sr-hexaferrite samples the real part of the initial permeability of Ba-hexaferrite samples are showing the same characteristics throughout the observed frequency region i.e., permeability remains independent of the frequency. With the simultaneous addition of CaO and SiO_2 the permeability of the Ba-hexaferrites have been found to be increased compared to the undoped samples. This might have been connected with the increase in density of the samples whenever a controlled amount of CaO and SiO_2 is added to the Ba-hexaferrite samples. Throughout the investigation it has also been observed that the real part of the complex initial permeability remains unaffected by the frequency whenever (CaO + SiO_2) added to the BaM or not.

5.8 Resistivity Measurement

Resistivity is an intrinsic property of a magnetic material. Ferrites materials are technically very important because of their high resistivity and low eddy current losses. Eddy current losses are inversely proportional to resistivity of the ferrite samples. Therefore, the measurement of resistivity is very crucial for the ferrite materials. The following table 5.17 and table 5.18 shows the d. c. resistivity of the Sr- and Ba-hexaferrite samples sintered at 1260°C in air for 2 hours. It has been

observed from the resistivity data of the Sr-hexaferrite samples that as the amount of La-content is increased the resistivity of the samples is decreased. With the simultaneous addition of CaO and SiO_2 the resistivity of the hexaferrites is increased. This is because SiO_2 is acting as the dead layer on the hexaferrite samples.

Table 5.17

Room temperature resistivity of the Sr-hexaferrite samples measured sintered at 1260°C in air for 2 hours

Composition	x	Resistivity (kΩ)
$(SrO)_{1-x}(La_2O_3)_x$ 5.7 Fe_2O_3	0.00	1.35
	0.04	1.31
	0.08	1.12
SrO 5.7 Fe_2O_3 + [0.7 wt% CaO + 0.3wt% SiO_2]	-------	1.71

Table 5.18

Room temperature resistivity of the Ba-hexaferrite samples measured sintered at 1260°C in air for 2 hours

Composition	x	Resistivity (kΩ)
$(BaO)_{1-x}(La_2O_3)_x$ 5.7 Fe_2O_3	0.00	1.23
	0.04	1.44
	0.08	3.51
BaO 5.7 Fe_2O_3 + [0.7 wt% CaO + 0.3wt% SiO_2]	-------	1.35

In the case of Ba-hexaferrites it has been found that the resistivity of the samples increases linearly with the addition of La_2O_3. Similar result is also noted whenever a controlled amount of CaO and SiO_2 was simultaneously added in the barium hexaferrite samples. According to the study of Wang et. al. [5.6] addition of SiO_2, a non-magnetic layer on the surface of the hexaferrite samples, the oxygen vacancies and morphology could also be important factors in determining the electrical and magnetic properties of the samples. To improve the oxygen

vacancies of samples is a valid way to enhance the magnetic properties of the hexaferrites. The increase in resistivity in doped sample is related to the decrement of conductivity due to the formation of Fe^{2+} ions in the octahedral sublattice when La^{3+} ions are substituted for $(SrBa)^{2+}$ [5.9]. The substitution of La for (SrBa) leads to a change of valence of Fe^{3+} ions to Fe^{2+} ions at the $4f_2$ position in the octahedral sublattice. The increase in resistivity might have been related with the increase in grain size with substitution amount which has been demonstrated in microstructure analyses of the samples. Resistivity of the samples depends upon the porosity and high resistivity is needed for low losses. Considering the above factors, we can select an optimum sintering temperature for each sample from the microstructure study. For the samples with small grains, pores are found at the grain boundaries. For the samples with large grains, the majority of pores are trapped inside the grains at large distance from the grain boundaries, which might affect the permeability, density and resistivity.

5.9 Measurement of Hysteresis Parameters

The hysteresis characteristics of the Sr- and Ba-hexaferrite samples prepared by ceramic technique have been measured by quantum design physical property measurement system (PPMS) vibrating sample magnetometer (VSM). Figs 5.15 (a, b, c and d) and fig-5.16 (a, b, c and d) show the magnetization curves and M-H loops for the Sr- and Ba-hexaferrites respectively with and without the addition of La_2O_3 and ($CaO + SiO_2$) measured parallel to the preferred magnetization direction for a magnetic field ranging from -5000 Oe to +5000 Oe.

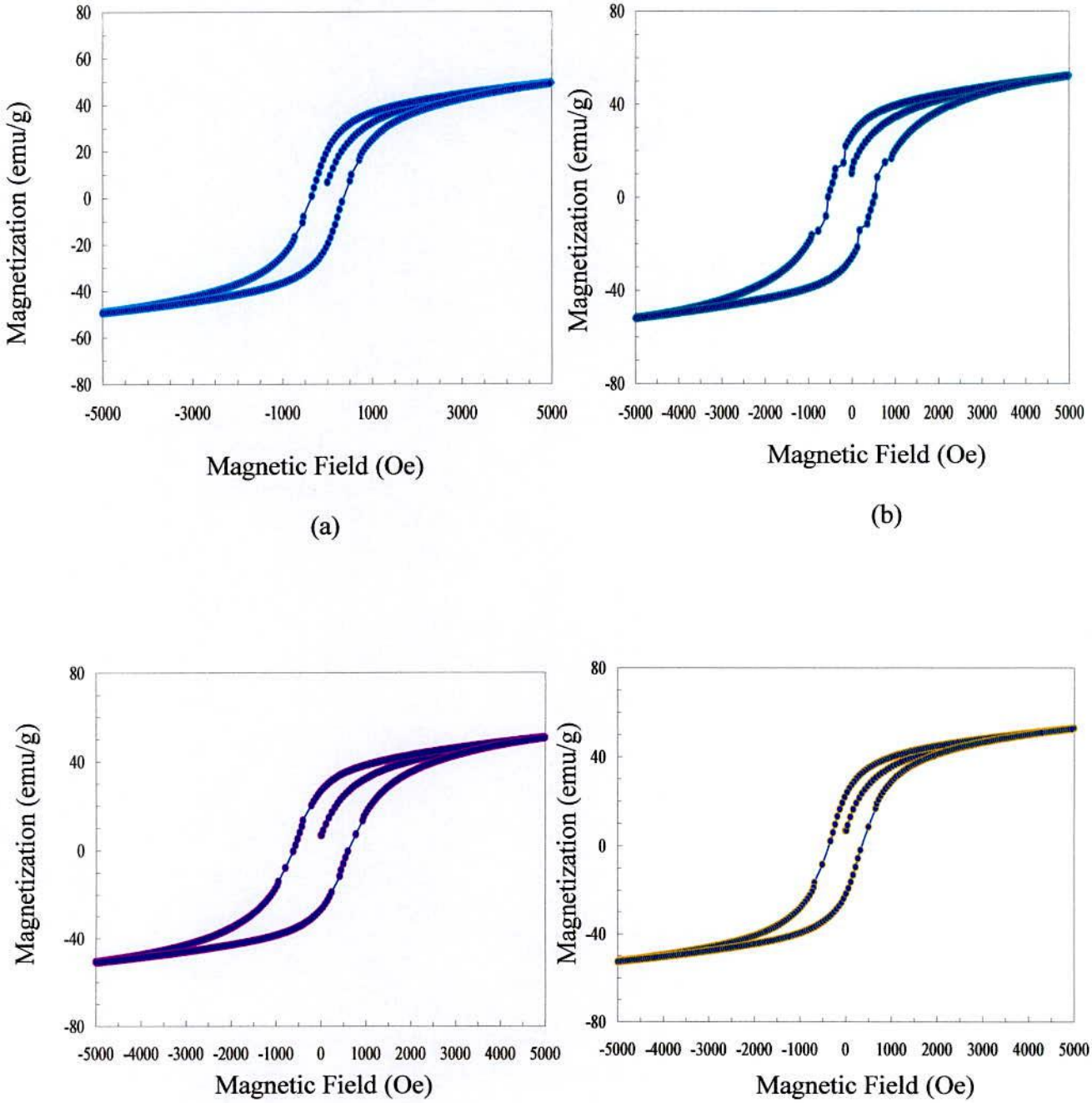

Fig- 5.15 : Hysteresis loops of composition $(SrO)_{1-x}(La_2O_3)_x$ 5.7 Fe_2O_3, where (a) x = 0.00, (b) x = 0.04, (c) x = 0.08 and (d) SrO 5.7 Fe_2O_3 + [0.7wt% CaO + 0.3wt% SiO_2] sintered at 1245°C

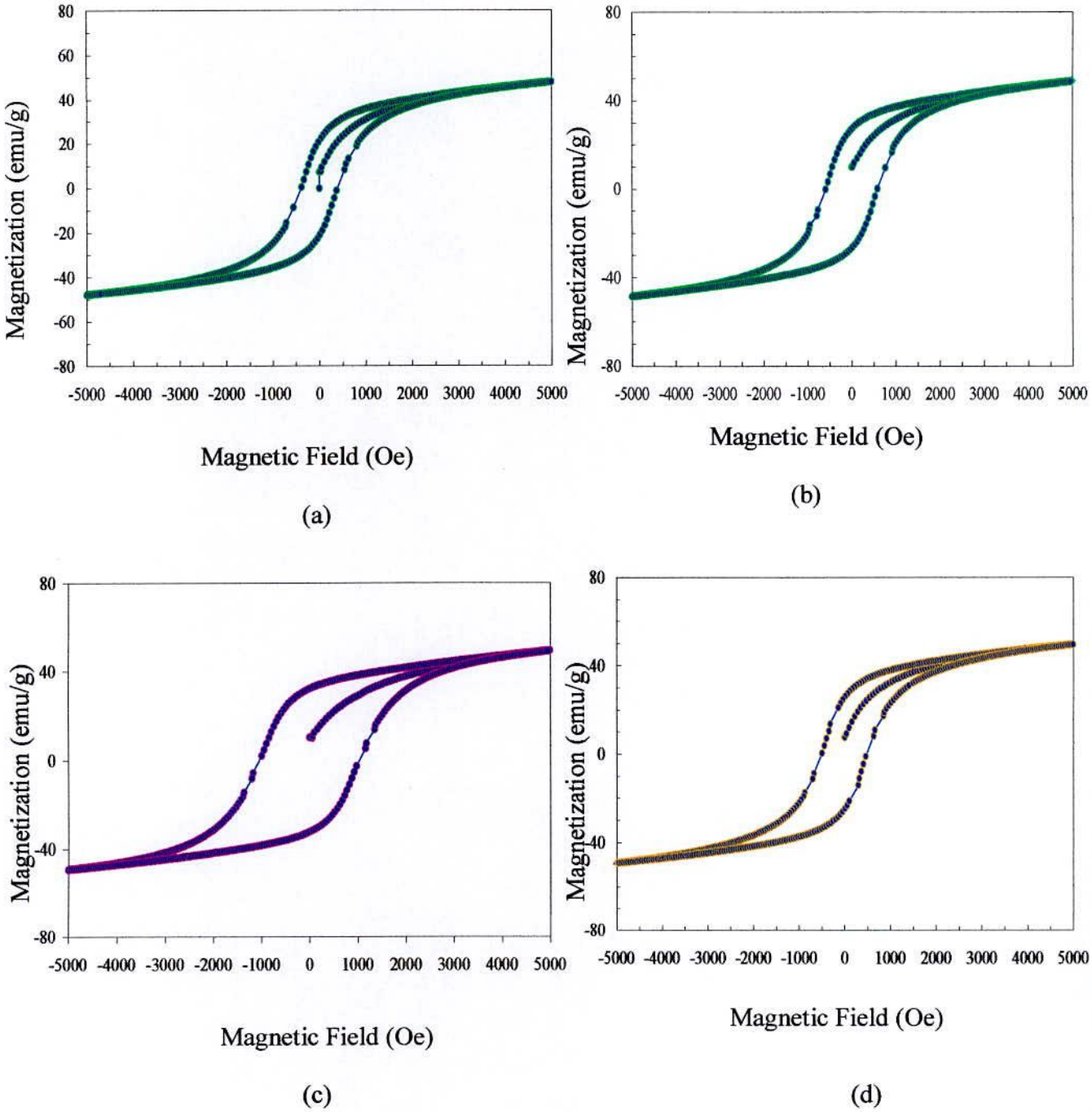

Fig-5.16 : Hysteresis loops of composition $(BaO)_{1-x}(La_2O_3)_x$ 5.7 Fe_2O_3, where (a) x = 0.00, (b) x = 0.04, (c) x = 0.08 and (d) BaO 5.7 Fe_2O_3 + [0.7wt% CaO + 0.3wt% SiO_2] sintered at 1245°C

The samples were sintered at 1245°C in air for 2 hours. Using the hysteresis loops the hysteresis parameters such as saturation magnetization M_s, coercivity H_c, remanent magnetization M_r, and $\frac{M_r}{M_s}$ ratio for Sr- and Ba-hexaferrite samples has been calculated and presented in table 5.19 and table 5.21. A comparison of the improvement or decrement of the magnetic qualities of the Sr- and Ba-hexaferrite samples has also been calculated which are displayed in table 5.20 and table 5.22.

Table 5.19

Remanent magnetization, coercivity, saturation magnetization and $\frac{M_r}{M_s}$ ratio of Sr-hexaferrite samples sintered at 1245°C

Composition	x	Remanent Magnetization, M_r (emu/g)	Coercivity, H_c (Oe)	Saturation Magnetization, M_s (emu/g)	$\frac{M_r}{M_s}$
$(SrO)_{1-x}$ $(La_2O_3)_x$ 5.7 Fe_2O_3	0.00	24.4	344	70.5	0.35
	0.04	28.8	592	72.2	0.40
	0.08	26.7	617	68.0	0.39
SrO 5.7 Fe_2O_3 + [0.7 wt% CaO + 0.3 wt% SiO_2]	------	23.8	326	68.7	0.35

Table 5.20

A comparison of magnetic properties of Sr-hexaferrite samples sintered at 1245°C

Without the addition of La_2O_3, H_c (Oe)	With the addition of La_2O_3, H_c (Oe)	% of improvement
344	592	72
	617	79
Without the addition of [CaO + SiO_2], H_c (Oe)	With the addition of [CaO + SiO_2], H_c (Oe)	% of decrement
344	326	5

Table5.21

Remanent magnetization, coercivity, saturation magnetization and $\frac{M_r}{M_s}$ ratio of Ba-hexaferrite samples sintered at 1245°C

Composition	x	Remanent Magnetization, M_r (emu/g)	Coercivity, H_c (Oe)	Saturation Magnetization, M_s (emu/g)	$\frac{M_r}{M_s}$
$(BaO)_{1-x}$ $(La_2O_3)_x$ 5.7 Fe_2O_3	0.00	20.7	382	66.5	0.31
	0.04	26.4	595	68.9	0.38
	0.08	32.0	991	69.0	0.46
BaO 5.7 Fe_2O_3 + [0.7wt% CaO + 0.3 wt% SiO_2]	-----	25.8	492	68.1	0.38

Table 5.22

A comparison of magnetic properties of Ba-hexaferrite samples sintered at 1245°C

Without the addition of La_2O_3, H_c (Oe)	With the addition of La_2O_3, H_c (Oe)	% of improvement
382	595	56
	991	159
Without the addition of [CaO + SiO_2], H_c (Oe)	With the addition of [CaO + SiO_2], H_c (Oe)	% of improvement
382	492	29

5.9.1 Measurement of Saturation Magnetization, M_s

As is well known, the overall magnetic properties of materials are governed by a sometimes complex combination of intrinsic and extrinsic properties. An intrinsic property such as M_s is controlled by the composition whereas an extrinsic property by the microstructure that is in turn governed by the processing techniques. The magnetization of magnetic materials is a structure sensitive static property (intrinsic property), the magnetic field required to produce the saturation value varies according to the relative geometry of the field to the easy axes and other metallurgical conditions of the material. The value of saturation magnetization M_s can be calculated from a numerical analysis of the magnetization curve based on the law of approach to saturation (LAS) with magnetic field ranging from -5000 Oe to + 5000 Oe [5.21-5.23] using the following equation:

$$M(H)=M_s(1-\frac{a}{H}-\frac{b}{H^2}-\frac{c}{H^3})+\chi_0 H \qquad (5.6)$$

where a, b, c.....χ_0 are constants. The term $\chi_0 H$ represents an increase in spontaneous magnetization when a high field is applied to reduce the misalignments of spins caused by thermal agitation. In the fields over a few

thousands the term $\frac{a}{H}$ is usually dominant, so that the above expression reduces to

$$M(H)=M_s(1-\frac{a}{H}) \qquad (5.7)$$

The value of saturation magnetization M_s has been calculated from the slope of the plot of $\frac{1}{H}$ vs M; when the plot becomes a straight line. The following figs- 5.17 (a, and b representative diagrams) and figs-5.18 (a, b, c and d) show the variation of magnetization with $\frac{1}{H}$ of the Sr- and Ba-hexaferrite samples. For all the cases the curves have been found to follow a straight line.

Investigation on the magnetic properties of Sr-hexaferrite particles coated with uniform SiO_2 layer reported that the value of M_s decreases from 85.7 to 20.00 emu/g with the addition of SiO_2 [5.4]. It is clearly evident from tables 5.19 and 5.21 that the value saturation magnetization decreases with addition of CaO and SiO_2. This may be attributed mainly to the contribution of the volume of the non-magnetic coating layer to the total sample volume. At the same time coercivity, which represents the property of a magnetic material and is determined by the strength and number of magnetic dipole in magnetic domain and relations between adjacent magnetic domains does not show large change (only 5.06% decrement) comparing to the La_2O_3 addition. This is because the nonmagnetic coating layer can be considered as a magnetically dead layer at the surface, thus affecting the uniformity or magnitude of magnetization due to quenching of surface moments [5.24-5.25]. The doping effect on the crystal structure and magnetic properties of chromium substituted Sr-hexaferrite nanoparticles having a composition $SrFe_{12-x}Cr_xO_{19}$, x = 0.00 to 1.00 showed that saturation magnetization increases with the increase in x and reaches to a maximum value at x = 0.20 reflecting that a small amount of the Cr doping leads to the increase of M_s [5.5]. When x > 0.40 the saturation magnetization reduces rapidly indicating that non-magnetic phase α-

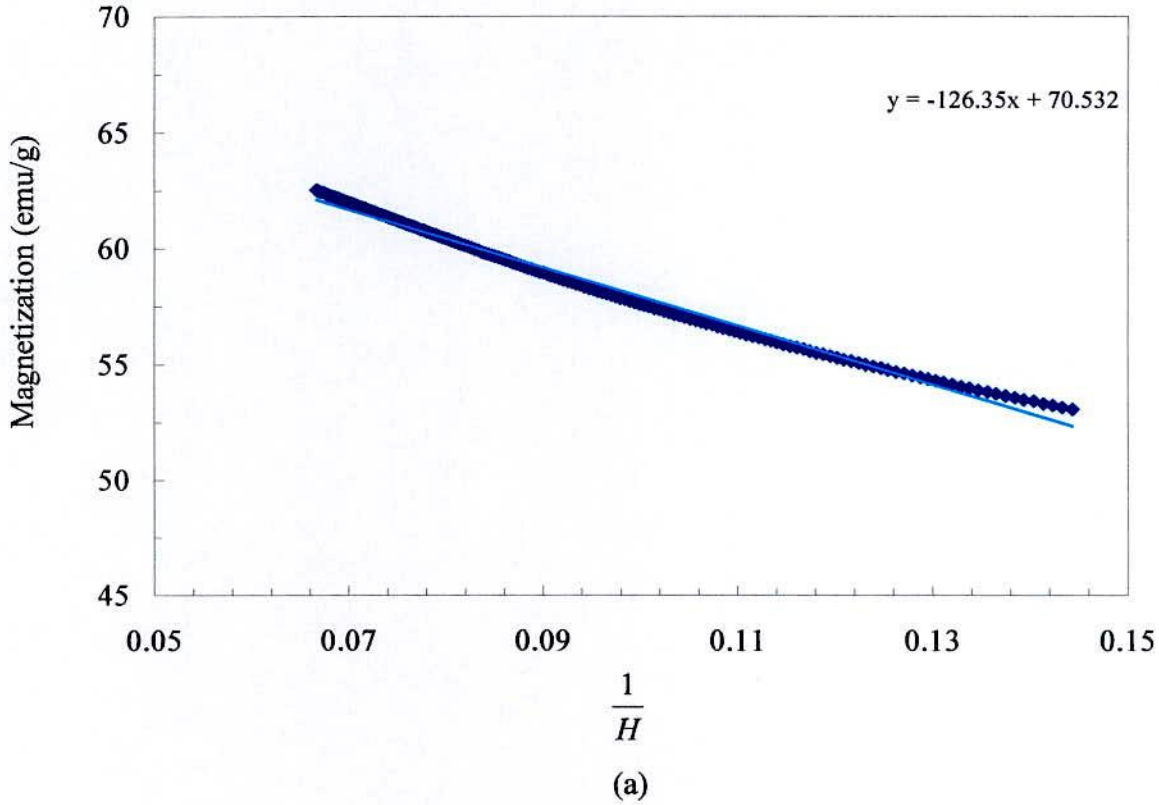

(a)

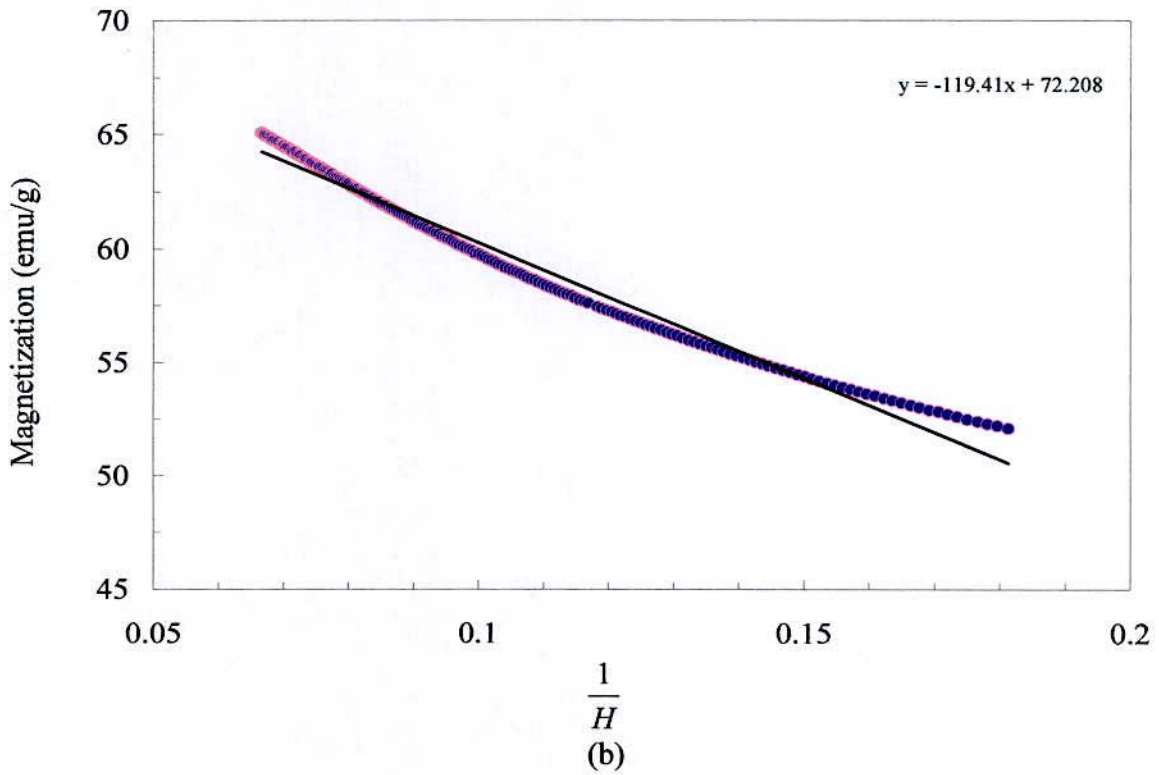

(b)

Fig-5.17:Variation of magnetization with $\frac{1}{H}$ for the composition $(SrO)_{1-x}$ $(La_2O_3)_x$ 5.7 Fe_2O_3, where (a) x = 0.00, (b) x = 0.04

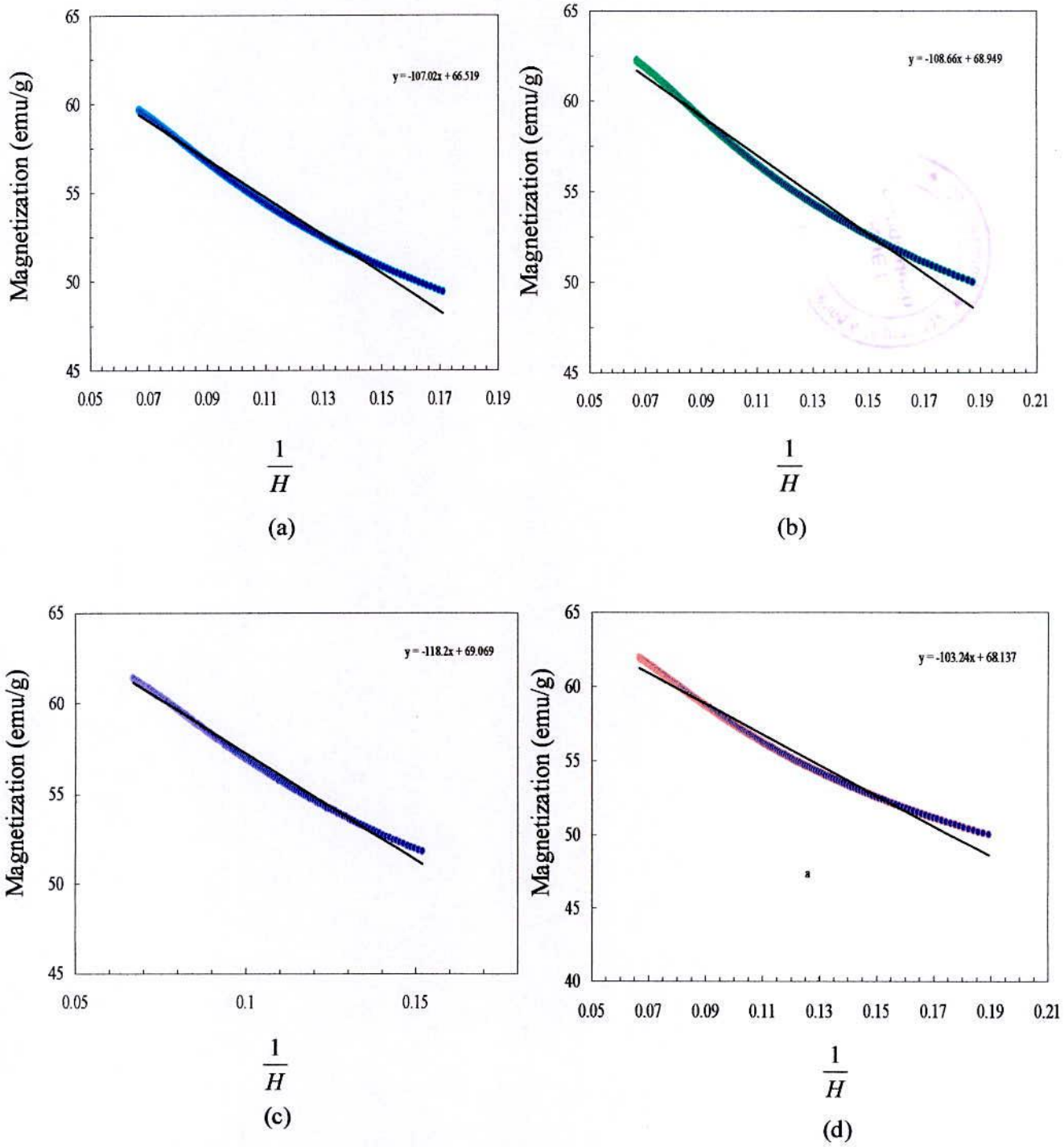

Fig-5.18:Variation of magnetization with $\frac{1}{H}$ for the composition $(BaO)_{1-x}$ $(La_2O_3)_x$ 5.7 Fe_2O_3, where (a) x = 0.00, (b) x = 0.04, (c) x = 0.08 and (d) BaO 5.7 Fe_2O_3 + [0.7wt% CaO + 0.3wt% SiO_2] sintered at 1245°C

Fe_2O_3 appears and its strength increases with the increase in x. Authors reported the value of saturation magnetization for Sr-hexaferrite samples is 64 emu/g.

In our investigation it has been found that suitable amount of La^{3+} substitution may remarkably increases the saturation magnetization and coercivity. With the La^{3+} addition for the same sintering temperature saturation magnetization increases first and then decreases. Saturation magnetization increases from M_s = 70.53 at x = 0.00 to M_s = 73.84 emu/g at x = 0.04 for the same sintering temperature. At the same time the coercivity increases from 344 Oe to 617.08 Oe. The magnetic properties of M-type Sr-hexaferrites are also influenced by sintering temperature. High sintering temperature is not suitable for ultrafine particles with high coercivity because magnetic alignment is difficult to achieve and high temperature sintering always leads to a reduction in coercivity due to particle growth. This could be caused by a great amount of hard magnetic phase and grain growth. In our case we have measured the coercivity of the samples sintered at 1245°C this might have been caused to reduce the coercivity of the hexaferrites. To get much better results of coercivity low temperature sintering is quite important factor to take into consideration.

The M_s values are closely related to the concentrations of La ions on the ferrite system and a deviation of the M_s values of the doped samples from that of the pure samples are observed. Three following factors are connected for interpreting the magnetization behavior of doped ferrites:

i) Hyperfine field enhancements with increase in Fe^{3+} — O — Fe^{3+} superexchange interaction strength and supertransfer fields: The suitable amount of La^{3+} substitution may remarkably increase the saturation magnetization and intrinsic coercivity according to the ref [5.16]. The authors reported that the saturation magnetization increases from 65.3emu/g at x = 0.00 to 69.8 emu/g at x = 0.20 for sintering temperature 1240°C and then decreases rapidly to 49.5 emu/g for x = 0.50 up to 0.20

emu/g for x = 1.0. This is due to superexchange interaction i.e., the coupling of magnetic moments of transition metal ion oxides could take place through excited states of intervening oxygen ions. For M-type ferrites, this phenomenon arises primarily from two types of factors. The first is an amounting number of Fe^{3+} ions with spin up orientation and superexchange interaction.

ii) Spin canting (non-collinear magnetic order): Spin canting or non-collinear magnetic order is a behavior in which spin orientations of magnetic ions align by making angles from the preferred direction (c-axis M structure ferrites), this causes to decrease in M_s [5.8, 5.26]. For M-type Sr-hexaferrite the magnetic moments of Fe^{3+} ions arranged collinearly due to the existence of superexchange interaction. The superexchange interaction determines the orientation of magnetic moment of Fe^{3+} ions. Substitution of divalent Ba or Sr by trivalent La associated with a valence change of one Fe^{3+} per formula unit to Fe^{2+} can reduce the strength of this interaction due to the Fe^{2+} ions while the substituted amount is too much. Hence a deviation from collinear to non-collinear arrangement will occur known as canting spin structure that is coherent with the decreasing T_c with substitution of La^{3+}.

iii) Magnetic dilution with valence state change of Fe^{3+} ($3d^5$ high spin) ions into Fe^{2+} ($3d^6$ low spin) ions after being substituted on the Sr^{2+} sites by La^{3+} ions for balancing the change of hexaferrite system. The magnetic dilution causes to decrease the value of M_s. Substitution of Sr with La would partially disturbed Fe^{3+} — O — Fe^{3+} superexchange interactions, attribute to an iron valence change from Fe^{3+} to Fe^{2+} on 2a site. The Fe^{3+} ions were also partially substituted by Fe^{2+} ions [5.8, 5.26]. The Fe^{2+} — O — Fe^{3+} exchange interaction is weaker than the Fe^{3+} — O — Fe^{3+} superexchange interaction. This provides evidence that the Fe^{3+} — O —

Fe^{3+} superexchange interaction could be diluted and distributed by Fe^{2+} ions [5.8, 5.26].

The curves shown in fig-5.16 (a, b, c and d) show the M-H loops for BaM-ferrites sintered at 1245°C in air for 2 hours. The value of coercivity is obtained from the demagnetization curves. The hysteresis loops of La-substituted hexaferrites show the behavior of the hard magnets with high H_c. The loops are broadened showing an increase in coercivity with the increase of La_2O_3 content and decreases again. The value of saturation magnetization was found to be increased for La-substituted barium hexaferrite of composition $Ba_{1-x}La_xFe_{12}O_{19}$ up $x = 0.00$ to $x = 0.15$ and then decreases again for $x > 0.15$ see ref. [5.27]. The rare-earth (Re) ion substituted M-type hexaferrites have improved magnetic properties largely associated with the increase of both magnetocrystalline anisotropy and coercivity and magnetization [5.26]. The Re ions may contribute to a change of new magnetic interactions, resulting in an improvements of magnetic properties.

The hysteresis loops of Ba-hexaferrites exhibit a high saturation magnetization M_s = 67.3 emu/g [5.6]. X-ray diffraction studies on aluminum substituted barium hexaferrites samples were performed by Mishra [5.28] and observed that remanent magnetization decreases from 21.0 emu/g to 9.45 emu/g with the aluminum substituted amount. Angeles [5.8] performed the magnetic studies of Zn-Ti substituted barium hexaferrites prepared by mechanical milling and shown that the value of saturation magnetization for pure barium hexaferrite is 60.90 emu/g and linearly decreases with the Zn-Ti substitution. When the substitution of Zn-Ti continues to increase the amount of iron ions replaced by non-magnetic ions increases too, leading to weakening of the all exchange interactions and consequently M_s decreases. Authors also reported that the remanent magnetization decreases with the substitution level. The coercivity of the samples was also found to be decreased with amount of substitution of Zn-Ti.

Babu [5.14] reported that the magnetization curves are almost saturated and it shows large coercive force. The authors found that the saturation magnetization value varies from 0.85 to 0.95 T and that seemed to be lower than the values reported by other investigators [5.29]. The lower magnetization may be due to the formation of $BaFe_{12}O_{19}$ and it is supposed to decrease the net saturation magnetization of the sample.

5.9.2 Measurement of Remanent Magnetization, M_r

A research work on the influence of SiO_2 and CaO additions on the microstructure and magnetic properties of sintered Sr-hexaferrite shows that with SiO_2 concentrations increasing from 0.6 wt% to 1 wt% the density of the magnets sintered at 1280°C is reduced to below 5 gm/cc and thus remanent magnetization is also increased [5.12]. The increased non-magnetic additive phase contributes to the reduced B_r. Study of Babu [5.14] reported that with the addition of La_2O_3, which as a grain refiner the remanent induction of the barium hexaferrite samples increases from 537 mT to 543 mT. The appropriate La_2O_3 amount and small SiO_2 doping contribute to the creation of needle shape particles with the size of a single domain, leading to an increase in magnetization as well as the magnetic anisotropies (both the magneto-crystalline anisotropy and shape anisotropy of the particles) which in turn causes an increase in the remanent induction.

In our investigation it has been observed that the value of remanent magnetization of Sr-hexaferrite samples increases first with the addition of La_2O_3. As the amount of additive is increased the value of M_r found to be decreased. The effect of addition of CaO and SiO_2 also causes a decrease in remanent magnetization. But in the case of Ba-hexaferrite samples it has been found that as the amount of La_2O_3 is increased the value of remanent magnetization has also been found to be increased linearly. A similar effect has also been investigated whenever a controlled amount of CaO and SiO_2 has been added simultaneously with the Ba-hexaferrite samples. Niem [5.9] studied the influence of La doping on the properties of Sr-Ba

hexagonal ferrites and observed that doping of La not only improves the remanent magnetization but also coercivity of the samples. Substitution of La for (Sr, Ba) leads to the following relation:

$$(Sr, Ba)^{2+} + Fe^{3+} \rightarrow La^{3+} + Fe^{2+}$$

The formed Fe^{2+} ions possibly are located at the $4f_1$ and $4f_2$ positions. This leads to an increase in remanent magnetization and coercivity. The magnetic properties of a new family of rare-earth substituted ferrites were studied by Grossinger [5.17] and reported that La-Co substitution cause an increase of the anisotropy and consequently of the coercivity of the Sr-hexaferrite samples. The reason for this favorable behavior is that Co enters special lattice sites. Angeles [5.8] studied the magnetic properties of Zn-Ti substituted barium hexaferrites prepared by mechanical milling and found the value of remanent induction for pure barium hexaferrite sample to be 34.8 emu/g. X-ray diffraction studies on the aluminum substituted barium hexaferrites by Mishra [5.28] has been shown the value of remanent magnetization decreases from 21.0 emu/g to 9.45 emu/g with substitution amount [5.30].

5.9.3 Measurement of Coercivity, H_c

The main intrinsic parameters governing the coercive field are the spontaneous magnetization, the magnetocrystalline anisotropy constant and saturation magnetization M_s, and magnetostriction. Microstructures affecting H_c are the types defects leading to inhomogeneties of the intrinsic magnetic material parameters: point defects, dislocations, antiphases and grain boundaries, surface inhomogeneties and precipitates.

In our experimental measurement it has been found that the magnetic properties of Sr-hexaferrites do not change significantly with SiO_2 addition because the coercivity represents the property of the magnetic materials which is determined by the strength and number of the magnetic dipole in magnetic domain and relations between adjacent magnetic domains. The suitable amount of La_2O_3

substitution may remarkably increase the coercivity, H_c. The coercivity has a minimum value of 344 Oe for x = 0.00 and a maximum of 617 Oe for x = 0.30 at sintering temperature 1245°C.

Different authors have been studied the coercivity and grain size of hard ferrites and found there is a reciprocal relationship between them. Several reports discussed to understand what factors govern the coercivity of barium hexaferrites to increase with the doping content [5.13]. The authors found their results were consistent with the previous published values, which shown the fact that the coercivity of barium hexaferrite depends on the temperature and grain size [5.31-5.35]. In a polycrystalline sample, the density of grain boundary is in inverse proportion to the grain size. Accordingly, the pinning of magnetization at the grain boundaries is the most likely cause determining the coercivity. The coercivity of a multi-domain grain sample probably depends on the factors within the grain rather than grain boundaries. In a small grain sample, the grain boundaries can act as pinning centres, which lead to impede the domain wall motion or the domain nucleation. This is the reason for what the coercivity increases with the small grain size. This suggests that the coercivity of barium ferrite samples can be controlled by grain morphology.

The hysteresis curves of barium hexaferrites exhibit a high value coercive force H_c [5.6]. As far as we are concerned, there are at least two factors resulting in the increase of coercivity with the addition of La_2O_3. First, one possible reason is related to the shape anisotropy. The effective anisotropy contributes to the coercivity. For hexaferrite samples, the effective anisotropy of each particle is the sum of the contributions of the magnetic anisotropy and shape anisotropy. Secondly, with a decrease of particles' size, corresponds to magnetic single domain, which is consistent with the increase of coercivity with the addition of La_2O_3. Hoque [5.1] in their study of the synthesis and characterization of BaSr hexaferrite using hematite and magnetite from Cox's Bazar beach sand measured

the average value of coercivity to be 2.2 kOe. It has been reported by the investigators that the presence of Al_2O_3 in beach sand magnetite as an impurity might have reduced the value of coercivity for the samples. Investigation of the influence of La doping on the properties of SrBa hexagonal ferrites of composition $(Sr_{0.75}Ba_{0.25})_{0.94}$ $(La_2O_3)_{0.03}$ $5.3Fe_2O_3$ by Niem [5.9] shows that the doping of La improves the coercivity from 1.926 kOe to 3.371 kOe for x = 0.00 to x = 0.06.

In our experimental measurement for Ba-hexaferrite samples the value of coercivity has been found to be increased remarkably with substitution of La_2O_3. The H_c has a minimum value 382 Oe for x = 0.00 and a maximum value 991 Oe for x = 0.08 at sintering temperature T_s = 1245°C. The addition of La_2O_3 which acts as a grain refiner increases the coercivity of Ba-hexaferrite samples a maximum of 159% due to the finer microstructure with the decrease in grain size. That is the grain size decreases with the La_2O_3 content and magnetic properties is enhanced satisfactorily. In our observation it has also been found that with the simultaneous addition of CaO and SiO_2 on the Ba-hexaferrite samples increases coercivity is 29%.

CHAPTER SIX

Conclusion

In the present investigation, we have studied the effect of Sr^{+2} and Ba^{2+} substitutions by lanthanum oxide on the structural and magnetic properties of the hexaferrites at different sintering temperature. It has been found that the quality, physical and magnetic properties of M-type hexaferrites are strongly dependent upon the synthesis technique used. The density of the sintered Sr- and Ba-hexaferrite samples was found to be increased with the sintering temperature. During the study it has been observed that the porosity of the Ba-hexaferrite samples increases linearly with the addition of La-content and the increase of porosity is the highest whenever CaO and SiO_2 was added.

The X-ray diffraction (XRD) studies confirm that the samples prepared for the investigation are of single phase M-type hexagonal structure which indicates that the ferrite powders are of quite homogeneous and highly pure. In the case of Sr-hexaferrite, the lattice parameters a and c have been found to be fluctuating somewhat with increase in La_2O_3 content. These slight changes in lattice parameter c may have been caused by the difference between the ionic radii of La^{3+} (1.22 Å) and Sr^{2+} (1.32 Å) and, between Fe^{3+} (0.67 Å) and Fe^{2+} (0.80 Å). The unit cell volume of the Sr-hexaferrite samples has been found to be decreased with the increase in La_2O_3-content. This variation in unit cell volume might have been associated with the larger ionic radii of La^{3+} (1.22 Å) and Sr^{2+} (1.32 Å) compared with that of Fe^{3+} (0.67 Å) and Fe^{2+} (0.80 Å).These results suggest that most of the La ions are dissolved both in the SrM grains and the grain boundaries, which lead to deviation of the unit cell volume comparing with the undoped one. It is seen that the lattice parameter a and c of the pure samples are slightly higher compared to that of the doped samples due to higher Ba^{2+} ionic radii compared to those of La^{3+} ionic radii. In our investigation it has been found that the unit cell volume of the Ba-hexaferrite increases linearly with the increase in La-substitution. The Curie temperature of the Sr-hexaferrite samples has been found to be constant with the addition La_2O_3 but with the addition of CaO and SiO_2 the Curie temperature was found to be increased a little. Curie temperature of Ba-hexaferrite samples

decreases with the addition of La_2O_3 and increases with the simultaneous addition of ($CaO + SiO_2$).

The particle morphology of SrM and BaM hexaferrite samples sintered at different temperatures with and without La_2O_3 has been investigated using scanning electron microscope (SEM). The micrographs show the irregular elongated shaped particles. It has been observed that La_2O_3 has remarkable effect on the particle size. With the addition of La_2O_3 it has been found that the grain size of all the samples were reduced significantly. It has also been observed that the addition of La_2O_3 has the effect of not only reducing grain size but also forming very dense microstructure causing an increase of coercivity of the samples. Throughout the study it has been observed that with the simultaneous addition of CaO and SiO_2 remarkably reduced the grain size as well as the density. During the investigation it has also been observed that sintering temperature has a significant effect on the microstructure of the hexaferrites. Low temperature sintering decreases the grain size, narrows grain size distribution. However, from the observation it may be expected that the hard magnetic characteristics of the hexaferrites could have been improved when sintered at low temperature.

The optimization of the dynamic properties such as complex permeability in the high frequency range requires a precise knowledge of the magnetization mechanisms involved. The magnetization mechanisms contributing to the complex permeability, $\mu = \mu' - \mu''$, in polycrystalline ferrites have been a controversial subject for a long time and remain unsolved satisfactorily. Throughout the frequency range investigated up to 13 MHz the permeability has been found to be almost constant i.e., independent of the frequency. No relaxation or resonance has been observed. When the polycrystalline ferrites are considered the bulk resistivity arises from a combination of the crystallite resistivity and the resistivity of the crystallite boundaries. The resistivity of the Sr-hexaferrites has been found to be decreased with the addition of La_2O_3 may be attributed to the low

activation energy of the ferrite samples at room temperature. It has been noticed that with the simultaneous addition of ($CaO + SiO_2$) the resistivity of Sr-hexaferrite samples is increased. In the case of Ba-hexaferrite samples it has been found that with the addition of La_2O_3 and simultaneous addition of ($CaO + SiO_2$) the resistivity of the hexaferrites is increased which may be attributed to the increase of grain boundary resistivity due to the microscopic segregation of the additives at the grain boundary. The boundary resistivity is much greater than that of crystallite resistivity. So the boundaries have the greatest influence on the d. c. resistivity.

Quantum design physical property measurement system (PPMS) vibrating sample magnetometer (VSM) measurements show that in the case of Sr-hexaferrites the value of saturation magnetization increases first with the addition of La_2O_3 and then decreases as the amount of additive is increased. This magnetization behavior might have been contributed by the increase in hyperfine fields on some Fe sites, disruption of collinear spin structure (spin canting) and magnetic dilution. It is clearly evident from the hysteresis data that with addition of ($CaO + SiO_2$) in the Sr-hexaferrite samples both the value of saturation magnetization, M_s and coercivity, H_c decreases which may be attributed to the fact that the addition SiO_2, a non-magnetic layer affects the uniformity of magnetization due to quenching of surface moments.

But in the case of Ba-hexaferrite samples the value of saturation magnetization increases linearly from a value of $M_s = 66.52$ for $x = 0.00$ to a value of $M_s = 69.07$ emu/g for $x = 0.08$. With the addition of CaO and SiO_2 the value of saturation magnetization was found to be $M_s = 68.14$ emu/g. During the study it was found that the coercivity and remanent magnetization increases with the addition of La_2O_3 and ($CaO + SiO_2$) to the Ba-hexaferrite samples.

Rare-earth oxide, La_2O_3 acts as a grain refiner and CaO promotes the plate like grain growth-oriented perpendicular to the basal plane while SiO_2 activates the reaction kinetics. The rare-earth (Re) substituted hexaferrites have the enhanced magnetic properties due to the increase in magnetocrystalline anisotropy with the doping of La_2O_3. Usually, the Re ions were used as substituents for Ba and Sr taking into account the ionic radii of the elements resulting in new magnetic interactions and hence improving the magnetic properties of the samples.

CHAPTER SEVEN

Bibliography

Bibliography

Chapter-I

[1.1] **Alex Goldman**, "Hand Book of Modern Ferromagnetic Materials" Modern Ferrite Technology, VanNostrand Reinhold, New York, 1990

[1.2] **Robert C. O. Handley**, "Modern Magnetic Materials" John Wiley & Sons, Inc. New York, (2000) 485

[1.3] **S. M. Yunus, F. U. Ahmed, I. Kamal, T. K. Datta, A. K. Azad, A. K. M. Zakaria, M. A. Hakim, M. A. Mazid**, Turkish. J. of Physics, 21 (1997) 904

[1.4] **T. Ogasawara, M. A. S. Oliveria**, "Microstructure and hysteresis curves of barium hexaferrite from Co-precipititation by organic agent", J. Magn. Magn. Mater. 27 (2000) 147

[1.5] **V. Babu, P. Padaikathan**, "Structure and Hard Magnetic Properties of barium hexaferrite with and without La_2O_3 prepared by ball milling", J. Magn. Magn. Mater. 241 (2002) 85-88

[1.6] **N. K. Dung, N. Chau, D. I. Minh and B. T. Cong**, " The Nature of High hard magnetic properties of Sr-ferrite substituted by La" Int. Con. On Mat. Sci. & Tech. held on 23-25 October 1999, 40, Dhaka, Bangladesh

[1.7] **Y. kaneko, S. Anamoto and A. Hamamura**, "Improvement of magnetic properties of permanent magnetic properties of the permanent magnets: Effect of CaO and SiO_2 additives on the sintered compact of Sr-ferrite", J. Japanese Soc. Powder and powder metallurgy, 34 (1987) 169

[1.8] **F. Kools and B. Hanket**, "The effect of Al_2O_3 substitution on the microstructure and coercivity of polycrystalline $SrFe_{12}O_{19}$", Proc. ICF-5 (1989) 417, held at Bombay, India

[1.9] **G. B. The**, et al. J. Solid State Chem. 167 (2002) 254

[1.10] **J. Kreijel et al.**, J. Magn. Magn. Mater. 213 (2003) 262

[1.11] **P. Tenaud, A. Morel, F. Kools, J. M. Breton, L. Lechevallier**, J. Alloys and Comp. 370 (2004) 331-334

[112] **D. Mishra**, Ph. D thesis, Berhampur university, Berhampur, India, 2003

[1.13] **J. C. Bernica**, Mater. Sci. Eng. A 109 (1989) 233

[1.14] **J. Kreijel et al.**, J. Magn. Magn. Mater. 213 (2003) 262

[1.15] **B. T. Shirk, W. R. Buessem**, J. Am. Ceram. Soc. 53 (1970) 192

[1.16] **M. Matsuoka, Y. Hoshi, M. Naoe, S. Yamanaka**, IEEE Trans. Magn. 18 (1982) 1119

[1.17] **F. Licci, T. Besagni**, IEEE Trans. Magn. MAG- 20 (1984) 1639

[1.18] **R. H. Anendt**, J. solid state Chem. 8 (1973) 339

[1.19] **T. Gonzalez-Carreo, M. P. Morales, C. J. Serna, Johal**, J. Magn. Magn. Mater. 223 (2001) 55

[1.20] **G. K. Thompson, B. J. Evans**, J. Appl. Phys. 73 (1993) 6295

[1.21] **J. J. Went, G. W. Rathenom, E. W. Gorter, G. W. Van Oosterhout**, Philips. Tech. Rev. 13 (1952) 194

[1.22] **C. A. M. Brock, A. L. Stuijts**, Philips Tech. Rev. 37 (1977) 157

[1.23] **E. W. Gorter**, G. W. Van Oosterhout, Philips Tech. Rev. 13 (1952)194

[1.24] **D. Bueno-Baques, E. Padron Hernandz, J. Matutes-Aquino, S. M. Rezende, D. R. Cornejo,** J. Alloys and Comp. 369 (2004) 158

[1.25] **P. Hernandz-Gomez, C. Torres, C. de Francisco, J. Munoz, O. Alejos, J. I. Iniguez, V. Rapso,** J. Magn. Magn. Mater. E. 1843 (2000) 272-276

[1.26] **X. Liu, W. Zhong, B. Gu, Y. Du**, J. Appl. Phys. 92 (2000) 1021

[1.27] **P. G. Bercoff, H. R. Bertorello**, J. Magn. Magn. Mater. 205 (1999) 261

[1.28]. **Xiansong Liu, Wei Zhong, Sen Yang, Zhi Yu, Benxi Gu, Youwei Du**, "Influences of La^{3+} substitution on the structure and magnetic properties of M-type strontium ferrites", J. Magn. Magn. Mater. 238 (2002) 207-214

[1.29] **Q. Q. Fang, Y. M. Liu, P. Yin, X. G. Li**, J. Magn. Magn. Mater. 234 (2002) 366

[1.30] **J. M. Bai, X. X. Liu, H. Xu, F. L. Wei, Z. Yang,** Acta. Phus. Sin. 49 (2000) 1595

[1.31] **H. C. Fang, C. K. Ong, X. Y. Zhang, Y. Li, X. Z. Wang, Z. Yang**, J. Magn. Magn. Mater. 191 (1999) 277

[1.32] **Qingqing Fang, Hui Chang, Kai Huang, Jinzhi Wang, Rui Li, Yonfang Jiao,** "Doping effect on crystal structure and magnetic properties of chromium substituted strontium hexaferrite nanoparticles" J. Magn. Magn. Mater. 294 (2005) 281-286

[1.33] **H. yamamoto, M. Nagakuma, H. Tarada**, IEEE Trans. Magn. 26 (1990) 1144

[1.34] **H. Taguchi, T. Takeishi, K. Suwa, K. Masuzawa, Y. Minachi**, J. Phys. IV(France) 7(1997) C1-311

[1.35] **M. Sagawa, H. Nagate, T. Wantanabe, O. Itatazi**, J. Phys. IV(France) 7 (1997) C1-307

[1.36] **N. K. Dung, N. Chau, B. T. Cong, D. L. Minh**, N. X. Phuc, J. Phys. IV(France) 7 (1997) C1-313

[1.37] **N. K. Dung, N. Chau, B. T. Cong, D. L. Minh, N. X.** Phuc, "Proceedings of the third international workshop on materials science (IWOMS '99) Hanoi, November 2-4, (1999) 357

[1.38] **Pham Quang Niem, Nguyem Chau, Nguyem Hoang Luong, Dang Le Minh**, "Influence of La doping on the properties of SrBa hexagonal ferrites", Physica B 327 (2003) 266-269

[1.39] **C. S. Kim, S. W. Lee, S. Y. An**, J. Appl. Phys. 87 (2000) 6244

[1.40] **Ounnunkad, S.,** "Improving magnetic properties of barium hexaferrites by La or Pr substitution", Solid State Communications 138 (2006) 472-475

[1.41] **Joonghoe Dho, E. K. lee, J. Y. Park, N. H. Hur,** "Effect of the grain boundary on the coercivity of barium ferrite $BaFe_{12}O_{19}$" J. Magn. Magn. Mater. 285 (2005) 164-168

[1.42] **H. Kojima, in: Wohlfarth** (Ed.), Ferromagnetic Materials, vol. 3, North-Holland, Amsterdam, , Chapter V, 1982, pp. 305-391

[1.43] **R. Grossinger, C. Tellez Blanco, M. Kupferling, M. Muller, G. Wiesinger**, "Magnetic properties of a new family of rare-earth substituted ferrites", Physica B 327 (2003) 202-207

[1.43] **K. Ida, Y. Minachi, K. Majuzawa, H. Nishio, H. Taguchi**, J. Magn. Soc. Japan 23 (1999) 1093

[1.44] **D. Mishra, S. Anand, R. K. Panda, R. P. Das,** "X-ray diffraction studied on aluminium substituted barium hexaferrites", Materials Letters 58 (2004) 1147-1153

[1.45] **Hart W.** The global magnetic materials market past, present and future. In proceedings of the conference "Iron Oxides for Hard/Soft Ferrites" Gorham-Intertec, Pitsburgh, 1996

[1.46] **F. Kools**, "Reaction induced grain growth impediment during sintering of strontium hexaferrite with silica addition, Solid state ionics, 16 (1985) 251-260

[1.47] **F. Kools**, The action of silica additive during sintering of sintering of strontium hexaferrite" Sci. Sint., 17 (1985) 49-80

[1.48] **Kaneko, Y. Kitajima, K and Takusagawa, N.**, "Effects of CaO and SiO_2 addition on the microstructure and intrinsic coercivity of sintered Sr-ferrite", J. Ceram. Soc. Jpn. Intl. Ed. 100 (1992) 1413-1417

[1.49] **J. Tőpfer, S. Schwazer, S. Senz and D. Hesse**, "Influence of SiO_2 and CaO additions on the microstructure and magnetic properties on sintered Sr-hexaferrite", J. of the Euro. Cera. Soci. 25 (2005) 1681-1688

[1.50] **H. Taguchi, Y. Minacji, K. Majuzawa**, in: proceedings of the Eight International Conference on Ferrites, Kyoto, Japan, 18-21 September 2000, p. 405

[1.51] **Y. Kubota, T. Takansi, Y. Ogata,** in: proceedings of the Eight International Conference on Ferrites, Kyoto, Japan, 18-21 September 2000, p. 410

[1.52] **F. Kools, A. Morel, P. Tanaud, M. Rossignol, O. Insard, R. Grossinger, J. M. Le Breton, J. Teillet,** in: proceedings of the Eight International Conference on Ferrites, Kyoto, Japan, 18-21 September 2000, p. 437

[1.53] **R. Grossinger, J. C. Tellez-Blanco, F. Kools, A. Morel, P. Tanaud, ,** in: proceedings of the Eight International Conference on Ferrites, Kyoto, Japan, 18-21 September 2000, p. 428

[1.54] **S. Manjura Hoque, M. A. Hakim and D. K. Saha**, "Synthesis and Characterization of Ba-Sr hexaferrite using hematite of analytical grade and magnetite from Cox's Bazar beach sand", Nuclear Sci. and Applications, Vol. 15, No. 1, June 2006, p. 65-70

Bibliography

Chapter-2

[2.1] http://en.wikipedia.org/wiki/crystal structure

[2.2] **B.D. Cullity**, "Element of X-ray Diffraction", Addition-Wesley publishing company, Inc. (1967).

[2.3] **Alex Goldman**, "Hand Book of Modern Ferromagnetic Materials" Modern Ferrite Technology, VanNostrand Reinhold, New York, 1990.

[2.4] **T. Ogasawara and M. A. S. Oliveira**, J. Mag. Mag. Mater. 217 (2000) 147

[2.5] **C. W. Chen**, Magnetism and Metallurgy, of Soft Mag. Mat. , North - Holland Pub. Com. XV (1977) 288

[2.6] **B. D. Cullity**, Elements of X-ray Diffraction, Addison- Wesley Publishing Com. Inc. (1977) 49

[2.7] **E. P. Wohlfarth**, Ferromagnetic Materials, A handbook on the properties of magnetically ordered substances, North-Holland Publishing Company, Amsterdam, New york, Oxford 2(1980) 337

[2.8] **J. Smit and H. P. J. Wijin**, Ferrites, John Wiley & Sons- Philips Technical library (1959) 175-211

[2.9] **J. M. Williams, J. Adetunji, M. Gregori**. J. Magn. Magn. Mater. 220 (2000) 124

[2.10] **P. B. Braun**, Philips Res. Rep. 12, 491-548 (1957). The Crystal Structure of a new group of Ferromagnetic Compounds

[2.11] **A. K. M. Abdul Hakim**, Ph. D Thesis, Bangladesh University of Engineering and Technology, 1995

[2.12] **David Jiles**, Introduction to Magnetism and Magnetic Materials, Chapman& Hall (1991) 111

[2.13] **B. D. Cullity**, Introduction to Magnetic Materials, Addison- Wesley Publishing Com. (1972) 181

[2.14] **W. P. Wolf**, Ferrimagnetism, Reports on Progress in Physics Vol. xx**1**v (1961) 213

[2.15] **Y. Yafet and C. Kittel**, Phys. Rev. **87** (1952)

[2.16] **J. B. Goodenough**, J. Phys. Chem. Solids, 6 (1958)

Bibliography

Chapter-3

[3.1] **K. V. Krishna**, Proc. Of the Int. School on Powder Diffraction (ISPD '98), IACS, Calcutta, India, 7-10 October (1998) 109

[3.2] **B. D. Cullity**, Elements of X-ray Diffraction, Addision-Wesley Publication Company, Inc., USA, 2nd Edition (1959) 378

[3.3] **D. K. Saha**, "Concentration and impurities study of Cox's Bazar beach Sand Minerals Magnetite and Ilmenite using X-ray Diffraction Method", Materials Science Division, AEC, Dhaka, Bangladesh

[3.4] Beach sand Exploitation Centre, Cox's Bazar report, June 1994, Published by Scientific Information division, BAEC, Bangladesh

[3.5] **O. Kubo, T. Ido, H. Yokoyama,** , IEEE Trans. Magn. MAG- 18 (1982) 1122

[3.6] Tohoku Metal Industries Ltd., Magnetic Recording Powders, Jpn. Patent. 59207 C4 (1984) 6

[3.7] **T. Ogasawara, M. A. S. Oliveria**, J. Magn. Magn. Mater. 27 (2000) 147

[3.8] **D. Mishra**, Ph. D thesis, Berhampur university, Berhampur, India, 2003

[3.9] **J. C. Bernica**, Mater. Sci. Eng. A 109 (1989) 233

[3.10] **P. G. Bercoff, H. R. Bertorello**, J. Magn. Magn. Mater. 205 (1999) 261

[3.11] **B. T. Shirk, W. R. Buessem**, J. Am. Ceram. Soc. 53 (1970) 192

[3.12] **M. Matsuoka, Y. Hoshi, M. Naoe, S. Yamanaka**, IEEE Trans. Magn. 18 (1982) 1119

[3.13] **F. Licci, T. Besagni**, IEEE Trans. Magn. MAG- 20 (1984) 1639

[3.14] **R. H. Anendt**, J. Solid State Chem. 8 (1973) 339

[3.15] **T. Gonzalez-Carreo, M. P. Morales, C. J. Serna, Johal**, J. Magn. Magn. Mater. 223 (2001) 55

[3.16] **G. K. Thompson, B. J. Evans**, J. Appl. Phys. 73 (1993) 6295

[3.17] **V. Babu, P. Padaikathan**, J. Magn. Magn. Mater. 241 (2002) 85-88

[3.18] **J. J. Went, G. W. Rathenom, E. W. Gorter, G. W. Van Oosterhout**, Philips. Tech. Rev. 13 (1952) 194

[3.19] **C. A. M. Brock, A. L. Stuijts**, Philips Tech. Rev. 37 (1977) 157

[3.20] **D. Bueno-Baques, E. Padron Hernandz, J. Matutes-Aquino, S. M. Rezende, D. R. Cornejo**, J. Alloys and Comp. 369 (2004) 158

[3.21] **P. Hernandz-Gomez, C. Torres, C. de Francisco, J. Munoz, O. Alejos, J. I. Iniguez, V. Raposo**, J. Magn. Magn. Mater. E 1843 (2000) 272-276

[3.22] **X. Liu, W. Zhong, B, Gu, Y. Du**, J. Appl. Phys 92 (2000) 1021

[3.23] **C.W. Chen**, Magnetism and Metallurgy, Soft Mag. Mat. , North - Holland Pub. Com. xv (1977) 219-229

[3.24] **C.W. Chen**, Magnetism and Metallurgy, Soft Mag. Mat. , North - Holland Pub. Com. xv (1977) 288

[3.25] **Kuezynski, G. C.**, Powder Metallurgy, Lesynski, w. ed. (Interscience, NY) (1961) 11

[3.26] **Burke, J. E.**, Kinetics of High- Temperature Processes, Kingery, W. D., ed. (Wiley, NY) 1959

[3.27] **P. I. Slick**, Ferrites for Non-microwave Applications, ferromagnetic materials, Vol.2 Ed. E .P. Wolfarth, 1980, North Holland Pub. Co. 2 (1890)

Bibliography

Chapter-4

[4.1]**B. D. Cullity**, Introduction to Magnetic Materials, Addision-Wisley Publishing Company, Inc., California (1972)

[4.2] **B. D. Cullity**, Elements of X-ray Diffraction, Second Edition, Addision-Wisley Publishing Company, Inc. (1978) 335

[4.3] **C. Kittel**, Introduction to Solid State Physics, 7^{th} edition, John Wiley & Sons, Inc.,Singapore (1996)

[4.4] **J. Smit and H. P. J. Wijin**, Ferrites (1959) 250

[4.5] **Atkins, P. W.**, Physical Chemistry. Oxford University Press, New York, (1998) 775-777

[4.6] **B. S. Bahl, G. D. Tuli, Arun Bahl**, Elements of Physical Chemistry, S. Chand & Comp. Ltd., Ramnagar, New Delhi-110055 (1999) 633

[4.7] **B. D. Cullity**, Introduction to Magnetic Materials, Addison-Wesley, Massachausetts, (1972) 347

[4.8] **Z. Yang, H. –X. Zeng, D. –H. Han, J. –Z. Liu, S. –Z. Geng**, J. magn. Magn. Mater. 115 (1992) 77

[4.9] **R. Grossinger**, J. Magn. Magn. Mater. 28 (1982) 137

[4.10] **C.W. Chen**, Magnetism and Metallurgy, Soft Mag. Mat. , North - Holland Pub. Com. XV (1977) 106-109

[4.11] **Jan Evetts**, Concise Enciclopedia of Magnnetic & Superconducting Materials, Pergamon Press, First Edition (1992) 72-73

Bibliography

Chapter-5

[5.1] **S. Manjura Hoque, M. A. Hakim and D. K. Saha**, "Synthesis and Characterization of Ba-Sr hexaferrite using hematite of analytical grade and magnetite from Cox's Bazar beach sand", Nuclear Sci. and Applications, Vol. 15, No. 1, June 2006, p. 65-70

[5.2] **A. M. Gadala, H. E. Schutz and H. W. Hennicke**, "Effect of some additions on the sinterability and magnetic properties of Ba-hexaferrites", *J. Magn. Magn. Mater.* 1 (1976) 24-25

[5.3] **A. A. Sattar, H. M. El-Sayed, K. M. El-Shokrofy and M. M. El-Tabey**, " Improvement of the magnetic properties of Mn- Ni- Zn ferrite by the non magnetic Al^{3+} ion substitution", J. Appl. Sci. 5(1) (2005) 162

[5.4] **Wuyou Fu, Haibin Yang, Qingjiang Yu, Jing Xu, Xiaofen Pang, Guang Zou**, "Preparation and Magnetic Properties of $SrFe_{12}O_{19}/SiO_2$ Nanoparticles with Core Shell Structure", Materials Letters, 61, 11-12 (2007) 2187-2190

[5.5] **Qingqing Fang, hui Cheng, Kai Huang, Jinzhi Wang, Rui Li, Yongfang Jiao**, "Doping Effect on Crystal Structure and Magnetic Properties of Chromium Substituted Strontium Hexaferrite Nanoparticles", J. Magn. Magn. Mater. 294 (2005) 281-286

[5.6] **Jun Wang, Yejun Wu, Yuejin Zhu, Peiqing Wang**, "Formation of rod-shaped $BaFe_{12}O_{19}$ nanoparticles with well magnetic properties", Materials Letters, 61, 7 (March 2007) 1522-1525

[5.7] **Xiansong Liu, Pablo Hernandez-Gomez, Kai Huang, Shengqiang Zhou, Yong Wang, Xia Cai, Hongjun Sun, Bao Ma,** *J. Magn. Magn. Mater.* 305 (2006) 524-528

[5.8] **A. Gonzelez-Angeles, G. Mondoga-Suarez, A. Gruskova, M. Papanova, J. Slama**, "Magnetic studies of Zn-Ti substituted barium

hexaferrites sample prepared by mechanical milling" *Materials Letters* 59 (2005) 26-31

[5.9] **Pham Quang Niem, Nguyem Chau, Nguyem Hoang Luong, Dang Le Minh**, "Influence of La doping on the properties of SrBa hexagonal ferrites", Physica B 327 (2003) 266-269

[5.10] **X. Zhang, Yuping Duen, Hongtao Guan, Shunhua Liu, Bin Wen**, "Effect of Doping MnO_2 on Magnetic Properties for M-type barium Hexaferrite" J. Magn. Magn. Mater. 311, 2 (2007) 507-511

[5.11] **S. L. Blum** "Microstructure and Properties of Ferrites" Journal of the American Ceramic Society 41 (11) (1958) 489–493

[5.12] **J. Tőpfer, S. Schwazer, S. Senz and D. Hesse**, *J. of the Euro. Cera. Soci.* 25 (2005) 1681-1688

[5.13] **Joonghoe Dho, E. K. lee, J. Y. Park, N. H. Hur,** "Effect of the grain boundary on the coercivity of barium ferrite $BaFe_{12}O_{19}$" J. Magn. Magn. Mater. 285 (2005) 164-168

[5.14] **V. Babu, P. Padaikathan**, "Structure and Hard Magnetic Properties of barium hexaferrite with and without La_2O_3 prepared by ball milling", J. Magn. Magn. Mater. 241 (2002) 85-88

[5.15] **A. Cochardt**, J. Appl. Phys. 37 (1966) 1112

[5.16] **Xiansong Liu, Sen Yang, Zhi Yu, Benxi Gu, Youwei Du,** J. Magn. Magn. Mater. 238 (2002) 207-214

[5.17] **R. Grossinger, C. Tellez Blanco, M. Kupferling, M. Muller, G. Wiesinger**, "Magnetic properties of a new family of rare-earth substituted ferrites", Physica B 327 (2003) 202-207

[5.18] **C. S. Kim, S. W. Lee, S. Y. An**, *J. Appl. Phys.* 87 (2000) 6244

[5.19] **J. Smit and H. P. J. Wijin**, Ferrites, *John Wiley & Sons- Publishers*, 1959.

[5.20] **Jiles, David**. Introduction to Magnetism and Magnetic Materials. London: Chapman & Hall/CRC, 1998

[5.21] **B. D. Cullity**, Introduction to Magnetic Materials, Addison-Wesley, Massachausetts, (1972) 347

[5.22] **Z. Yang, H. –X. Zeng, D. –H. Han, J. –Z. Liu, S. –Z. Geng**, J. magn. Magn. Mater. 115 (1992) 77

[5.23] **R. Grossinger**, J. Magn. Magn. Mater. 28 (1982) 137

[5.24] **M. Ma, Y. Zhang, X. Li, D. Fu, H. Zhang, N. Gu**, Colloids Surf., A Physicochem. Eng. Asp. 262 (2005) 87

[5.25] **R. Kaiser, G. Miskolezy**, J. Appl. Phys. 41 (1970) 1064

[5.26] **X. Liu, W. Zhong, S. Yang, Z. Yu, B. Gu, Y. Du**, Phys. Status Solidi A 193 (2002) 314

[5.27] **N. K. Dung, N. Chau, B. T. Cong, D. C. Minh, N. X. Phuc**, Proceedings of the Third International Workshop on Materials Science (IWOMS '99) Hanoi, November 2-4 (1999) 357

[5.28] **Ounnunkad, S**,. *Solid State Communications* 138 (2006) 472-475

[5.29] **D. Mishra, S. Anand, R. K. Pandu, R. P. Das**, "X-ray Diffraction Studies on Aluminium Substituted Barium Hexaferrite" Materials Letters, 58 (2004) 1147-1153

[5.30] **T. Ogsawara, M. A. S. Oliveria**, J. Magn. Magn. Mater. 217 (2000) 147

[5.31] **T. Suzuki. K. Kani, K. Warri, S. Kawakami, Y. Torii**, J. Mater. Sci. Lett. 11 (1992) 83-895

[5.32] **H. Koijima**, Ferromagnetic Materials, in: E. P. Wohlfarth (Ed.), North-Holland, New York, 1982

[5.33] **F. Kools**, J. Physique 46 (1985) C6-349

[5.34] **G. Turilli, A. Paoluzi, M. Lucenti**, J. Magn. Magn. Mater. 104 (1992) 1143

[5.35] **W. A. Kuezmarek, B. W. Ninham**, J. Appl. Phys. 76 (1976) 6065

[5.36] **T. L. Hylton, M. A. Parker, U. Ullah, K. R. Coffey, U. Umphress, J. K. Howard**, J. Appl. Lett. 75 (1994) 5960